iScience

CellPress

Article

A Quinoline-Appended Cyclodextrin Derivative as a Highly Selective Receptor and Colorimetric Probe for Nucleotides

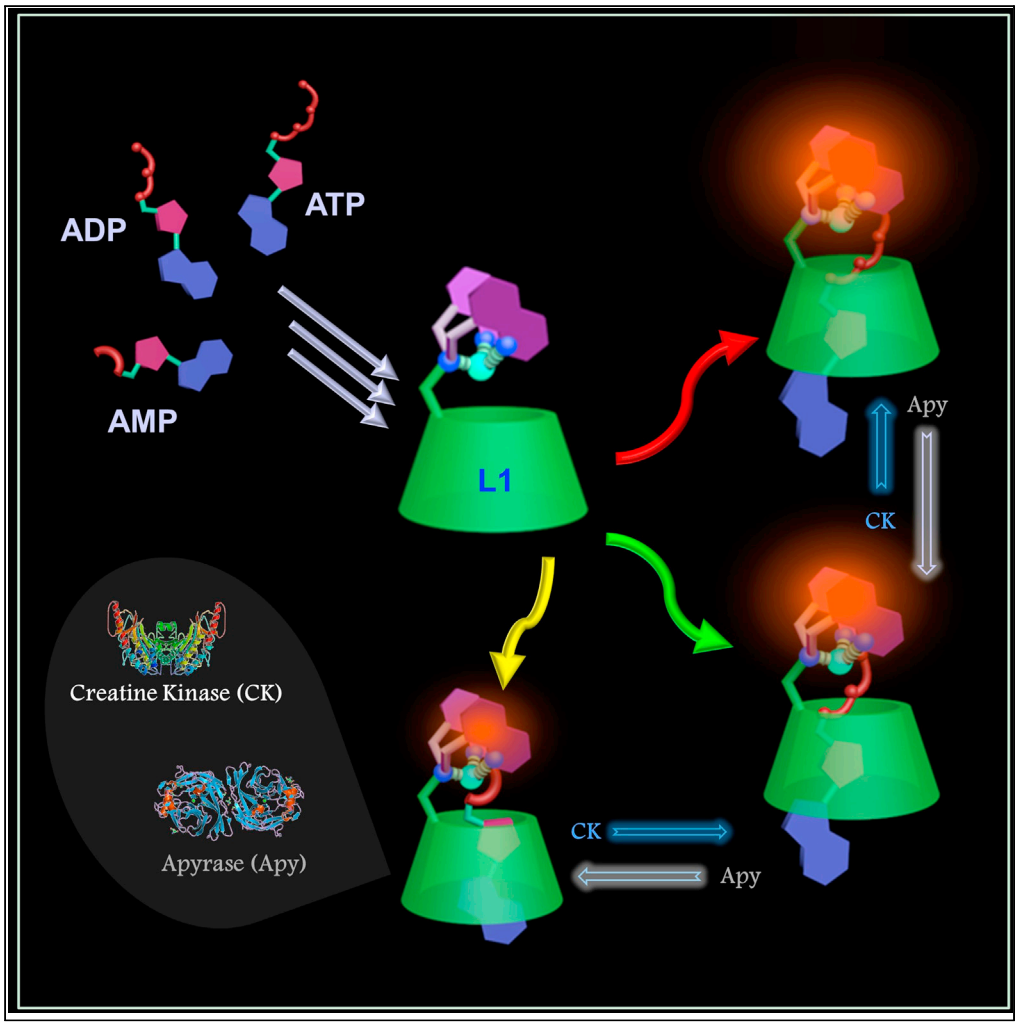

Kuppusamy Kanagaraj, Chao Xiao, Ming Rao, ..., Wanhua Wu, Jason J. Chruma, Cheng Yang

victor.borovkov@scuec.edu.cn (V.B.)
wuwanhua@scu.edu.cn (W.W.)
yangchengyc@scu.edu.cn (C.Y.)

HIGHLIGHTS

Bis-quinoline CDXs as sensing probes to differentiate the nucleotide homologs in water

Its responses in the visible range allowed for a naked-eye colorimetric differentiation

The mechanism is proposed based on divergent spatial orientations of guests binding

Differentiation is realized by *in situ* enzymatic ATP hydrolysis and AMP phosphorylation

Kanagaraj et al., iScience *23*, 100927
March 27, 2020
https://doi.org/10.1016/j.isci.2020.100927

iScience

CellPress

Article

A Quinoline-Appended Cyclodextrin Derivative as a Highly Selective Receptor and Colorimetric Probe for Nucleotides

Kuppusamy Kanagaraj,[1] Chao Xiao,[1] Ming Rao,[1] Chunying Fan,[1] Victor Borovkov,[2,*] Guo Cheng,[1] Dayang Zhou,[3] Zhihui Zhong,[1] Dan Su,[1] Xingke Yu,[1] Jiabin Yao,[1] Taotao Hao,[1] Wanhua Wu,[1,*] Jason J. Chruma,[1] and Cheng Yang[1,4,*]

SUMMARY

The design and development of specific recognition and sensing systems for biologically important anionic species has received growing attention in recent years, as they play significant roles in biology, pharmacy, and environmental sciences. Herein, a new supramolecular sensing probe L1 was developed for highly selective differentiation of nucleotides. L1 displayed extremely marked absorption and emission differentiation upon binding with nucleotide homologs of AMP, ADP, and ATP, due to the divergent spatial orientations of guests upon binding, which allowed for a naked-eye colorimetric differentiation for nucleotides. A differentiating mechanism was unambiguously rationalized by using various spectroscopic studies and theoretical calculations. Furthermore, we successfully demonstrated that L1 can be applied to the real-time monitoring of the enzyme-catalyzed phosphorylation/dephosphorylation processes and thus demonstrated an unprecedented visualizable strategy for selectively differentiating the structurally similar nucleotides and real-time monitoring of biological processes via fluorescent and colorimetric changes.

INTRODUCTION

Ubiquitously present enzymatic active sites, where target substrates are selectively extracted from a complex mixture (e.g., biological fluid) and transformed with efficient rate accelerations, predetermined geometry (beneficial orientation and conformation), and superb stereocontrol under physiological conditions (at *ca* 36°C, in aqueous media at pH 7), represent the paradigmatic ideal for supramolecular chemistry (Kirby, 1996; Cacciapaglia et al., 2004; Ringe and Petsko, 2008). The construction of various artificial supramolecular receptors that mimic enzymes with highly selective binding of biologically important molecules in aqueous media has received substantial attention in recent years (Hembury et al., 2008; Liu and Bonizzoni, 2014; Zhou et al., 2011; Hargrove et al., 2011; You et al., 2015; Busschaert et al., 2015; O'Neil and Smith, 2006; Martinez-Manez and Sancenon, 2003; Molina et al., 2017). Cyclodextrins (CDXs), which are prominent naturally occurring host molecules that possess tunable hydrophobic cavities capable of selectively binding specific substrates in water via non-covalent interactions, are of particular interest in this regard (Szejtli, 1998; Rekharsky and Inoue, 1998). These fascinating properties of CDXs can be further enhanced by selective modifications that enable them to be used in various applications such as catalysis, enzyme mimetic, and molecular sensing (You et al., 2015; Busschaert et al., 2015; O'Neil and Smith, 2006; Martinez-Manez and Sancenon, 2003; Molina et al., 2017; Ogoshi and Harada, 2008; Szente and Szeman, 2013; Hapiot et al., 2012). This CDX-based supramolecular sensing approach, in which selectivity and sensitivity can be tuned to the desired analyte by choosing the specific cavity size, shape, and charge complementarity, has apparent advantages over conventional analytical chemistry techniques and instruments, such as ionic conductivity, mass spectrometry, electrochemical sensing, bio-polymer-based sensing, and indicator displacement methods (You et al., 2015). Taking advantage of multiple weak non-covalent interactions involved in the formation of supramolecular complexes, CDX-based systems are able to produce novel and important practical functions.

Nucleotides are composed of a five-carbon sugar (ribose or deoxyribose) unit connected to a hydrophobic nitrogenous base at the anomeric carbon and one to three negatively charged phosphate groups on the primary hydroxyl moiety. Among all nucleotides, adenosine 5′-monophosphate (AMP), adenosine 5′-diphosphate (ADP), and adenosine 5′-triphosphate (ATP) are particularly important since these

[1]Key Laboratory of Green Chemistry & Technology, College of Chemistry, State Key Laboratory of Biotherapy, West China Medical Center, and Healthy Food Evaluation Research Center, Sichuan University, Chengdu 610064, China

[2]College of Chemistry and Materials Science, South-Central University for Nationalities, Wuhan 430074, China

[3]Comprehensive Analysis Center, ISIR, Osaka University, Japan

[4]Lead Contact

*Correspondence: victor.borovkov@scuec.edu.cn (V.B.), wuwanhua@scu.edu.cn (W.W.), yangchengyc@scu.edu.cn (C.Y.)

https://doi.org/10.1016/j.isci.2020.100927

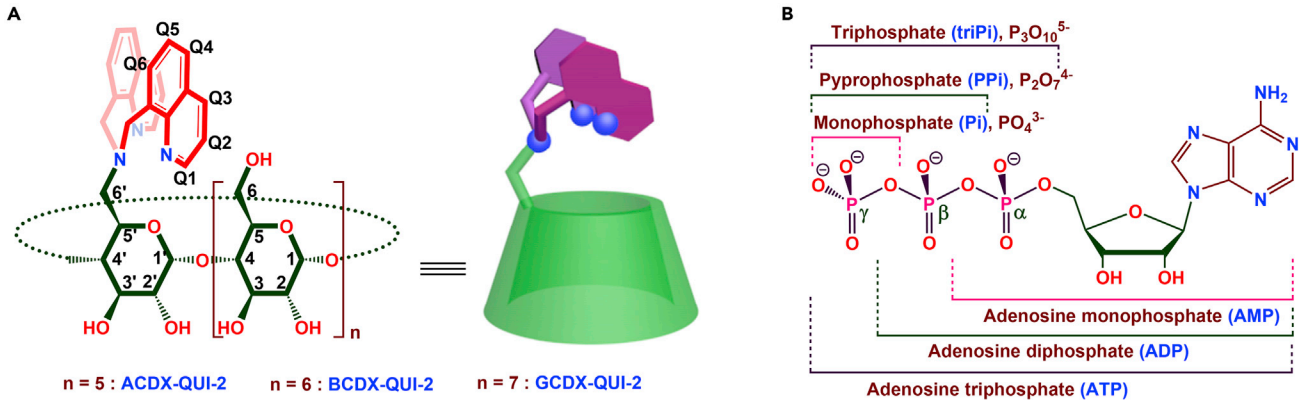

Scheme 1. Structures of the Supramolecular Receptors and Analytes.

Structure of the (A) designed supramolecular A/B/GCDX-QUI-2 receptors and (B) nucleotides (AMP, ADP, and ATP) and inorganic phosphates (Pi, PPi, and triPi).

nucleotides play a decisive and fundamental role in metabolism at the cellular level and they are involved in several processes including cellular signal transmission and transduction, modulation of ion channels, bioenergetics, and the transfer of genetic information (Knowles, 1980; Berg et al., 2002). ATP is a universal energy supplier in living cells, with the required energy for the cell accomplished by metabolic conversion of the nucleotide back into its precursors ADP and/or AMP (Knowles, 1980; Berg et al., 2002). Therefore, effective differentiation of ATP from ADP and AMP by artificial sensors is highly important to quantify the amount of each of these nucleotides in a cell. Based on the ATP/AMP ratio, one can understand and control the accompanying metabolic pathways in the cell that generate and consume ATP. Indeed, this is one of the most efficient methods to determine the amount of energy required for a cell. Furthermore, as ADP and ATP have different biochemical roles in metabolic processes, their interaction with proteins and other biomolecules are varied. Remarkably, PII proteins are one of the most widely distributed families of signal transduction proteins in nature and their competitive interaction with ATP and ADP serves as a sensor for the "energy charge" of bacteria (Wolfe et al., 2007; Jiang and Ninfa, 2007; Huergo et al., 2013). Therefore, sensing and distinguishing these nucleotides using supramolecular fluorescent probes (in aqueous medium) is an urgently needed yet challenging task for researchers, and the development of such a sensor is in high demand. It is important to note that these specially designed supramolecular receptors should distinguish the structurally similar nucleotides based on their different total anionic charge densities via differential binding affinities.

Many selective fluorescent and/or colorimetric chemosensing probes for adenosine nucleotides have been developed (Zhou et al., 2011; Martinez-Manez and Sancenon, 2003; Ramaiah et al., 2010; Zhao and Huang, 2010; García-Espana et al., 2012; Wu et al., 2017; Agafontsev et al., 2019; Ojida et al., 2006; McCleskey et al., 2003; Xu et al., 2009; Huang et al., 2015; Kumar et al., 2014a, 2014b; Shi et al., 2013; Das et al., 2017; Sancenon et al., 2001; Jose et al., 2007; Li et al., 2005; Wang et al., 2016). A singular sensing probe with a differential signaling response to the three phosphorylation states of adenosine, however, has not been reported. Indeed, the design of most previously reported receptors is mainly focused on targeting the negatively charged phosphate group via interactions with a metal or cationic unit tethered to a fluorophore. Moreover, such sensors are typically employed in organic or aqueous-organic media (You et al., 2015; Busschaert et al., 2015; O'Neil and Smith, 2006; Martinez-Manez and Sancenon, 2003; Molina et al., 2017; Ramaiah et al., 2010; Zhao and Huang, 2010; García-Espana et al., 2012; Wu et al., 2017; Agafontsev et al., 2019; Ojida et al., 2006; McCleskey et al., 2003; Xu et al., 2009; Huang et al., 2015; Kumar et al., 2014a, 2014b; Shi et al., 2013; Das et al., 2017; Sancenon et al., 2001; Jose et al., 2007); while only a few systems are able to function in a complex aqueous media though being not suited for practical applications (Ramaiah et al., 2010; Zhao and Huang, 2010; García-Espana et al., 2012; Wu et al., 2017; Agafontsev et al., 2019; Kumar et al., 2014a, 2014b; Shi et al., 2013; Das et al., 2017; Sancenon et al., 2001). Furthermore, when designing an aqueous media nucleotide sensor system, the selectivity for nucleotides over related inorganic phosphate analogues with similar anionic charge densities, such as phosphate (Pi), diphosphate (PPi), and triphosphate (triPi, Scheme 1), must be taken into account. Many studies have collectively reported on selective binding and diverse recognition interactions between positively charged CDXs and

various nucleotide phosphates (Hargrove et al., 2011; Eliseev and Schneider, 1993, 1994; Schwinte et al., 1998; Vizitiu and Thatcher, 1999; Cotner and Smith, 1998; Hauser et al., 2000; Mourtzis et al., 2007; Yuan et al., 2007; Aggelidou et al., 2009; Yang et al., 2015; Formoso, 1973, 1974). Nevertheless, such highly adaptable systems have yet to yield selective chemosensors for real-time applications. Recently, Hayashita and co-workers disclosed a guest-targeting azo/coumarin-modified CDX-copper complex as a probe for distinguishing ATP from AMP and ADP (Fujita et al., 2017; Yamada et al., 2018). The majority of known sensors, however, suffer from a low selectivity and sensitivity toward structurally similar nucleotides, and they demonstrate significantly reduced binding affinity in complex aqueous media, thus making them inappropriate for applications under biologically relevant conditions (Ramaiah et al., 2010; Zhao and Huang, 2010; García-Espana et al., 2012; Wu et al., 2017; Agafontsev et al., 2019). There are only a few examples of selective nucleotide sensors available (You et al., 2015; Busschaert et al., 2015; O'Neil and Smith, 2006; Martinez-Manez and Sancenon, 2003; Molina et al., 2017; Ramaiah et al., 2010; Zhao and Huang, 2010; García-Espana et al., 2012; Wu et al., 2017; Agafontsev et al., 2019; Ojida et al., 2006; McCleskey et al., 2003; Xu et al., 2009; Huang et al., 2015; Kumar et al., 2014a, 2014b; Shi et al., 2013; Das et al., 2017; Sancenon et al., 2001; Jose et al., 2007), and these examples still are not well suited to the requirements of chemosensing probes, owing to poor solubility in pH-buffered solutions, competitive interference from similar anionic analytes, inefficient detecting ability in competitive aqueous media, poor bio-compatibility, unacceptably low bio-sensing responses in cells and biological fluids, or response in high analyte concentrations. Therefore, the design and development of a single supramolecular sensor that is able to distinguish between structurally similar nucleotides based on their different total anionic charge densities is a fascinating goal for many researchers working in biological and supramolecular chemistry.

Indeed, introduction of fluorophores with functional groups to the primary or secondary side arms of CDXs gives two advantages for the development of selective nucleotide probes: an external additional binding site and a fluorogenic signaling unit for guest molecules. Quinoline motifs frequently are used as sensing probes (Meng et al., 2012; Tang et al., 2016; Mikata et al., 2017; Pramanik and Das, 2009; Cai et al., 2013) for various analytes owing to their desirable structure and unique photophysical properties such as relatively high photostability, long-wavelength absorption, and moderate fluorescence emission. Therefore, many mono-quinoline-appended CDX derivatives have been used as sensing probes for cations and neutral analytes (Liu et al., 2003, 2004, 2007a, 2007b, 2009; Liu and Bonizzoni, 2014; Yu et al., 2010; Chen et al., 2007; Zhai et al., 2013; Li et al., 2014; Cheng and Dong, 2016; Cheng et al., 2015). Herein, for the first time, we designed bis-quinoline receptors, A/B/GCDX-QUI-2 (Scheme 1), which contain two main recognition sites: the CDX cavity as a hydrophobic guest binding site and the appended mono-*N*-bis-(8-methylaminoquinolyl) unit acting simultaneously as a fluorophore and metal-binding unit. This combination is indispensable to the substrate/analyte-specific response function. In the present study, the copper-coordinated BCDX-QUI-2 receptor (probe **L1**) was used as a differentiating fluorescence and colorimetric sensor for detecting adenosine-based nucleotides (AMP, ADP, and ATP), and it demonstrated significant selectivity toward AMP and ATP in aqueous media. A unique binding mechanism is proposed on the basis of UV-vis absorption, fluorescence measurements, NMR experiments, and theoretical simulations.

RESULTS AND DISCUSSION

Conformational Analysis of Sensing Receptors

In general, the cavity of a CDX host provides a chiral microenvironment to the tethered achiral chromophoric moiety and generates a corresponding induced circular dichroism (ICD) signal (Harata and Uedaira, 1975; Kajtar et al., 1982; Kodaka, 1993) that depends on the mutual spatial arrangement of the CDX axis and chromophore position. It is important to note that the geometry of molecules with two chromophores linked to a single nitrogen atom of amine as coordinating functional group attaching to the chiral carbon could be controlled by oxidation state of complexing metal ion, hence resulting in the opposite sign of exciton-coupled circular dichroism (ECCD) spectra, which was dependent upon the cationic oxidation form (Harada and Nakanishi, 1972; Zahn and Canary, 1999, 2000; Canary et al., 1998). We herein synthesized the A/B/GCDX-QUI-2 receptors with different cavity sizes and analyzed the effect of the CDX cavity size and solvent used on the conformation of the tethered mono-*N*-bis-(8-methylquinolyl) chromophoric moiety.

The supramolecular receptors, A/B/GCDX-QUI-2 (Scheme 1), were synthesized by reacting two equivalents of 8-(bromomethyl)quinoline with the respective mono-6-amino-α/β/γ-CDXs (see Scheme S3). The

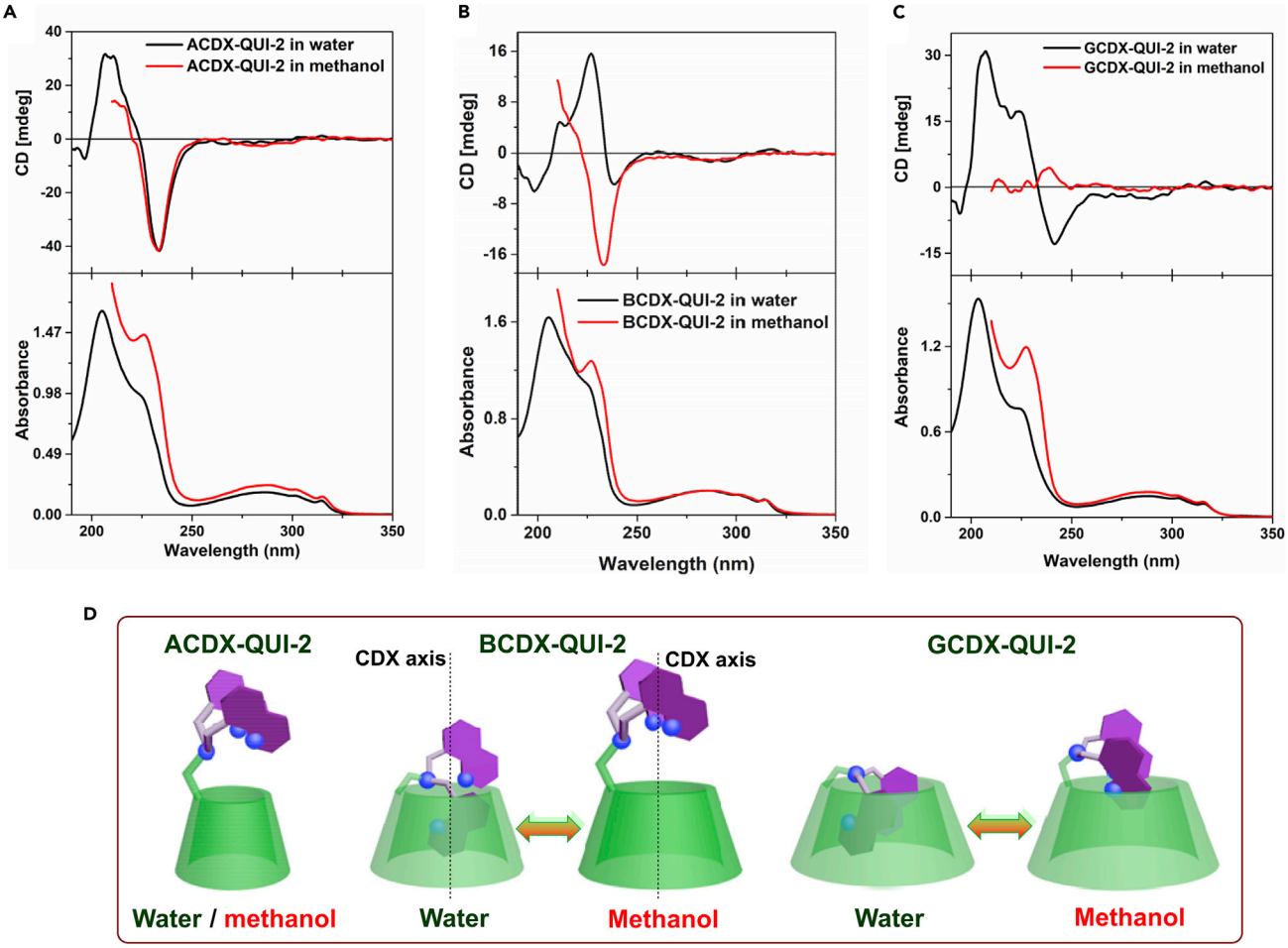

Figure 1. Conformational Analysis of Sensing Receptors

Circular dichroism and UV-vis absorption spectra of receptors (A) ACDX-QUI-2 (3.95×10^{-5} M), (B) BCDX-QUI-2 (3.68×10^{-5} M), and (C) GCDX-QUI-2 (3.17×10^{-5} M) in water and methanol at 25°C. (D) Schematic representation of the quinoline chromophore conformations proposed by applying the empirical rule on the ICD phenomena of CDX complexes (Harata and Uedaira, 1975; Kajtar et al., 1982; Kodaka, 1993) and the exciton chirality theory (Harada and Nakanishi, 1972; Zahn and Canary, 1999, 2000; Canary et al., 1998) to the CD spectra of A/B/GCDX-QUI-2.

synthetic A/B/GCDX-QUI-2 derivatives were fully characterized by using various analytical techniques (see Figures S4–S19), and their conformations in water and methanol were analyzed by CD (Harata and Uedaira, 1975; Kajtar et al., 1982; Kodaka, 1993) and ^{1}H and 2D NMR spectroscopic studies. The UV-vis absorption spectra of A/B/GCDX-QUI-2 have similar absorption maxima at 206, 226 (shoulder), 284, and 315 nm and a single emission band observed at 427 nm upon excitation (λ_{exc}) at 315 nm in both water and methanol (Figures 1 and S23). The absorption bands at 226, 284, and 315 nm are attributed to the long (^1B_b) and short ($^1L_{a,b}$)-axis polarized π-π^* transitions of the quinoline chromophore (Meng et al., 2012; Tang et al., 2016; Mikata et al., 2017; Pramanik and Das, 2009; Cai et al., 2013; Liu et al., 2004, 2007a, 2007b, 2009; Chen et al., 2007; Zhai et al., 2013; Li et al., 2014; Cheng and Dong, 2016; Cheng et al., 2015). As shown in Figure 1, the chiroptical behaviors in water and methanol of the three CDX-QUI-2 sensors depend significantly upon the CDX cavity size.

In the CD spectra of A/B/GCDX-QUI-2 derivatives (Figure 1), the ICD signals of the two quinoline chromophores appeared at ~230 and 290 nm and are attributed to the corresponding ^1B_b and $^1L_{a,b}$ electronic transitions. ACDX-QUI-2 has almost the same CD profile in both water and methanol, and this result is indicative of conformational similarities of the quinoline moieties in either solvent (Figure 1A). BCDX-QUI-2 and GCDX-QUI-2, on the other hand, demonstrate different chiroptical behavior in these two solvents, apparently as a result of solvent-dependent conformational variability. Specifically, the CD spectra of

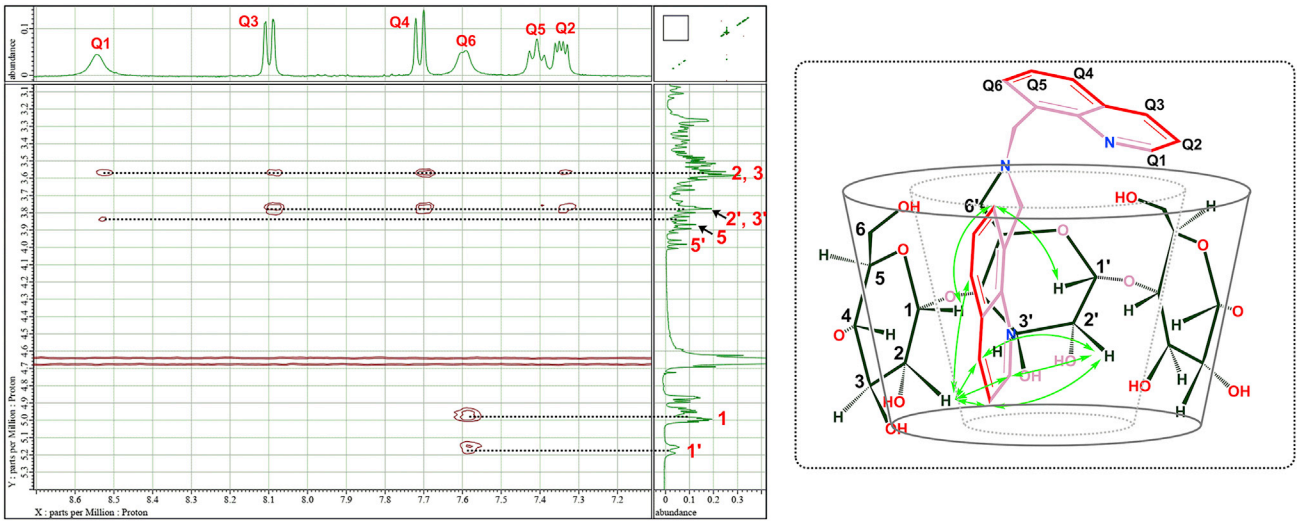

Figure 2. ^{1}H–^{1}H ROESY Spectrum of BCDX-QUI-2 in D_2O at 25°C with a Mixing Time of 250 ms (400 MHz) and Proposed Conformation

BCDX-QUI-2 and GCDX-QUI-2 in water consist of a negative couplet (a weak negative Cotton effect [CE] signal located at low energy of the spectrum followed by a strong positive CE signal located at high energy of the spectrum) appearing around 234 and 233 nm, respectively (Figures 1B and 1C). According to the empirical rule on the ICD phenomena of CDX complexes (Harata and Uedaira, 1975; Kajtar et al., 1982; Kodaka, 1993), the observed CD signals of BCDX-QUI-2 and GCDX-QUI-2 indicate that the anchored quinoline chromophores locate inside the CDX cavities with the long $^{1}B_b$ transition band being parallel to the CDX axis and the short $^{1}L_{a,b}$ transition band being almost vertical to the CDX axis. Both the quinoline chromophores (in GCDX-QUI-2) or only one quinoline chromophore (in BCDX-QUI-2) accommodated inside the CDX cavity (see below) resulted in the counterclockwise orientation of its electronic transitions that correspond to the negative exciton chirality ECCD signals (a negative CE followed by positive CE, reading from a longer to shorter wavelength) according to the exciton chirality method (Harada and Nakanishi, 1972; Zahn and Canary, 1999, 2000; Canary et al., 1998). In methanol, BCDX-QUI-2 shows a relatively strong negative couplet, hence indicating that both of the quinoline chromophores are outside the CDX cavity and are relatively in proximity to each other. This conformational mode is a result of the high solvation and its location at the primary hydroxyl rim with the long $^{1}B_b$ transitions being slightly tilted to the CDX axis. Similarly, because of its smaller cavity size, ACDX-QUI-2 gives a strong negative exciton couplet in both water and methanol, implying that both quinoline chromophores locate outside of the CDX cavity (Figure 1A). The weak positive CE peak at around 239 nm observed for GCDX-QUI-2 in methanol indicates that both of the quinoline chromophores are not completely excluded from the CDX cavity. This is because the large accommodating cavity size of the γ-CDX host results in the parallel orientation of the $^{1}B_b$ electronic transitions to the CDX axis, hence producing a positive CD signal (Figure 1C).

The solvent-dependent conformational change of the three CDX-QUI-2 derivatives when transitioning from deuterated water to deuterated methanol was further analyzed by NMR measurements (Figures 2 and S24–S30). The ^{1}H NMR spectra of the CDX-QUI-2 derivatives show complicated patterns with multiple overlapped signals from the CDX protons appearing between 3.0 and 4.2 ppm and well-resolved quinoline protons observed further downfield (7.0–9.0 ppm, Figures S24–S30). The CDX protons of both BCDX-QUI-2 and GCDX-QUI-2 in D_2O experienced corresponding up-field shifts observed at around 3.0–3.25 ppm in comparison with those in CD_3OD. This clearly indicates that the appended quinoline chromophore is self-included into the CDX cavity as a predominant conformer (Figure 1D). The self-included pattern of BCDX-QUI-2 was also confirmed by the appearance of cross peaks between the quinoline protons and adjacent CDX protons in the 2D ROESY spectrum (Figures 2 and S28A). In CD_3OD, the absence of these up-field shifted protons from CDX and the broadening of the quinoline signals indicate that both the quinoline moieties are located outside the cavity. This proposal was supported by the absence of the corresponding cross contour peaks in the 2D ROESY spectrum (Figure S28B). ACDX-QUI-2 also shows the absence of the up-field shift for the CDX protons. This feature, along with the strong negative exciton

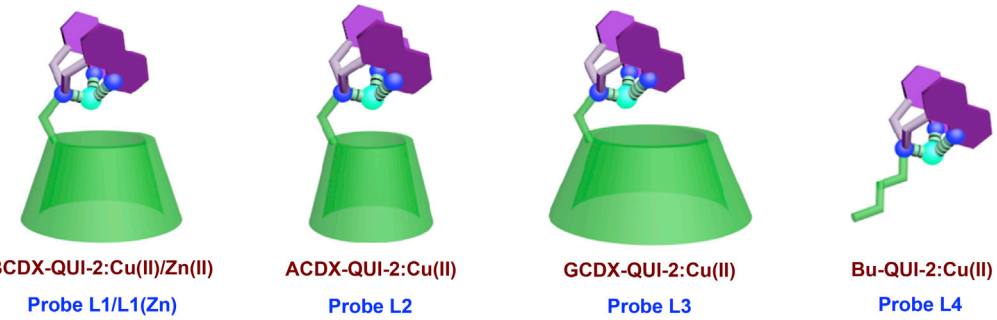

Scheme 2. Structures of Probes L1-L4

Schematic structures for probes **L1** and **L1(Zn)**, as well as control compounds **L2-L4** (green cone, CDX moiety; purple, quinoline groups; dark blue, chelating nitrogen atoms; light blue, Cu(II) or Zn(II) cation).

couplet signals in both water and in methanol, clearly indicate that ACDX-QUI-2 exists as a single conformer with both the quinoline chromophores located outside the CDX cavity (Figure 1D).

The Q1 proton of quinoline moieties proved to be the best conformational indicator. Hence, in all CDX-QUI-2 derivatives the proton provided a sharp and intense signal in D_2O, whereas in CD_3OD, the resulting signal was less intense. This is evidence that the quinoline chromophores are expelled from the CDX cavity via strong solvation in the organic solvent. The expelled quinoline subunits can interchange their positions at a rate substantially faster than the NMR timescale, hence resulting in less intense and broadened NMR signals for the Q1 proton. According to the aforementioned discussion about conformational switching, in aqueous solution, the hydrophobic quinoline chromophores are expected to be immersed in the chiral microenvironment of appropriately sized CDX cavities, but this is not necessarily when using less polar methanol as solvent. Combining the results from CD and NMR experiments provides strong support for the existence of the proposed A/B/GCDX-QUI-2 conformers in both water and methanol (Figure 1D).

The relationship between solvent and conformation was further investigated for BCDX-QUI-2. In organic solvents such as $CDCl_3$, DMSO-d_6, CD_3OD, and acetone-d_6, the primary conformation of BCDX-QUI-2 appears to be one in which the quinoline chromophores are expelled from the chiral hydrophobic CDX cavity (Figure S31). It should be noted that the presence of small organic molecules such as isopropanol and ethyl acetoacetate do not affect the predominant self-included conformer of BCDX-QUI-2 in D_2O, with the corresponding co-inclusion complexes forming instead (Figure S32).

Application of Adenosine Nucleotide Sensing Probe

Although positively charged CDXs with mono/per-aminomethyl and guanidine moieties have been reported to strongly bind nucleotides like AMP, ADP, and ATP (Eliseev and Schneider, 1993, 1994; Schwinte et al., 1998; Vizitiu and Thatcher, 1999; Cotner and Smith, 1998; Hauser et al., 2000; Mourtzis et al., 2007; Yuan et al., 2007; Aggelidou et al., 2009; Yang et al., 2015; Formoso, 1973, 1974), the design and construction of such supramolecular systems as chemical sensors for nucleotides under practical applications remains a challenging task. Introduction of fluorophores to the primary or secondary side arms of CDXs may provide additional binding sites and fluorogenic signaling units, which can be used as artificial sensing receptors for biologically important small molecules and anions (Zhong et al., 2009; Ngo et al., 2012; Kumar et al., 2012, 2014a, 2014b). The fluorogenic bis-quinoline motifs in A/B/GCDX-QUI-2 are able to form the corresponding chelated complexes with Cu(II) and Zn(II) ions (Schemes 2 and S5, Figures S33–S36), which can be used as sensing and differentiating receptors for nucleotides and inorganic phosphates. As will be detailed below, the selective response of the BCDX-QUI-2:Cu(II) complex **L1** toward various adenosine-based nucleotides in an aqueous medium was clearly demonstrated via UV-vis absorption and fluorescence spectroscopic studies and further supported by control experiments, ^{1}H and ^{31}P NMR spectroscopy, mass spectrometry analysis, and theoretical simulations.

Selective Response of Probe L1 in the Presence of Various Nucleotides and Inorganic Phosphates

The selective response of β-CDX-derived probe **L1** toward various adenosine nucleotides and inorganic phosphates was investigated by using UV-vis and fluorescence titrations (Figures 3 and 4). The measurements were carried out by adding five equivalents of nucleotides and inorganic phosphates to a fixed

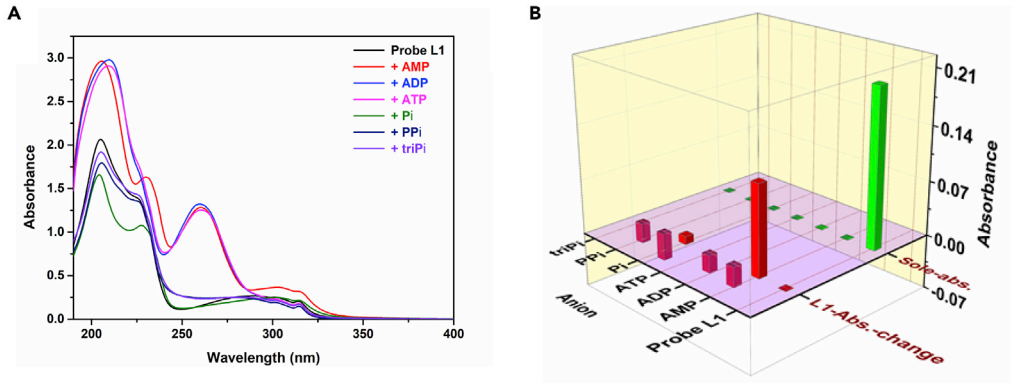

Figure 3. Absorption based Sensing Response of Probe L1 towards Various Analytes

(A) UV-vis absorption spectra of probe **L1** (37 μM) in the absence (black) and presence of nucleotides (5 equiv; AMP [red], ADP [blue], ATP [magenta]) and inorganic phosphates (5 equiv; Pi [green], PPi [navy], and triPi [violet]) in water at room temperature.

(B) UV-vis absorption change (at 315 nm) of probe **L1** (37 μM) toward the nucleotides (5 equiv) AMP, ADP, ATP and inorganic phosphates (5 equiv) Pi, PPi, and triPi in water at room temperature (green bars represents the sole absorbance of probe **L1** and nucleotides at 315 nm; red bars represents the observed absorbance changes [at 315 nm] of probe **L1** upon addition of nucleotides and inorganic phosphates, respectively).

amount of probe **L1**. Remarkably, among the analytes tested, only AMP exhibited an enhancement of the absorption maxima at 303 and 315 nm (Figure 3A), accompanied by a blue-shifted (from 427 to 377 nm, $\Delta\lambda_{em}$ = 50 nm) and quenched fluorescence emission (Figure 4A). ADP and ATP, on the other hand, both showed a small hypochromic effect in the absorption spectra and enhanced fluorescence emission at 427 nm ($\lambda_{exc.}$ = 315 nm). Inorganic phosphates exhibited a relatively negligible change in the absorption and the fluorescence emission of the probe **L1**. Most importantly, it was only upon addition of AMP to **L1** that the aqueous solution turned from colorless to light blue with corresponding absorption maxima appearing at 303 and 315 nm and a less intense ligand-to-metal charge transfer (LMCT) band around >325 nm. The relative absorption and fluorescence changes for selective sensing and the differentiating response of the probe **L1** in the presence of various nucleotides and inorganic phosphates are given in Figures 3B and 4B. This unique change and differential binding behavior of **L1** with AMP, ADP, and ATP allows the molecular probe to be used as an effective sensor for discriminating between structurally similar nucleotides using either spectral means or even the naked eye.

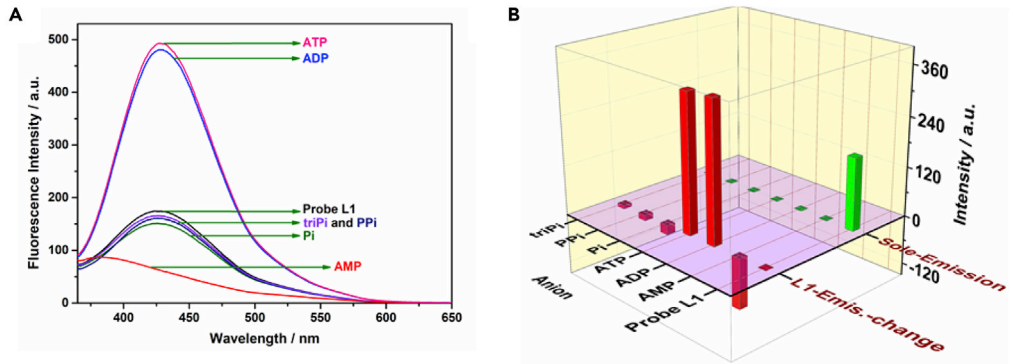

Figure 4. Fluorescence based Sensing Response of Probe L1 towards Various Analytes

(A) Fluorescence spectra of probe **L1** (37 μM) in the absence (black) and presence of nucleotides (10 equiv; AMP [red], ADP [blue], ATP [magenta]) and inorganic phosphates (10 equiv; Pi [green], PPi [navy], and triPi [violet]) in water at room temperature (λ_{exc} = 315 nm).

(B) Fluorescence response (at 427 nm) of probe **L1** (37 μM) toward the nucleotides (10 equiv) AMP, ADP, ATP and inorganic phosphates (10 equiv) Pi, PPi, and triPi in water at room temperature (green bars represents the sole fluorescence of probe **L1** and nucleotides at 427 nm; red bars represents the observed fluorescence changes (at 427 nm) of probe **L1** upon addition of nucleotides and inorganic phosphates, respectively).

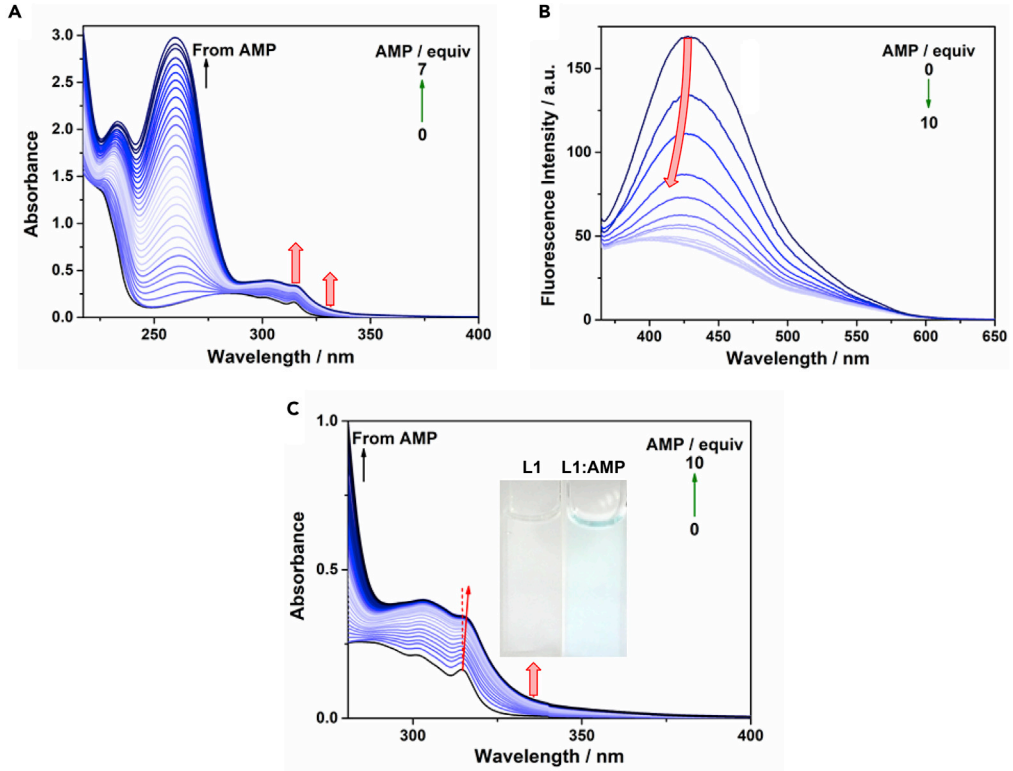

Figure 5. Absorption and Fluorescence Spectral Changes of Probe L1 towards AMP

(A) Absorption and (B) fluorescence spectral changes ($\lambda_{exc.}$ = 315 nm) of **L1** (37 μM) upon addition of AMP (0–10 equiv) in water at room temperature; (C) expansion of Figure 5A in the region of >280 nm. Inset: Color change of probe **L1** upon addition of AMP.

Investigation of Sensing and Differentiating Binding Response of Probe L1 with AMP, ADP, and ATP

In order to verify the differentiating binding response of probe **L1** with nucleotides AMP, ADP, and ATP, the corresponding absorption and emission titrations were carried out separately in water (Figures 5, 6, and 7). It was found that **L1** shows a moderate fluorescence emission observed at 427 nm ($\lambda_{exc.}$ = 315 nm) in water, which was blue shifted (from 427 to 377 nm, $\Delta\lambda_{em}$ = 50 nm) and considerably quenched upon addition of 0–10 equivalents of AMP (Figure 5B), which is most probably due to the charge interaction between the adenine moiety and the quinoline chromophore when **L1** binds with AMP (see "Theoretical Studies" for detail). In the UV-vis spectra there is a noticeable enhancement of the absorption maxima at 303 and 315 nm with small red shifts (~2–5 nm) and new long wavelength band (>325 nm) upon addition of AMP (Figure 5A). Moreover, the color of the solution turned from colorless to light blue upon increasing the AMP concentration (Figure 5C). Indeed, Cu(II) ions having empty *d*-orbitals are able to form an LMCT ternary complex with the probe **L1** and electron-rich phosphate group of AMP, hence exhibiting a longer wavelength absorption band and changing the solution color to light blue (Kim et al., 2009; Kim and Quang, 2007; Santis et al., 1995; de Silva et al., 2009; Guo et al., 2016; Wang et al., 2017). In contrast, addition of ADP and ATP to the probe **L1** resulted in a significant enhancement of the fluorescence emission at 427 nm ($\lambda_{exc.}$ = 315 nm) (Figures 6B and 7B), and they demonstrated hypochromic effects of absorption maxima at 303 and 315 nm in the absorption spectra (Figures 6A and 7A).

It is important to emphasize that poor binding efficiency has been observed for nucleotides upon interaction with native CDXs. For example, the association constant (k_a) of β-CDX with AMP is 41 M^{-1}, through non-specific hydrophobic interactions (Formoso, 1973, 1974). Nucleotide binding to CDX can be enhanced considerably, however, upon functionalization with a respective number of cationic amino groups on the primary side of the cyclic oligosaccharide framework (k_a of per-methylamino-β-CDX with AMP and ATP are 1.26 × 10^5 M^{-1} and 3.24 × 10^6 M^{-1}, respectively, whereas per-guanidino-β-CD with ADP or ATP form irreversible complexes due to the ionic/columbic interaction and salt bridge formation) (Hargrove

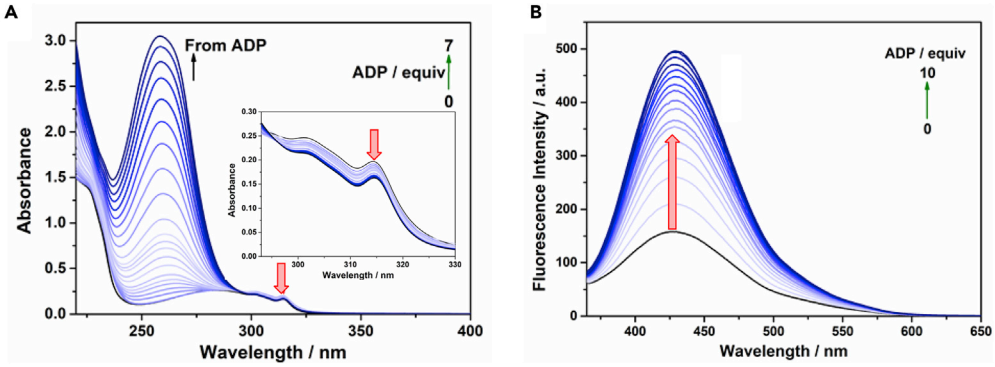

Figure 6. Absorption and Fluorescence Spectral Changes of Probe L1 towards ADP

(A) Absorption and (B) fluorescence spectral changes ($\lambda_{exc.}$ = 315 nm) of probe **L1** (37 μM) upon addition of ADP (0–10 equiv) in water at room temperature. Inset: Expansion of Figure 6A in the region of 293–330 nm.

et al., 2011; Eliseev and Schneider, 1993; Yuan et al., 2007). These results demonstrate that the sensing and binding response of probe **L1** with adenosine nucleotides differed based on the length of anionic phosphate esters attached to the hydrophobic adenine moiety. This response depends mainly on the coordinating ability of the phosphoric anion group to the metal ion and the nature of host:guest (H:G) interaction of the adenine moiety with the CDX cavity. The calculated k_a values of BCDX-QUI-2 with AMP, ADP, and ATP are 5.55 × 10^3, 443, and 308 M^{-1}, respectively (Table S1 and Figure S38), which are considerably less in comparison with the k_a values of probe **L1** with the same nucleotides (4.24 × 10^4, 4.78 × 10^4, and 5.15 × 10^4 M^{-1}, respectively; Table 1 and Figures S40–S42). This observation clearly indicates that the metal ion plays a key role in sensing and differentiating the binding response. It is interesting to find that the binding constants of nucleotides with **L1** are very much similar, despite their different charge in nucleotides in water. This is most probably due to the unique binding mode of **L1** with nucleotides, as only one phosphate group of nucleotides could bind the metal center of **L1**, whereas the hydrophobic part of the nucleotides that complexes with the CD cavity is exactly same.

Supramolecular Complex Stoichiometry

The stoichiometry of the supramolecular complexes are mainly found from the Job's method, which is a common method and powerful tool for the determination of the complex stoichiometry of an equilibria (Job, 1928). Job's plots based on absorption titrations suggest the formation of a 1:1 complex (Figure S43) between the probe **L1** and nucleotides AMP, ADP, or ATP.

NMR Studies

The origin behind the observed remarkable sensing and differentiating response of probe **L1** with the nucleotides was investigated by using ^{1}H NMR and ^{31}P NMR spectroscopy. Since the paramagnetic Cu(II) ion

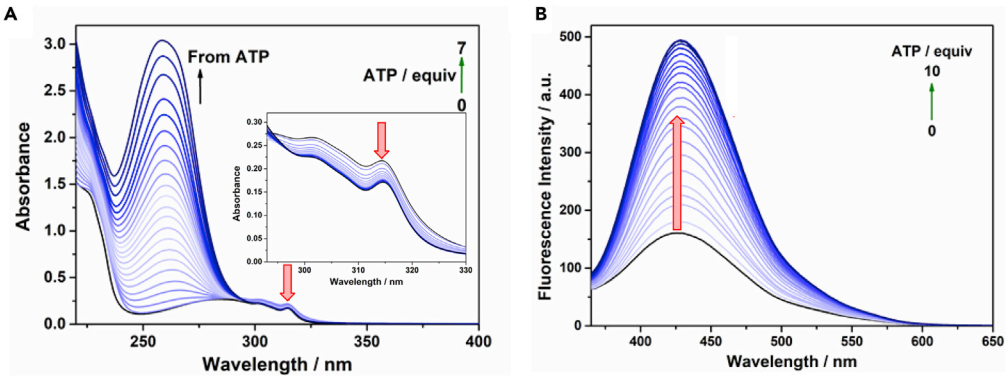

Figure 7. Absorption and Fluorescence Spectral Changes of Probe L1 towards ATP

(A) Absorption and (B) fluorescence spectral changes (λ_{exc} = 315 nm) of probe **L1** (37 μM) upon addition of ATP (0–10 equiv) in water at room temperature. Inset: Expansion of Figure 7A in the region of 293–330 nm.

Host	Guest	k_a/M^{-1}
Probe **L1**	AMP	4.24×10^4
Probe **L1**	ADP	4.78×10^4
Probe **L1**	ATP	5.15×10^4
Probe **L1**	Other anions[a]	–

Table 1. Association Constants (k_a) Determined for Probe L1 and Nucleotides in Aqueous Medium at Room Temperature

All of the nucleotides were added as sodium salts. k_a was determined by fitting the absorption change in the UV-vis titration spectra of probe **L1** upon addition of nucleotides.

[a]Other anions—not determined.

of **L1** is not suitable for the NMR studies, the analogous zinc complex **L1(Zn)** was used to examine the mode of binding of the formed complexes. It was found that the aromatic protons of quinoline are slightly shifted upfield and became broader upon sequential addition of AMP, ADP, and ATP. Additionally, the CDX protons (3.0–4.2 ppm) were completely broadened and also experienced a large upfield shift upon addition of the nucleotides (Figures S44–S46). This is due to the ring current effect from adenine aromatic ring strongly affecting the CDX protons. Upon complexation with AMP, the aromatic adenine signals of the included nucleotide base underwent upfield shifts. In the case of ADP complexation, signals for protons in the pyrimidine ring also showed an upfield shift, whereas signals from the imidazole ring experienced a downfield shift. For ATP complexation, the proton resonances of the aromatic adenine moiety were shifted downfield as a result of the interaction mode, in which the adenine moiety is located outside the CDX cavity and thus experienced the downfield shift. These observations clearly support the suggestion that the existence of significantly variable binding patterns of the adenine moiety and the involved H:G interactions between **L1(Zn)** and nucleotides are responsible for the differentiating and sensing response of probe **L1(Zn)** toward AMP, ADP, and ATP.

The ^{31}P NMR spectra of the complexes of the probe **L1(Zn)** with AMP, ADP, and ATP were recorded separately (Figure 8). It was revealed that the respective α-, β-, and γ-phosphorus atoms of AMP, ADP, and ATP (Scheme 1) showed different chemical shifts with respect to their distance from the metal center and the H:G interaction with the CDX cavity of **L1(Zn)**. In the case of AMP bound to **L1(Zn)**, there is a relatively large upfield shift ($\Delta\delta$ = +2.046 ppm) of the α-P signal from −3.819 to −1.773 ppm, indicating that the phosphate group strongly coordinates to the metal ion. On the other hand, the P signals of ADP (two signals) and ATP (three signals) show downfield shifts upon binding to **L1(Zn)**, which varied in extent with respect to the binding of terminal phosphate group to the Zn cation (Figure 8). For ADP, the α-P and β-P signals experienced a downfield shift ($\Delta\delta$ = −0.526 and −1.373 ppm, respectively). For both ADP and ATP, the shift of α-P resonance was relatively smaller than that of β-P resonance, hence indicating that the β-P atom of ADP strongly interacts with the Zn ion. Similarly, the α-, β-, and γ-P signals of ATP show downfield shifts ($\Delta\delta$ = −0.343, −2.956, and −3.478 ppm, respectively) upon complexation with the probe **L1(Zn)**, also suggesting that the γ-P atom of ATP strongly interacts with the metal center. These observations indicate that only the more negatively charged terminal phosphate groups (owing to the presence of two negative charges) play a key role in binding to the Zn ion. On the basis of literature data (Eliseev and Schneider, 1993, 1994; Schwinte et al., 1998; Vizitiu and Thatcher, 1999; Cotner and Smith, 1998; Hauser et al., 2000; Mourtzis et al., 2007; Yuan et al., 2007; Aggelidou et al., 2009; Yang et al., 2015; Formoso, 1973, 1974; Zhong et al., 2009; Ngo et al., 2012) and the observed results, the following differentiating models for binding of **L1** to AMP, ADP, and ATP can be illustrated schematically, as demonstrated in Scheme 3.

Importance of the CDX Cavity and Its Size

The observed differential binding responses between **L1** and the three different nucleotides, such as absorption changes, blue-shifted fluorescence quenching by AMP (Figure 5), hypochromic effects in absorption, and enhanced fluorescence emission at 427 nm by ADP and ATP (Figures 6 and 7), unambiguously indicate that the cavity of the β-CDX group in **L1** plays a crucial role in this structural selectivity. To rationalize this result, a reference molecule without the CDX cavity (Bu-QUI-2) was synthesized (Schemes 2 and S4) and its Cu(II) complex (**L4**) was used to study the corresponding sensing and differentiating response. These control experiments were carried out in the presence and absence of native

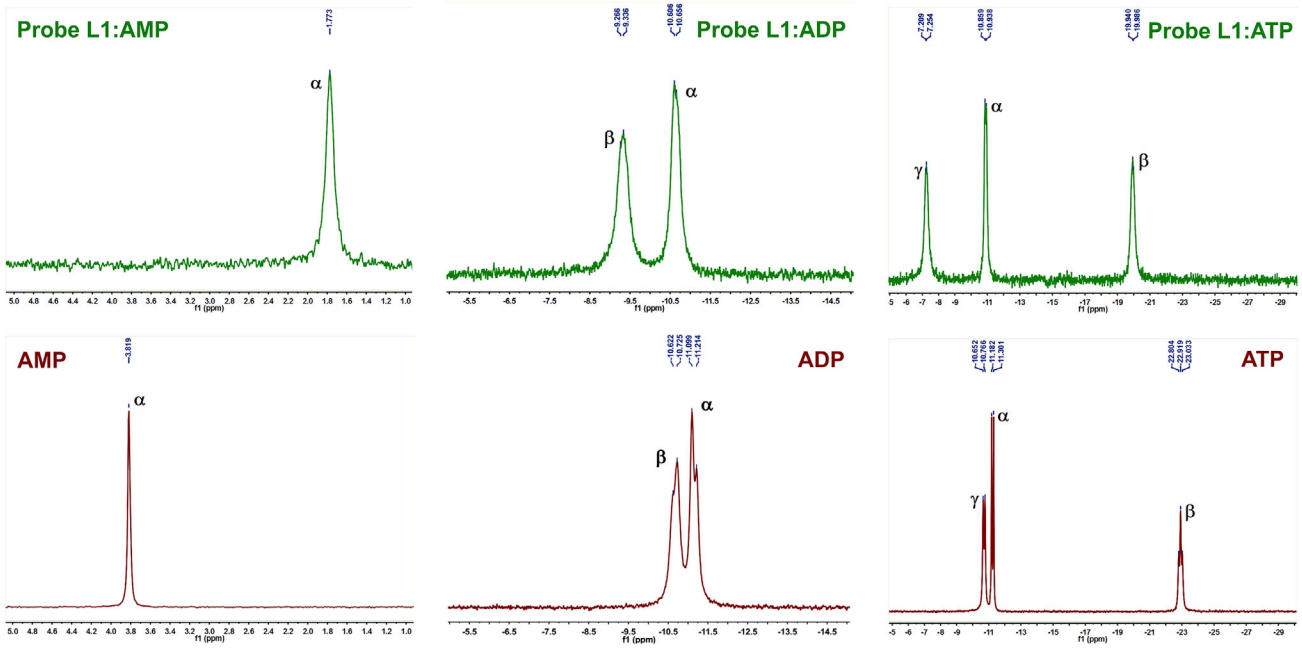

Figure 8. ^{31}P NMR Spectra of Nucleotides and its Complexes with Probe L1(Zn)

^{31}P NMR spectra of AMP, ADP, and ATP (lower panel) and its complexes with the probe **L1(Zn)** (upper panel)

(non-modified) β-CDX serving as an external host cavity. Upon addition of the nucleotides to an aqueous solution of **L4**, we found a negligible variation in the absorption spectra (Figure S48), both with and without β-CDX (Figure S49). This result indicates a synergistic contribution between the hydrophobic cavity of β-CDX and the covalently linked bis-quinoline moiety in **L1** toward generating the differentiating binding pattern and spectral response of the molecular probe. Additionally, control experiments with the complex between **L1** and the strongly binding guest molecule 1-adamantanecarboxylic acid (1-AdCA) (Chen et al., 2007) were carried out so as to validate the importance of β-CDX cavity in the probe **L1** for efficient binding of nucleotides. The **L1**:1-AdAC complex was titrated against nucleotides and showed no discernible spectral change (Figure S50). This result demonstrates that the strongly bound 1-AdCA effectively blocks access of the nucleotide to the CDX cavity, hence preventing the corresponding nucleotide binding.

In order to examine the effect of cavity size on the differential binding behavior of probe **L1** to nucleotides, we repeated the nucleotide binding studies with α-CDX-based **L2** and γ-CDX-derived probe **L3**, which possess smaller and larger cavity sizes, respectively, in comparison with **L1** (Figures 9 and S47). The titration of **L2** with the corresponding nucleotides showed an insignificant change in the absorption spectra and a small enhancement of the fluorescence emission upon addition of AMP, ADP, or ATP (Figures 9 and S47). Similar titration studies were also carried out with **L3** showing even less variation in the absorption spectra and relatively small changes in the fluorescence spectra (Figures 9 and S47). These results demonstrate the requirements of the CDX cavity for effective nucleotide binding, which in turn depends upon the size of the cavity acting as a portal for the sensing and differentiating response.

Theoretical Studies

The proposed differential binding mechanism is strongly supported by corresponding theoretical calculations. On the basis of these experimental results and in accordance with the literature data (Eliseev and Schneider, 1993, 1994; Schwinte et al., 1998; Vizitiu and Thatcher, 1999; Cotner and Smith, 1998; Hauser et al., 2000; Mourtzis et al., 2007; Yuan et al., 2007; Aggelidou et al., 2009; Yang et al., 2015; Formoso, 1973, 1974; Fujita et al., 2017; Yamada et al., 2018; Kim et al., 2009; Kim and Quang, 2007; Santis et al., 1995; de Silva et al., 2009; Guo et al., 2016; Wang et al., 2017; Butler, 2014; Hewitt et al., 2017; Wongkongkatep et al., 2017), the sensor probe **L1** and the corresponding nucleotide complexes (**L1**:AMP/ADP/ATP) were examined by density functional theory (DFT) and time-dependent density functional theory (TD-DFT) calculations at the B3LYP/6-31G(d) level by using the Gaussian 09 program (Figures 10, S51, and S52) (Frisch

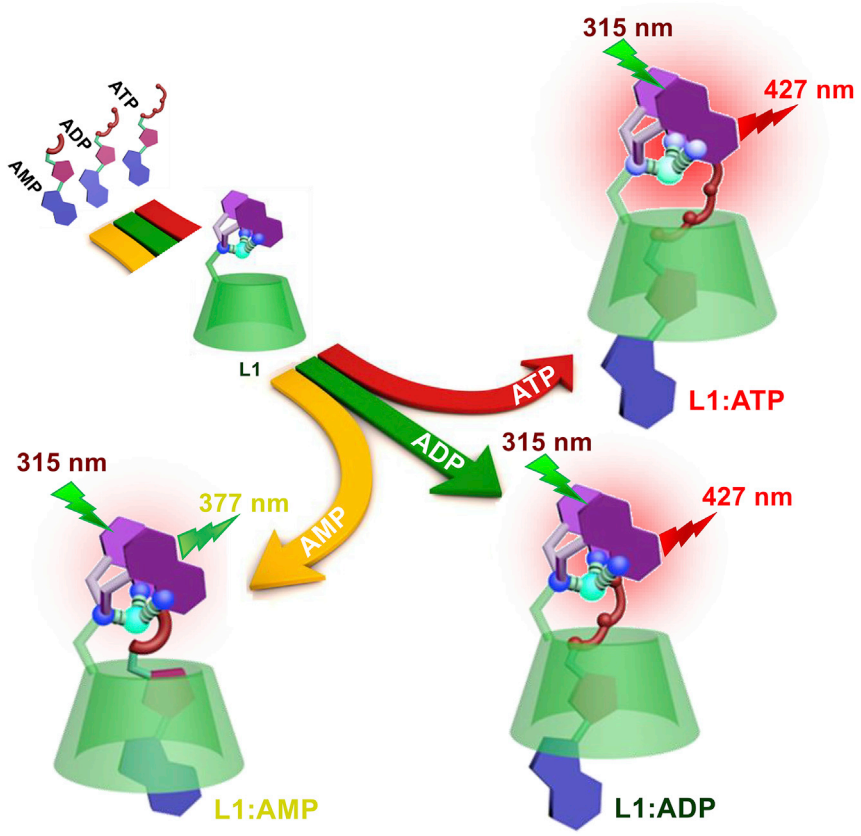

Scheme 3. Proposed Sense and Differentiating Mechanism
Proposed sense and differentiating binding patterns of **L1** with AMP, ADP, and ATP in water.

et al., 2010). For BCDX-QUI-2, both the highest occupied molecular orbital (HOMO) and lowest unoccupied molecular orbital (LUMO) are distributed on the tethered *N*-bis-8-methylamino part and quinolyl scaffolds, respectively, with an energy difference (ΔE) of 4.93 eV that decreased down to 4.60 eV upon coordination with Cu^{2+} in the probe **L1**. For comparison, the HOMO and LUMO of AMP, ADP, and ATP are located at the adenine moiety with ΔE values decreasing in the following order: 5.43, 5.42, and 5.35 eV,

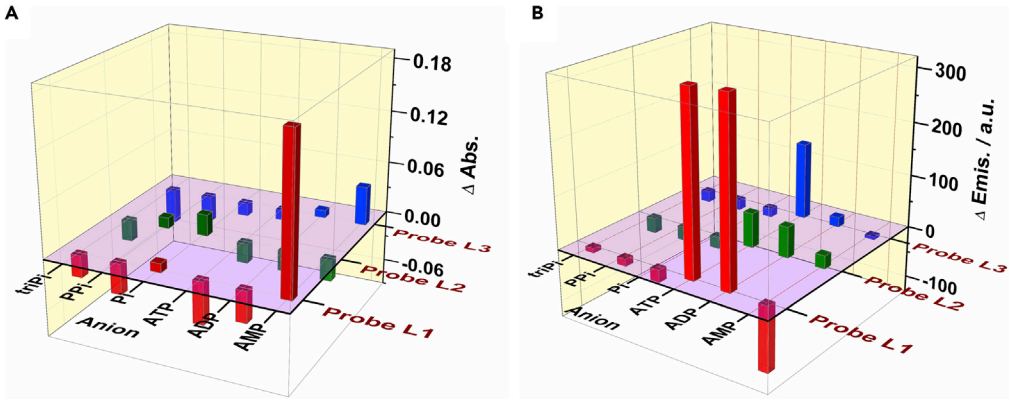

Figure 9. Absorption and Fluorescence Spectral Changes of Probe L1-L3 upon Binding with Analytes
Comparison of (A) absorption (ΔAbs.) and (B) fluorescence spectral changes (ΔEmis.; $\lambda_{exc.}$ = 315 nm) of probe **L1-3** upon addition of nucleotides (AMP, ADP, and ATP) and inorganic phosphates in aqueous medium at room temperature.

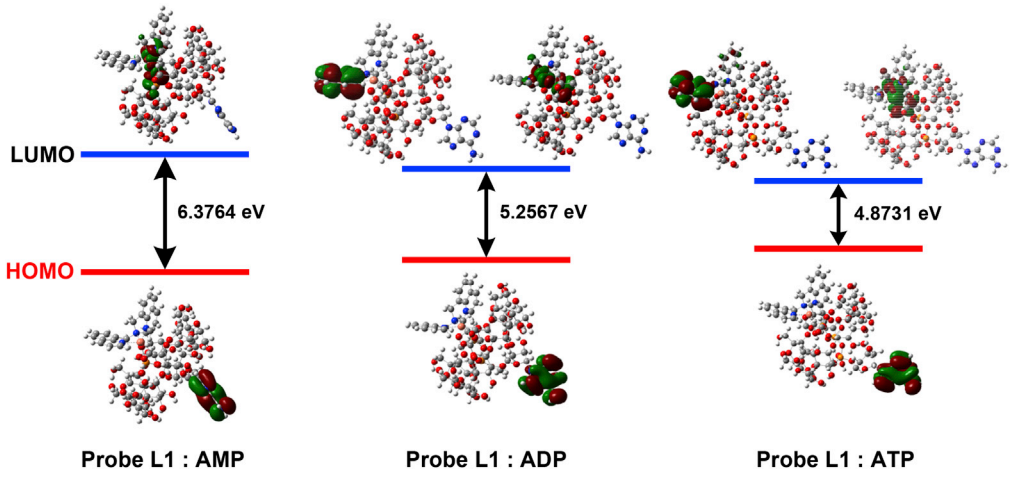

Figure 10. DFT Study of Probe L1: nucleotide Complexes

DFT optimized structures, HOMO-LUMO energy levels, and interfacial plots of the orbitals for the three proposed **L1**:nucleotide complexes

respectively, which correlate with increasing the number of phosphate groups. For gaining more insights into the binding pattern between the probe **L1** and these three nucleotides, the corresponding calculations were performed separately with the results shown in Figure 10.

The energy minimized structures of the complexes were acquired from the design strategy and the experimental results discussed above via the coordination of the terminal phosphate group of the nucleotide to the metal ion of **L1**. The calculated ΔE values of the **L1**:AMP/ADP/ATP complexes (6.3764, 5.2567, and 4.8731 eV, respectively) decreased considerably upon the increases in the number of phosphate groups in the nucleotides. Furthermore, the HOMO electron clouds of these complexes were only distributed on the adenine moiety, whereas the LUMO electron cloud distributions varied with the differential binding patterns of the different nucleotides with the probe **L1**. The LUMO level electron clouds for the complex **L1**:AMP is distributed on the *N*-bis-8-methylamino part only, whereas for the **L1**:ADP/ATP complexes, the LUMO electron clouds distributed on both the *N*-bis-8-methylamino part and quinoline scaffolds. This indicates a good match between the molecular size of AMP and probe **L1**, hence allowing the adenine base moiety in AMP to occupy the hydrophobic cavity region of *β*-CDX via corresponding non-covalent interactions (k_a = 4.24 × 10^4 M^{-1}). In turn, the CDX walls restrict the electron density shift process from the adenine moiety to the quinoline chromophore, which is consistent with the observed results (quenched fluorescence emission, enhanced absorption maxima at 303 and 315 nm, and new long wavelength absorption band at >325 nm with blue coloration upon addition of AMP to the probe **L1**). Binding of the terminal phosphate groups of ADP and ATP to the metal center of probe **L1** forces the adenine chromophore to sit outside of the CDX cavity, which simultaneously allows the electron density to be shifted from the adenine moiety to both the *N*-bis-8-methylamino part and the quinolyl chromophore. This shift in electron density also is consistent with the obtained experimental data (enhanced fluorescence emission, small hypochromic effect in the absorption maxima at 303 and 315 nm, and no optical color change upon addition of ADP or ATP to the probe **L1**). In addition, the TD-DFT ground and excited state calculations of **L1** and its nucleotide complexes provide the corresponding simulated absorption (303 and 315 nm) and emission (for AMP and ADP/ATP, 377 and 427 nm, respectively) bands, which are in full agreement with the experimentally observed results. Therefore, the present study establishes an effective design strategy for the differentiation of nucleotides by using the probe **L1**.

Enzyme and Stimuli Responsive *In Situ* Monitoring of Optical Signaling, Enzymatic ATP Hydrolysis, and AMP Phosphorylation

As nucleotides play a vital role in most fundamental biological reactions catalyzed by enzymes (Schlattner et al., 2006; Zimmermann, 1999; Chen and Urban, 2016), monitoring such enzymatic activity in real time has a significant practical importance to biological and medical science. Thus, on the basis of the established differentiating ability of the probe **L1** toward AMP, ATP, and ADP, a real-time monitoring of the enzymatic

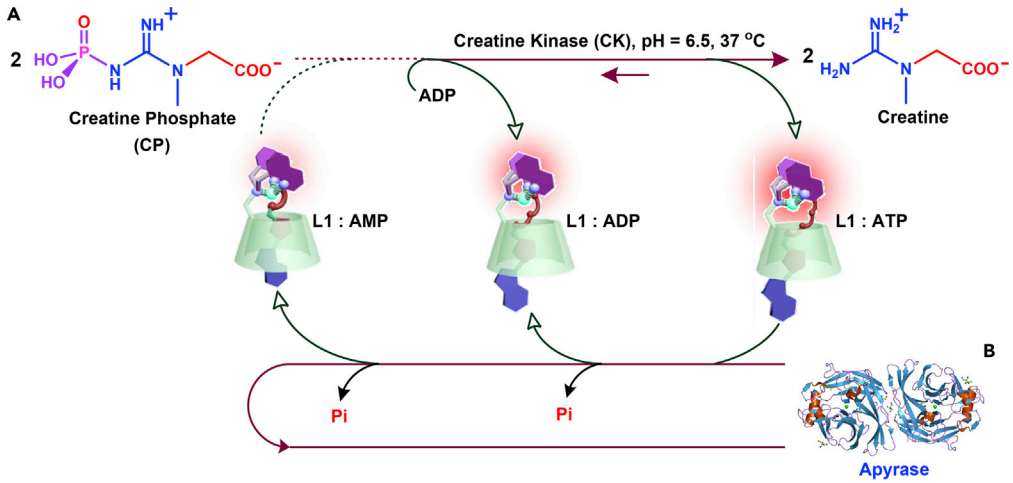

Scheme 4. Schematic Representation of Enzyme Catalyzed AMP/ADP Phosphorylation and ATP/ADP Hydrolysis Process

Two enzymatic reactions involving adenosine nucleotides and their products detected by using the differentiating probe **L1**, (A) creatine kinase (CK)-catalyzed phosphorylation of AMP and/or ADP using creatine phosphate (CP) to produce ATP and creatine, (B) hydrolytic enzyme apyrase-catalyzed dephosphorylation of ATP → ADP → AMP and Pi.

activity of the enzymes creatine kinase (CK, AMP/ADP → ATP) and apyrase (ATP → ADP → AMP) was tested (Scheme 4) (Kumar et al., 2012, 2014a, 2014b; Schlattner et al., 2006; Zimmermann, 1999; Chen and Urban, 2016).

The enzyme-catalyzed phosphorylation and dephosphorylation reactions were carried out with and without the probe **L1** and monitored by two different methods (Phosphorylation Method I/II (PM-I/II) and Dephosphorylation Method I/II (dPM-I/II); see Transparent Methods section in Supplemental Information and Figure S53). In both methods, under the catalysis by CK, ADP phosphorylated with creatine phosphate (CP) to produce ATP and creatine, and the fluorescence intensity of the probe **L1** thus increased over time due to the formation of the **L1**: ATP complex (Figures 11A and 11B). CK-catalyzed AMP phosphorylation with CP is comparatively less feasible in comparison with ADP (Figures S54 and S55 in SI). The fluorescence spectra of **L1** in the presence of substrate (ADP + CP) and product (ATP + creatine) were measured in water (Figure 11A). The observed fluorescence enhancements over time during the CK catalysis are in good agreement with the separate fluorescence measurements of **L1** in the presence of substrate and product. Similarly, the hydrolytic apyrase enzyme catalyzed the dephosphorylation of ATP and ADP and the reaction was also followed by monitoring the fluorescence of dissolved **L1** at different time intervals. Such studies showed a corresponding fluorescence quenching over time (Figures 11D and S57). The obtained results are comparable with the fluorescence emissions of **L1**:AMP/ADP/ATP and Pi complexes (Figures 11C and S56). In both cases, the fluorescence kinetic data indicate that the enzymatic conversion reaction rates of ADP → ATP and ATP → → AMP were accelerated upon increasing the relative concentration of the enzymes CK or apyrase, respectively (Figures 11B and 11D). The real-time monitoring of the enzymatic activity of apyrase (ATP → ADP → AMP and Pi) also was verified by ^{31}P NMR spectroscopy measurements at different time intervals with EDTA as a catalyst quencher (Figure S58). The observed ^{31}P NMR spectral peaks of a reaction mixture containing the probe **L1(Zn)**:ATP + apyrase revealed the ratio of hydrolyzed products (ADP and AMP) at different time intervals.

Conclusions

Herein, we designed and synthesized a series of *bis*-8-methylquinolyl chromophore-tethered CDX derivatives and studied their conformations in different solvents. The corresponding metal complexes **L1–L3** were utilized as efficient sensing and discriminating probes for nucleotide phosphates. *β*-CDX-based probe **L1** was found to serve as a specific supramolecular colorimetric (visible) and fluorescent sensor for discriminating between structurally similar nucleotide phosphates and their related inorganic phosphates in aqueous media. The present study establishes the obvious need of the CDX cavity for nucleotide binding,

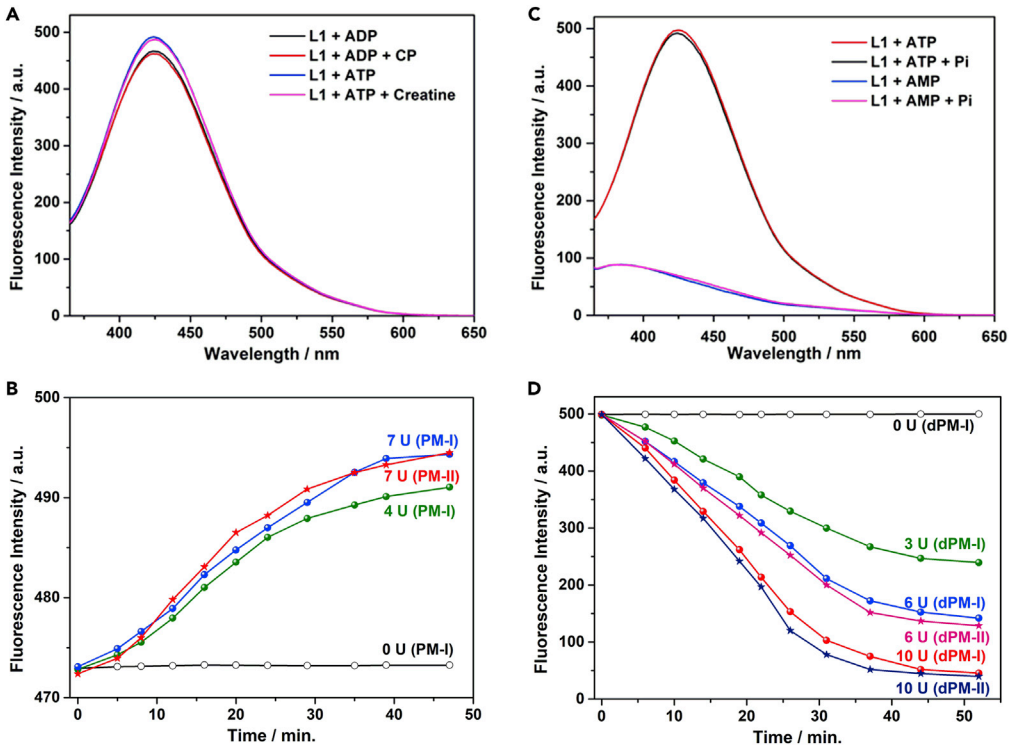

Figure 11. Results of Enzyme Catalyzed ADP Phosphorylation and ATP Hydrolysis

(A) Fluorescence spectra of the solution of **L1** (37 μM) + ATP or ADP (10 equiv), **L1** (37 μM) + ATP (10 equiv) + CP (10 equiv), and **L1** (37 μM) + ADP (8 equiv) + creatine (10 equiv) in water.

(B) Time-trace plots of CK-catalyzed ADP phosphorylation monitored by emission intensity at 427 nm in two different methods PM-I and PM-II, [ADP] = 300 μM, [CP] = 10 equiv, [CK] = 0, 4, and 7 units, MES buffer (10 mM, pH = 6.5) at 37°C (λ_{exc} = 315 nm, slit: 5 nm/5 nm).

(C) Fluorescence spectra of the solution of **L1** (37 μM) + ATP or AMP (10 equiv), **L1** (37 μM) + ATP (10 equiv) + Pi (10 equiv), and **L1** (37 μM) + AMP (10 equiv) + Pi (10 equiv) in water.

(D) Time-trace plots of apyrase-catalyzed ATP dephosphorylation monitored by emission intensity at 427 nm in two different methods PM-I and PM-II, [ATP] = 370 μM, [apyrase] = 0, 3, 6 and 10 units, HEPES buffer solution (10 mM, pH = 7.4) at 37°C (λ_{exc} = 315 nm, slit: 5 nm/5 nm).

which in turn depends on the specific cavity size for providing the interaction portals for the corresponding sensing and differentiating response. A mechanism for the signaling and nucleotide differentiation was established from control experiments and theoretical (DFT and TD-DFT) studies. The present sensor also can be applied efficiently for the fluorescent real-time monitoring of nucleotide phosphorylation and dephosphorylation processes catalyzed by enzymes such as creatine kinase and apyrase, respectively. This supramolecular probe-based sensing/differentiating approach and the real-time monitoring of the enzyme-catalyzed phosphorylation/dephosphorylation processes of nucleotides might open up new avenues for many interdisciplinary researchers; this present research results will also be expandable to the detection of other nucleotides and *in vivo* monitoring applications.

Limitations of the Study

The real-time monitoring of biological processes via fluorescent and colorimetric changes in this study was achieved *in vitro*; the enzyme-catalyzed phosphorylation and dephosphorylation reactions are surely more complicated *in vivo* and deserve further investigation but was limited by the present experimental conditions.

METHODS

All methods can be found in the accompanying Transparent Methods supplemental file.

SUPPLEMENTAL INFORMATION

Supplemental Information can be found online at https://doi.org/10.1016/j.isci.2020.100927.

ACKNOWLEDGMENTS

The authors gratefully acknowledge the financial assistance from the National Natural Science Foundation of China (No. 21871194, 21971169, 21572142, 21402129), National Key Research and Development Program of China (No. 2017YFA0505903), and Science and Technology Department of Sichuan Province (2019YJ0160, 2019YJ0090, and 2017SZ0021). V.B. acknowledges the start-up research grant (YZZ16005) from South-Central University for Nationalities. Comprehensive Training Platform of Specialized Laboratory, College of Chemistry, Prof. Peng Wu of Analytical &Testing Center, Sichuan University for characterization and photophysical properties measurement and Ms Jiao Lu, National Engineering Research Center for Biomaterials, Sichuan University for MALDI-TOF-MS measurement are greatly appreciated.

AUTHOR CONTRIBUTIONS

K.K., C.X., M.R., and C.F. carried out the experiment and analyzed the data; K.K. wrote the manuscript; G.C., D.Z., Z.Z., D.S., X.Y., J.Y., T.H., and J.J.C. analyzed the data and modified the manuscript; and V.B., W.W., and C.Y. conceived of the present idea and modified the manuscript.

DECLARATION OF INTERESTS

The authors declare no competing interests.

Received: December 23, 2019
Revised: January 18, 2020
Accepted: February 13, 2020
Published: March 27, 2020

REFERENCES

Agafontsev, A.M., Ravi, A., Shumilova, T.A., Oshchepkov, A.S., and Kataev, E.A. (2019). Molecular receptors for recognition and sensing of nucleotides. Chemistry *25*, 2684–2694.

Aggelidou, C., Mavridis, I.M., and Yannakopoulou, K. (2009). Binding of nucleotides and nucleosides to per(6-guanidino-6-deoxy) cyclodextrins in solution. Eur. J. Org. Chem. *2009*, 2299–2305.

Berg, J.M., Tymoczko, J.L., and Stryer, L. (2002). Biochemistry (W.H. Freeman and company).

Busschaert, N., Caltagirone, C., Rossom, W.V., and Gale, P.A. (2015). Applications of supramolecular anion recognition. Chem. Rev. *115*, 8038–8155.

Butler, S.J. (2014). Ratiometric detection of adenosine triphosphate (ATP) in water and real-time monitoring of apyrase activity with a tripodal zinc complex. Chemistry *20*, 15768–15774.

Cacciapaglia, R., Di Stefano, S., and Mandolini, L. (2004). Effective molarities in supramolecular catalysis of two-substrate reactions. Acc. Chem. Res. *37*, 113–122.

Cai, Y., Meng, X., Wang, S., Zhu, M., Pan, Z., and Guo, Q.X. (2013). A quinoline based fluorescent probe that can distinguish zinc(II) from cadmium(II) in water. Tetrahedron Lett. *54*, 1125–1128.

Canary, J.W., Allen, C.S., Castagnetto, J.M., Chiu, Y.-H., Toscano, P.J., and Wang, Y. (1998). Solid state and solution characterization of chiral, conformationally mobile tripodal ligands. Inorg. Chem. *37*, 6255–6262.

Cheng, Y., and Dong, X. (2016). Preparation of a molecularly imprinted fluorescent chemosensor using quinoline modified vinyl-β-cyclodextrin and acrylamide as monomers for the selective recognition of spermidine. Anal. Methods *8*, 5838–5842.

Chen, T.-R., and Urban, P.L. (2016). Mass spectrometry-guided refinement of chemical energy buffers. Proc. R. Soc. A. *472*, 20150812.

Chen, Y., Han, K.-Y., and Liu, Y. (2007). Effective switch-on fluorescence sensing of zinc(II) ion by 8-aminoquinolino-β-cyclodextrin/adamantaneacetic acid system in water. Bioorg. Med. Chem. *15*, 4537–4542.

Cheng, Y., Jiang, P., and Dong, X. (2015). Molecularly imprinted fluorescent chemosensor synthesized using quinoline-modified-β-cyclodextrin as monomer for spermidine recognition. RSC Adv. *5*, 55066–55074.

Cotner, E.S., and Smith, P.J. (1998). Phosphotyrosine binding by ammonium- and guanidinium-modified cyclodextrins. J. Org. Chem. *63*, 1737–1739.

Das, S., Sarkar, H.S., Uddin, M.R., Rissanen, K., Mandal, S., and Sahoo, P. (2017). Differential detection and quantification of cyclic AMP and other adenosine phosphates in live cells. Chem. Commun. (Camb.) *53*, 7600–7603.

de Silva, A.P., Moody, T.S., and Wright, G.D. (2009). Fluorescent PET (Photoinduced Electron Transfer) sensors as potent analytical tools. Analyst *134*, 2385–2393.

Eliseev, A.V., and Schneider, H.J. (1993). Aminocyclodextrins as selective hosts with several binding sites for nucleotides. Angew. Chem. Int. Ed. *32*, 1331–1333.

Eliseev, A.V., and Schneider, H.J. (1994). Molecular recognition of nucleotides, nucleosides, and sugars by aminocyclodextrins. J. Am. Chem. Soc. *116*, 6081–6088.

Formoso, C. (1973). The interaction of β-cyclodextrin with nucleic acid monomer units. Biochem. Biophys. Res. Commun. *50*, 999–1005.

Formoso, C. (1974). The interaction of β-cyclodextrin with dinucleoside phosphates. Biopolymers *13*, 909–917.

Frisch, M.J., Trucks, G.W., Schlegel, H.B., Scuseria, G.E., Robb, M.A., Cheeseman, J.R., Scalmani, G., Barone, V., Mennucci, B., Petersson, G.A., et al. (2010). Gaussian 09 (Gaussian, Inc.).

Fujita, K., Fujiwara, S., Yamada, T., Tsuchido, Y., Hashimoto, T., and Hayashita, T. (2017). Design and function of supramolecular recognition systems based on guest-targeting probe-modified cyclodextrin receptors for ATP. J. Org. Chem. *82*, 976–981.

Guo, A., Zhu, R., Ren, Y., Dong, J., and Feng, L. (2016). A "turn-on" fluorescent chemosensor for aluminum ion and cell imaging application.

Spectrochim. Acta A Mol. Biomol. Spectrosc. *153*, 530–534.

García-Espana, E., Belda, R., Gonzalez, J., Pitarch, J., and Bianchi, A. (2012). Receptors for nucleotides. In Supramolecular Chemistry: From Molecules to Nanomaterials, P.A. Gale and J.W. Steed, eds. (Wiley-VCH), pp. 1225–1257.

Harata, K., and Uedaira, H. (1975). The circular dichroism spectra of the β-cyclodextrin complex with naphthalene derivatives. Bull. Chem. Soc. Jpn. *48*, 375–378.

Harada, N., and Nakanishi, K. (1972). The exciton chirality method and its application to configurational and conformational studies of natural products. Acc. Chem. Res. *5*, 257–263.

Hapiot, F., Bricout, H., Tilloy, S., and Monflier, E. (2012). Functionalized cyclodextrins as first and second coordination sphere ligands for aqueous organometallic catalysis. Eur. J. Inorg. Chem. *10*, 1571–1578.

Hargrove, A.E., Nieto, S., Zhang, T., Sessler, J.L., and Anslyn, E.V. (2011). Artificial receptors for the recognition of phosphorylated molecules. Chem. Rev. *111*, 6603–6782.

Hauser, S.L., Johanson, E.W., Green, H.P., and Smith, P.J. (2000). Aryl phosphate complexation by cationic cyclodextrins. an enthalpic advantage for guanidinium over ammonium and unusual enthalpy-entropy compensation. Org. Lett. *2*, 3575–3578.

Hembury, G.A., Borovkov, V.V., and Inoue, Y. (2008). Chirality-sensing supramolecular systems. Chem. Rev. *108*, 1–73.

Hewitt, S.H., Parris, J., Mailhot, R., and Butler, S.J. (2017). A continuous luminescence assay for monitoring kinase activity: signaling the ADP/ATP ratio using a discrete europium complex. Chem. Commun. (Camb.) *53*, 12626–12629.

Huang, F., Hao, G., Wu, F., and Feng, G. (2015). Fluorescence sensing of ADP over ATP and PPi in 100% aqueous solution. Analyst *140*, 5873–5876.

Huergo, L.F., Chandra, G., and Merrick, M. (2013). P(II) signal transduction proteins: nitrogen regulation and beyond. FEMS Microbiol. Rev. *37*, 251–283.

Jiang, P., and Ninfa, A.J. (2007). Escherichia coli PII signal transduction protein controlling Nitrogen assimilation acts as a sensor of adenylate energy charge in vitro. Biochemistry *46*, 12979–12996.

Job, P. (1928). Formation and stability of inorganic complexes in solution. Ann. Chim. *9*, 1130–1203.

Jose, D.A., Mishra, S., Ghosh, A., Shrivastav, A., Mishra, S.K., and Das, A. (2007). Colorimetric sensor for ATP in aqueous solution. Org. Lett. *9*, 1979–1982.

Kajtar, M., Horvath-Toro, C., Kuthi, E., and Szejtli, J. (1982). A simple rule for predicting circular dichroism induced in aromatic guests by cyclodextrin hosts in inclusion complexes. Acta Chim. Acad. Sci. Hung. *110*, 327–355.

Kim, J.S., and Quang, D.T. (2007). Calixarene-derived fluorescent probes. Chem. Rev. *107*, 3780–3799.

Kim, M.J., Swamy, K.M.K., Lee, K.M., Jagdale, A.R., Kim, Y., Kim, S.J., Yoo, K.H., and Yoon, J. (2009). Pyrophosphate selective fluorescent chemosensors based on coumarin-DPA-Cu(II) complexes. Chem. Commun. (Camb.), 7215–7217.

Kirby, A.J. (1996). Enzyme mechanisms, models, and mimics. Angew. Chem. Int. Ed. *35*, 706–724.

Kodaka, M. (1993). A general rule for circular dichroism induced by a chiral macrocycle. J. Am. Chem. Soc. *115*, 3702–3705.

Knowles, J.R. (1980). Enzyme-catalyzed phosphoryl transfer reactions. Annu. Rev. Biochem. *49*, 877–919.

Kumar, M., Jonnalagadda, N., and George, S.J. (2012). Molecular recognition driven self-assembly and chiral induction in naphthalene diimide amphiphiles. Chem. Commun. (Camb.) *48*, 10948–10950.

Kumar, A., Prasher, P., and Singh, P. (2014a). A fluorescent probe for estimation of adenosine diphosphate and monitoring of glucose metabolism. Org. Biomol. Chem. *12*, 3071–3079.

Kumar, M., Brocorens, P., Tonnele, C., Beljonne, D., Surin, M., and George, S.J. (2014b). A dynamic supramolecular polymer with stimuli-responsive handedness for in situ probing of enzymatic ATP hydrolysis. Nat. Commun. *5*, 5793.

Li, C., Numata, M., Takeuchi, M., and Shinkai, S. (2005). A sensitive colorimetric and fluorescent probe based on a polythiophene derivative for the detection of ATP. Angew. Chem. Int. Ed. *44*, 6371–6374.

Li, N., Chen, Y., Zhang, Y.-M., Wang, L.-H., Mao, W.-Z., and Liu, Y. (2014). Molecular binding thermodynamics of spherical guests by β-cyclodextrins bearing aromatic substituents. Thermochim. Acta *576*, 18–26.

Liu, Y., and Bonizzoni, M. (2014). A supramolecular sensing array for qualitative and quantitative analysis of organophosphates in water. J. Am. Chem. Soc. *136*, 14223–14229.

Liu, Y., Song, Y., Wang, H., Zhang, H.-Y., Wada, T., and Inoue, Y. (2003). Selective binding of steroids by 2,2′-biquinoline-4,4′-dicarboxamide-bridged bis(β-cyclodextrin): fluorescence enhancement by guest inclusion. J. Org. Chem. *68*, 3687–3690.

Liu, Y., Song, Y., Chen, Y., Li, X.-Q., Ding, F., and Zhong, R.-Q. (2004). Biquinolin-modified β-cyclodextrin dimers and their metal complexes as efficient fluorescent sensors for the molecular recognition of steroids. Chemistry *10*, 3685–3696.

Liu, Y., Shi, J., and Guo, D.-S. (2007a). Novel permethylated β-cyclodextrin derivatives appended with chromophores as efficient fluorescent sensors for the molecular recognition of bile salts. J. Org. Chem. *72*, 8227–8234.

Liu, Y., Zhang, N., Chen, Y., and Wang, L.-H. (2007b). Fluorescence sensing and binding behavior of aminobenzenesulfonamidoquinolino-β-cyclodextrin to Zn^{2+}. Org. Lett. *9*, 315–318.

Liu, Y., Yu, M., Chen, Y., and Zhang, N. (2009). Convenient and highly effective fluorescence sensing for Hg^{2+} in aqueous solution and thin film. Bioorg. Med. Chem. *17*, 3887–3891.

Martinez-Manez, R., and Sancenon, F. (2003). Fluorogenic and chromogenic chemosensors and reagents for anions. Chem. Rev. *103*, 4419–4476.

McCleskey, S.C., Griffin, M.J., Schneider, S.E., McDevitt, J.T., and Anslyn, E.V. (2003). Differential receptors create patterns diagnostic for ATP and GTP. J. Am. Chem. Soc. *125*, 1114–1115.

Meng, X., Wang, S., and Zhu, M. (2012). Quinoline-based fluorescence sensors. In Molecular Photochemistry - Various Aspects, S. Saha, ed. (IntechOpen Limited), pp. 3–22.

Mikata, Y., Takekoshi, A., Kaneda, M., Konno, H., Yasuda, K., Aoyama, M., and Tamotsu, S. (2017). Replacement of quinolines with isoquinolines affords target metal ion switching from Zn^{2+} to Cd^{2+} in the fluorescent sensor TQLN (N, N,N′,N′-tetrakis(2-quinolylmethyl)-2,6-bis(aminomethyl) pyridine). Dalton Trans. *46*, 632–637.

Molina, P., Zapata, F., and Caballero, A. (2017). Anion recognition strategies based on combined noncovalent interactions. Chem. Rev. *117*, 9907–9972.

Mourtzis, N., Eliadou, K., Aggelidou, C., Sophianopoulou, V., Mavridis, I.M., and Yannakopoulou, K. (2007). Per(6-guanidino-6-deoxy)cyclodextrins: synthesis, characterisation and binding behaviour toward selected small molecules and DNA. Org. Biomol. Chem. *5*, 125–131.

Ngo, H.T., Liu, X., and Jolliffe, K.A. (2012). Anion recognition and sensing with Zn(II)-dipicolylamine complexes. Chem. Soc. Rev. *41*, 4928–4965.

Ogoshi, T., and Harada, A. (2008). Chemical sensors based on cyclodextrin derivatives. Sensors *8*, 4961–4982.

Ojida, A., Miyahara, Y., Wongkongkatep, J., Tamaru, S.-I., Sada, K., and Hamachi, I. (2006). Design of dual-emission chemosensors for ratiometric detection of ATP derivatives. Chem. Asian J. *1*, 555–563.

O'Neil, E.J., and Smith, B.D. (2006). Anion recognition using dimetallic coordination complexes. Coord. Chem. Rev. *250*, 3068–3080.

Pramanik, A., and Das, G. (2009). An efficient phosphate sensor: tripodal quinoline excimer transduction. Tetrahedron *65*, 2196–2200.

Ramaiah, D., Neelakandan, P.P., Nair, A.K., and Avirah, R.R. (2010). Functional cyclophanes: promising hosts for optical biomolecular recognition. Chem. Soc. Rev. *39*, 4158–4168.

Rekharsky, M.V., and Inoue, Y. (1998). Complexation thermodynamics of cyclodextrins. Chem. Rev. *98*, 1875–1918.

Ringe, D., and Petsko, G.A. (2008). How enzymes work. Science *320*, 1428–1429.

Sancenon, F., Descalzo, A.B., Martinez-Manez, R., Miranda, M.A., and Soto, J. (2001). A colorimetric

ATP sensor based on 1,3,5-Triarylpent-2-en-1,5-diones. Angew. Chem. Int. Ed. *40*, 2640–2643.

Santis, G.D., Fabbrizzi, L., Licchelli, M., Mangano, C., and Sacchi, D. (1995). Redox switching of anthracene fluorescence through the CuII/CuI couple. Inorg. Chem. *34*, 3581–3582.

Schlattner, U., Tokarska-Schlattner, M., and Wallimann, T. (2006). Mitochondrial creatine kinase in human health and disease. Biochim. Biophys. Acta *1762*, 164–180.

Schwinte, P., Darcy, R., and O'Keeffe, F. (1998). Ditopic binding of nucleotides by heptakis(6-hydroxyethylamino-6-deoxy)-β-cyclodextrin. J. Chem. Soc. Perkin Trans. *2*, 805–808.

Shi, L., Hu, P., Ren, Y., and Feng, G. (2013). An unexpected highly selective mononuclear zinc complex for adenosine diphosphate (ADP). Chem. Commun. (Camb.) *49*, 11704–11706.

Szejtli, J. (1998). Introduction and general overview of cyclodextrin chemistry. Chem. Rev. *98*, 1743–1754.

Szente, L., and Szeman, J. (2013). Cyclodextrins in analytical chemistry: host-guest type molecular recognition. Anal. Chem. *85*, 8024–8030.

Tang, L., Wu, D., Huang, Z., and Bian, Y. (2016). A fluorescent sensor based on binaphthol-quinoline Schiff base for relay recognition of Zn^{2+} and oxalate in aqueous media. J. Chem. Sci. *128*, 1337–1343.

Vizitiu, D., and Thatcher, G.R.J. (1999). Binding of phosphates to aminocyclodextrin biomimetics. J. Org. Chem. *64*, 6235–6238.

Wang, L., Yuan, L., Zeng, X., Peng, J., Ni, Y., Cheng, J., Xu, W., Agrawalla, B.K., Su, D., Kim, B., and Chang, Y.T. (2016). A multisite-binding switchable fluorescent probe for monitoring mitochondrial ATP level fluctuation in live cells. Angew. Chem. Int. Ed. *55*, 1773–1776.

Wang, Z., Wang, H., Meng, T., Hao, E., and Jiao, L. (2017). Synthetically simple, click-generated quinoline-based Fe^{3+} sensors. Methods Appl. Fluoresc. *5*, 024015.

Wolfe, D.M., Zhang, Y., and Roberts, G.P. (2007). Specificity and regulation of interaction between the PII and AmtB1 proteins in *Rhodospirillum rubrum*. J. Bacteriol. *189*, 6861–6869.

Wongkongkatep, J., Ojida, A., and Hamachi, I. (2017). Fluorescence sensing of inorganic phosphate and pyrophosphate using small molecular sensors and their applications. Top. Curr. Chem. *375*, 30.

Wu, Y., Wen, J., Li, H., Sun, S., and Xu, Y. (2017). Fluorescent probes for recognition of ATP. Chin. Chem. Lett. *28*, 1916–1924.

Xu, Z., Singh, N.J., Lim, J., Pan, J., Kim, H.N., Park, S., Kim, K.S., and Yoon, J. (2009). Unique sandwich stacking of pyrene-adenine-pyrene for selective and ratiometric fluorescent sensing of ATP at physiological pH. J. Am. Chem. Soc. *131*, 15528–15533.

Yamada, T., Fujiwara, S., Fujita, K., Tsuchido, Y., Hashimoto, T., and Hayashita, T. (2018). Development of dipicolylamine-modified cyclodextrins for the design of selective guest-responsive receptors for ATP. Molecules *23*, 635.

Yang, N., Wei, Y., Kang, X., and Su, Z. (2015). Selective recognition and sensing for adenosine triphosphate by label-free electrochemistry based on its inclusion with per-6-ammonium-β-cyclodextrin. Anal. Methods *7*, 10129–10135.

You, L., Zha, D., and Anslyn, E.V. (2015). Recent advances in supramolecular analytical chemistry using optical sensing. Chem. Rev. *115*, 7840–7892.

Yuan, D., Izuka, A., Fukudome, M., Rekharsky, M.V., Inoue, Y., and Fujita, K. (2007). Heptakis(6-deoxy-6-guanidino)-β-cyclodextrin: an artificial model for mitochondrial ADP/ATP carrier. Tetrahedron Lett. *48*, 3479–3483.

Yu, M., Chen, Y., Zhang, N., and Liu, Y. (2010). Construction and transmembrane dissociation behavior of supramolecular assembly of quinolinocyclodextrin with porphyrin. Org. Biomol. Chem. *8*, 4148–4154.

Zahn, S., and Canary, J.W. (1999). Absolute configurations of N,N-dialkyl α-amino acids and β-amino alcohols from exciton-coupled circular dichroism spectra of Cu(II) complexes. Org. Lett. *6*, 861–864.

Zahn, S., and Canary, J.W. (2000). Electron-induced inversion of helical chirality in copper complexes of N,N-dialkylmethionines. Science *288*, 1404–1407.

Zhai, S.-S., Chen, Y., and Liu, Y. (2013). Selective binding of bile salts by β-cyclodextrin derivatives with appended quinolyl arms. Chin. Chem. Lett. *24*, 442–446.

Zhao, X.J., and Huang, C.Z. (2010). Small organic molecules as fluorescent probes for nucleotides and their derivatives. TrAC-Trend. Anal. Chem. *29*, 354–367.

Zhou, Y., Xu, Z., and Yoon, Y. (2011). Fluorescent and colorimetric chemosensors for detection of nucleotides, FAD and NADH: highlighted research during 2004-2010. Chem. Soc. Rev. *40*, 2222–2235.

Zhong, C., Mu, T., Wang, L., Fu, E., and Qin, J. (2009). Unexpected fluorescent behavior of a 4-amino-1,8-naphthalimide derived β-cyclodextrin: conformation analysis and sensing properties. Chem. Commun. (Camb.) *2009*, 4091–4093.

Zimmermann, H. (1999). Two novel families of ectonucleotidases: molecular structures, catalytic properties, and a search for function. Trends Pharmacol. Sci. *20*, 231–236.

iScience, Volume *23*

Supplemental Information

A Quinoline-Appended Cyclodextrin Derivative as a Highly Selective Receptor and Colorimetric Probe for Nucleotides

Kuppusamy Kanagaraj, Chao Xiao, Ming Rao, Chunying Fan, Victor Borovkov, Guo Cheng, Dayang Zhou, Zhihui Zhong, Dan Su, Xingke Yu, Jiabin Yao, Taotao Hao, Wanhua Wu, Jason J. Chruma, and Cheng Yang

Supplemental Schemes

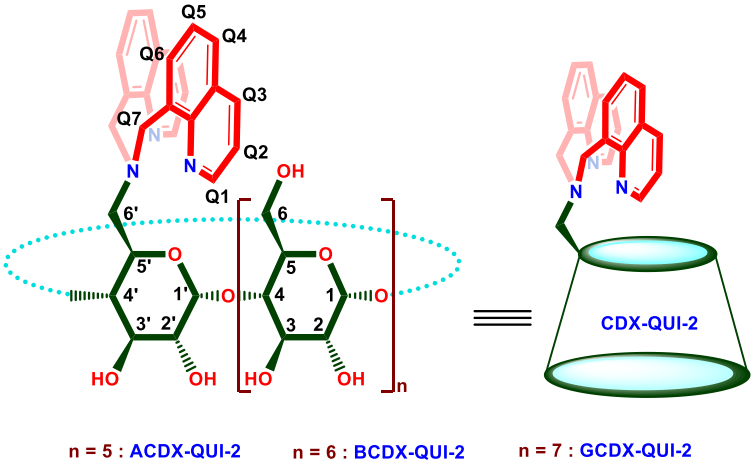

Scheme S1. Structure of CDX derivatives, Related to Scheme 1.

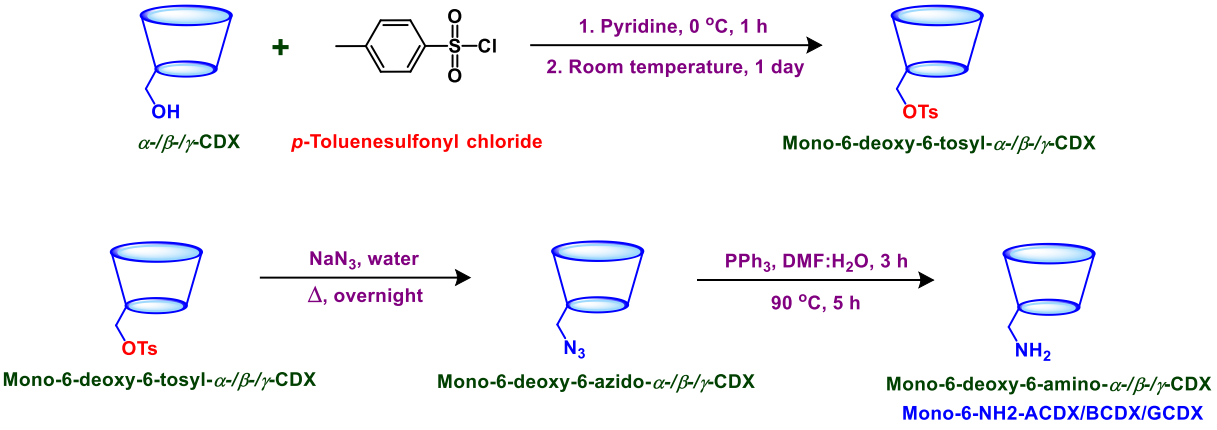

Scheme S2. Synthesis of mono-6-deoxy-6-amino-α-/β-/γ-CDX derivative (Mono-6-NH_2-ACDX/BCDX/GCDX), Related to Scheme 1.

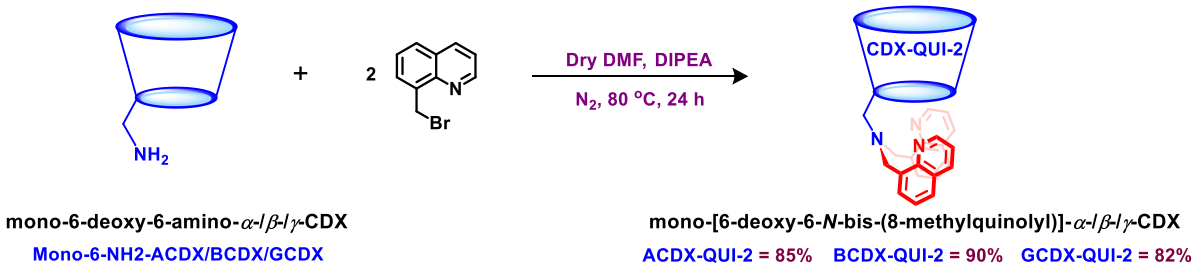

Scheme S3. Synthesis of CDX appended mono-*N*-bis-(8-aminomethylquinoline derivatives (CDX-QUI-2), Related to Scheme 1.

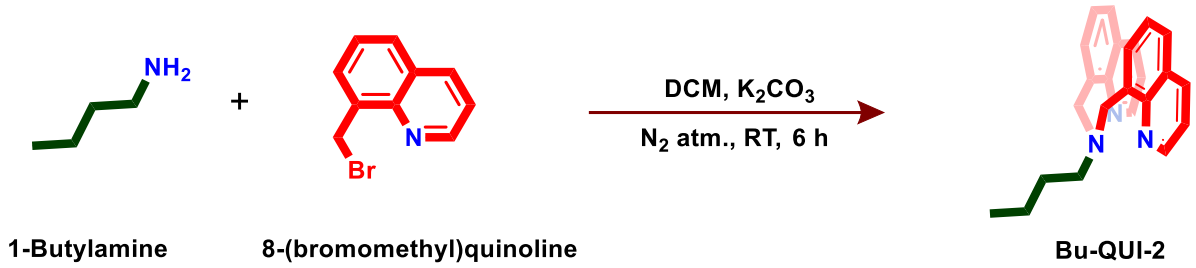

Scheme S4. Synthesis of control compound Bu-QUI-2, Related to Scheme 2.

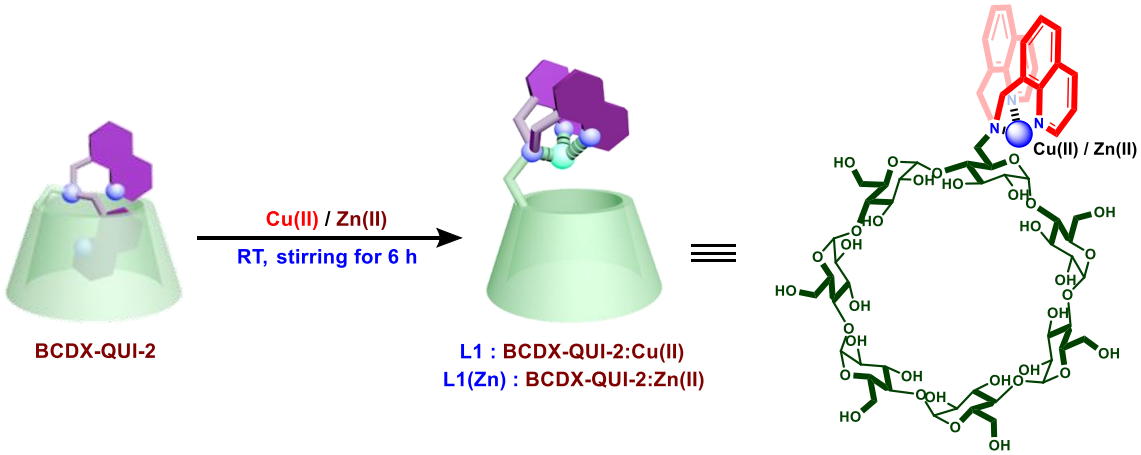

Scheme S5. Preparation of probe **L1** and **L1(Zn)**, Related to Scheme 2.

Supplemental Figures

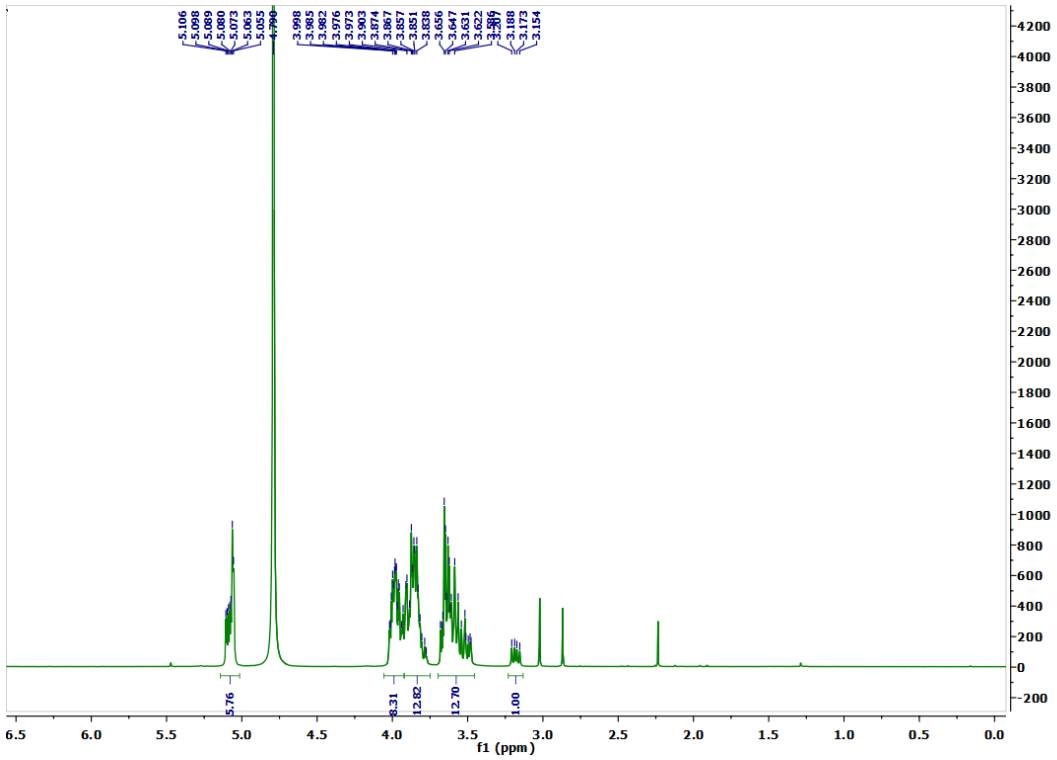

Figure S1. ^{1}H NMR Spectrum of mono-6-deoxy-6-amino-α-CDX (mono-6-NH_2-ACDX) (D_2O, 400 MHz, 25 °C), Related to Scheme 1.

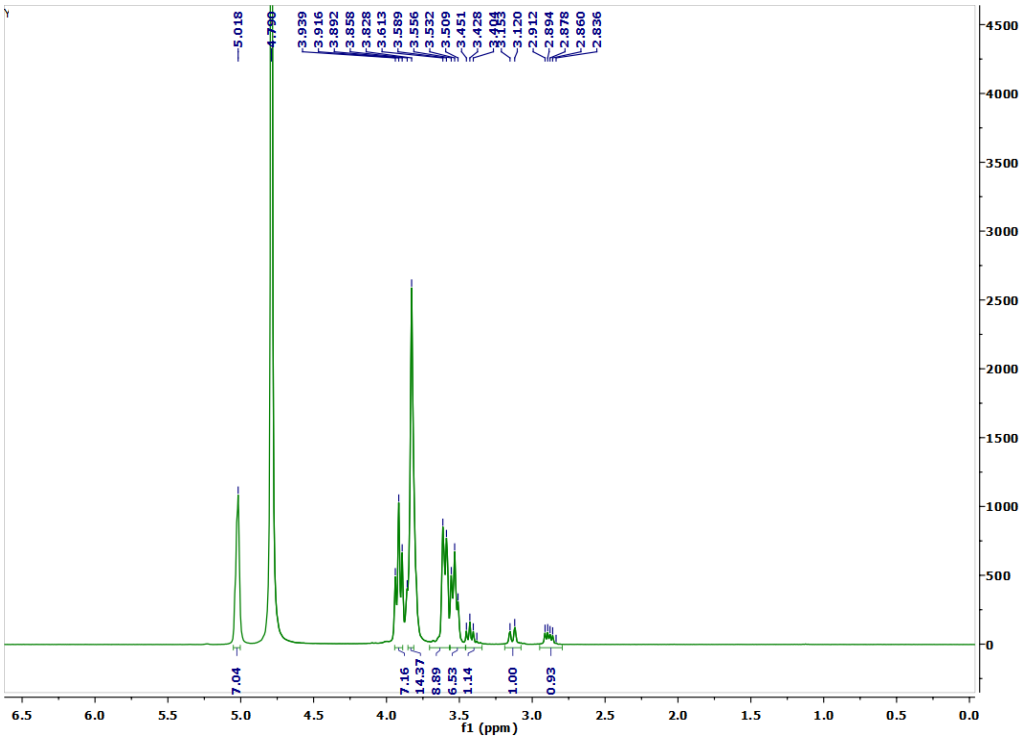

Figure S2. ^{1}H NMR Spectrum of mono-6-deoxy-6-amino-β-CDX (mono-6-NH_2-BCDX) (D_2O, 400 MHz, 25 °C), Related to Scheme 1.

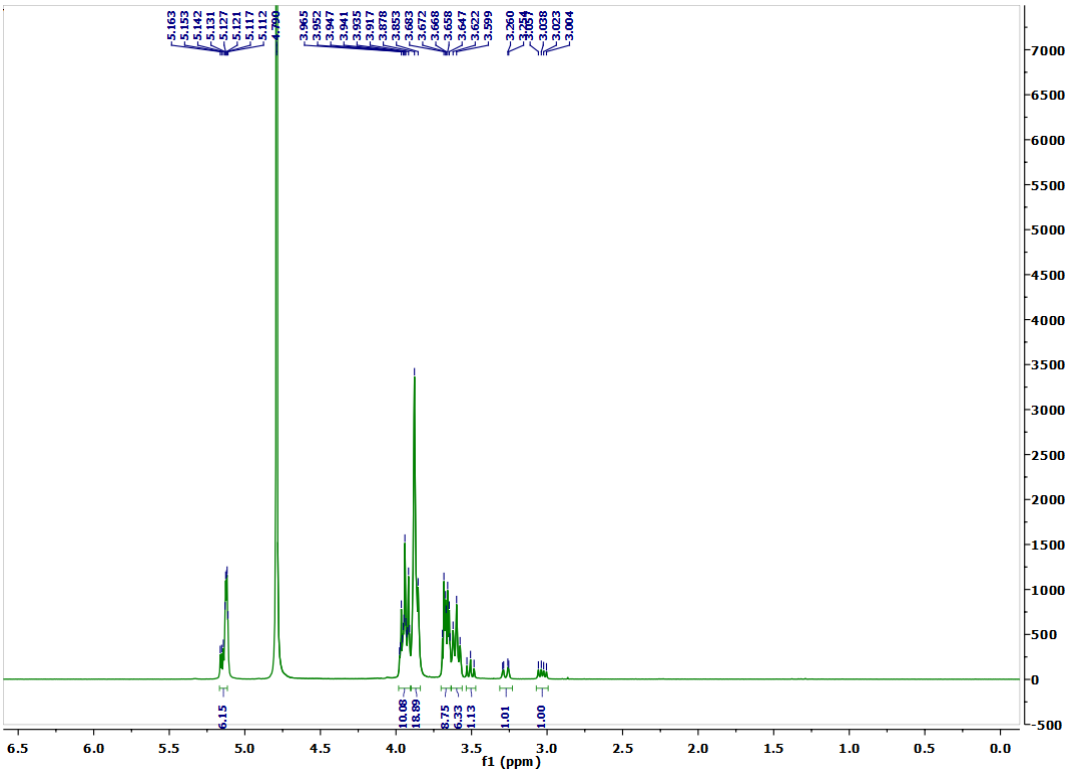

Figure S3. ^{1}H NMR Spectrum of mono-6-deoxy-6-amino-γ-CDX (mono-6-NH_2-GCDX) (D_2O, 400 MHz, 25 °C), Related to Scheme 1.

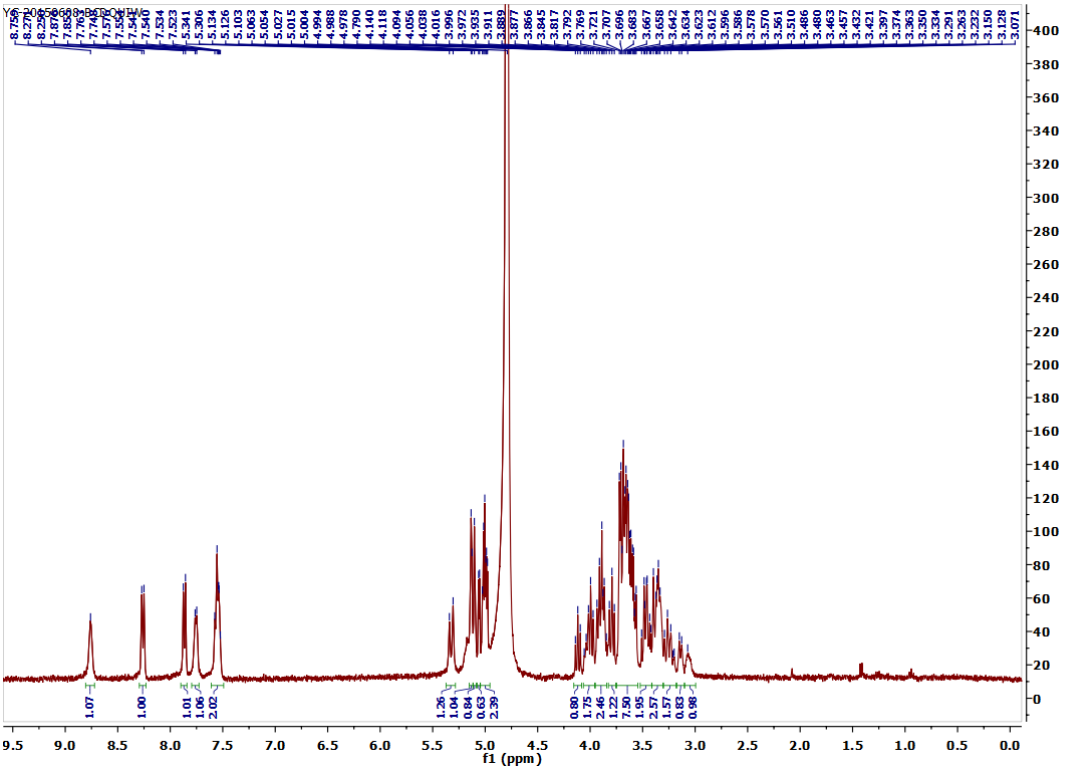

Figure S4. ^{1}H NMR Spectrum of BCDX-QUI-2 (D_2O, 400 MHz, 25 °C), Related to Scheme 1.

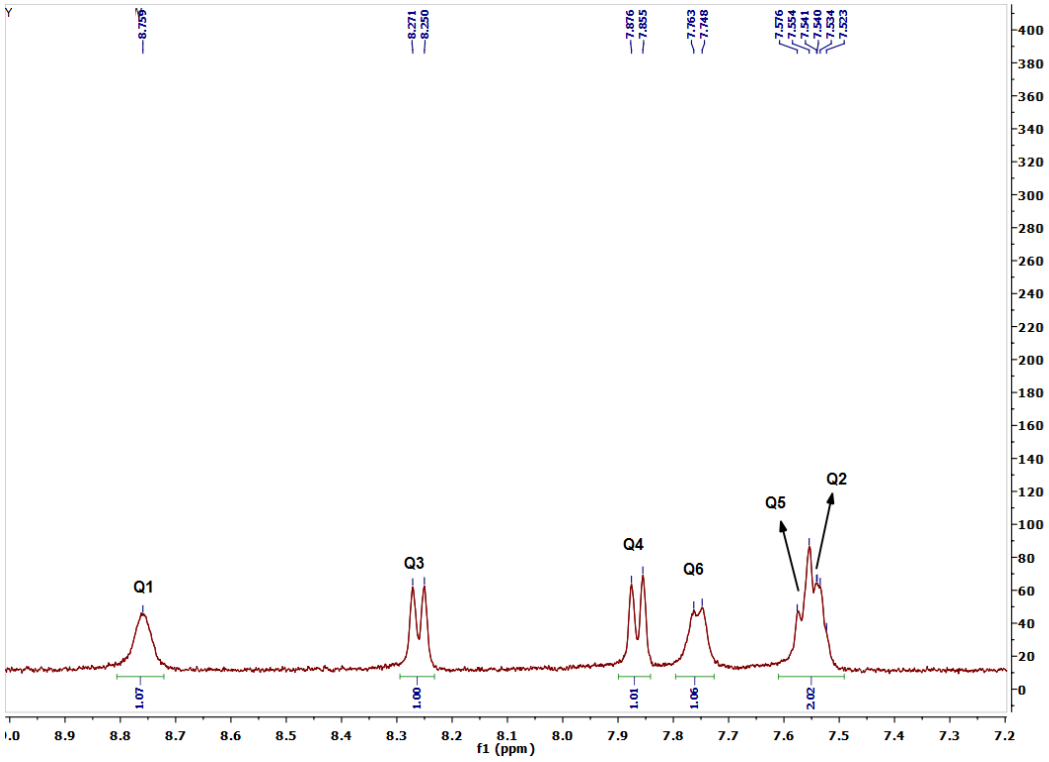

Figure S5. Expanded ^{1}H NMR spectrum of BCDX-QUI-2 (D_2O, 400 MHz, 25 °C), Related to Scheme 1.

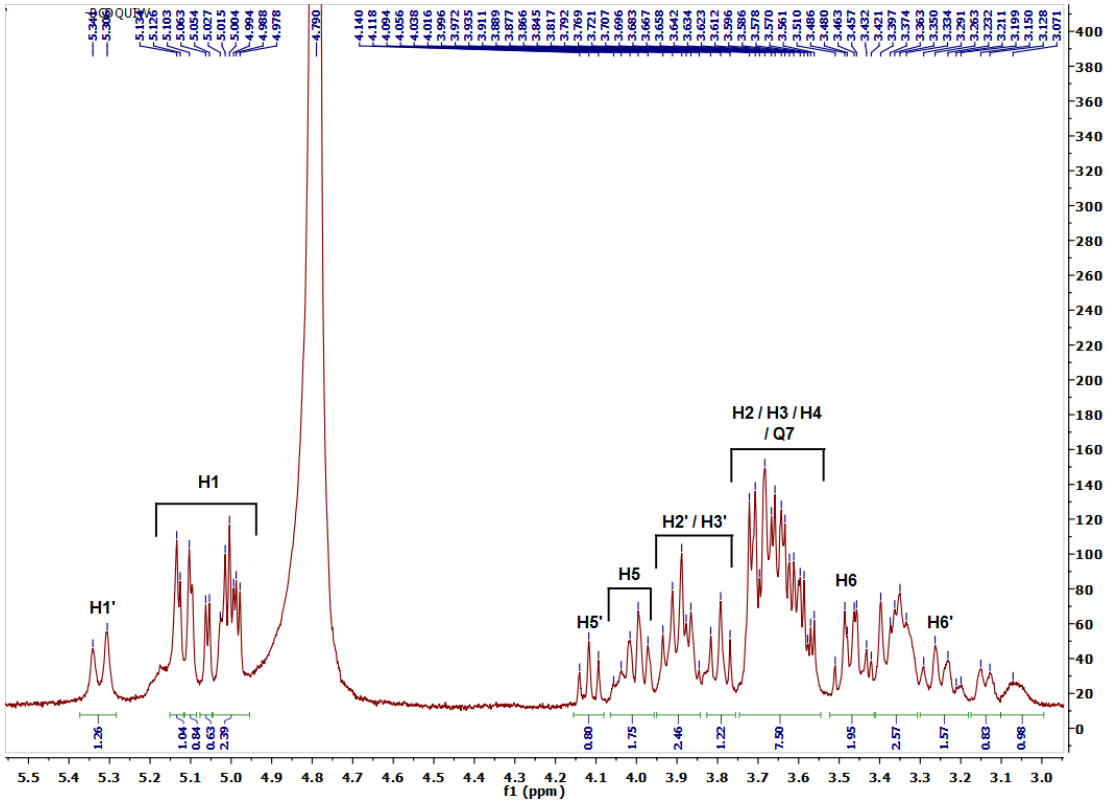

Figure S6. Expanded ^{1}H NMR spectrum of BCDX-QUI-2 (D_2O, 400 MHz, 25 °C), Related to Scheme 1.

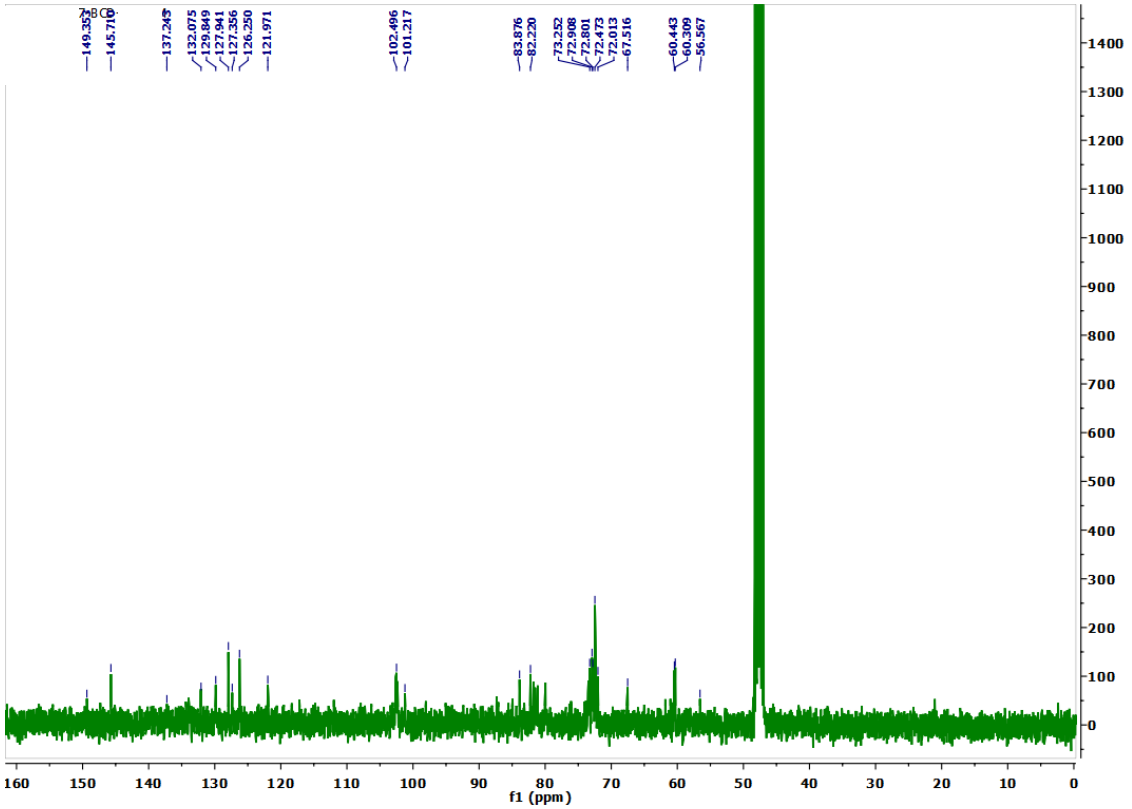

Figure S7. ^{13}C NMR Spectrum of BCDX-QUI-2 (CD_3OD, 101 MHz, 25 °C), Related to Scheme 1.

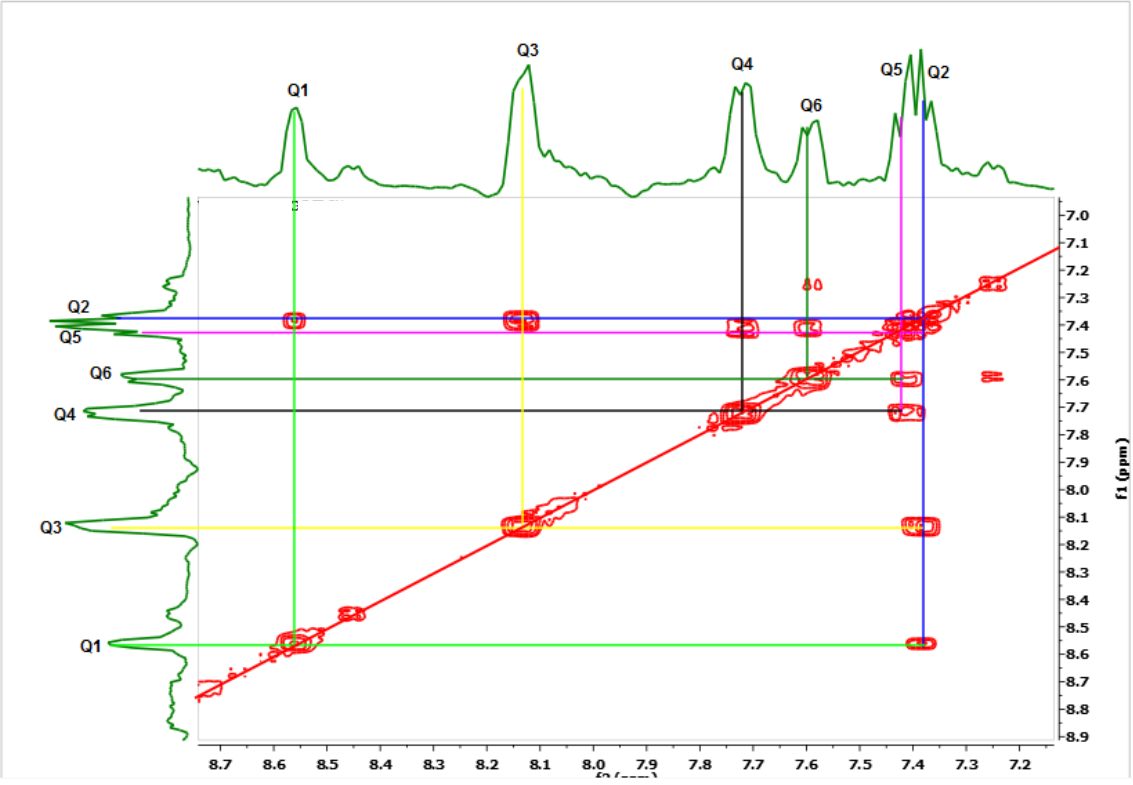

Figure S8. ^{1}H-^{1}H COSY Spectrum of BCDX-QUI-2 (D_2O, 400 MHz, 25 °C), Related to Scheme 1.

BCDX-QUI-2 Event#: 1 MS(E+)

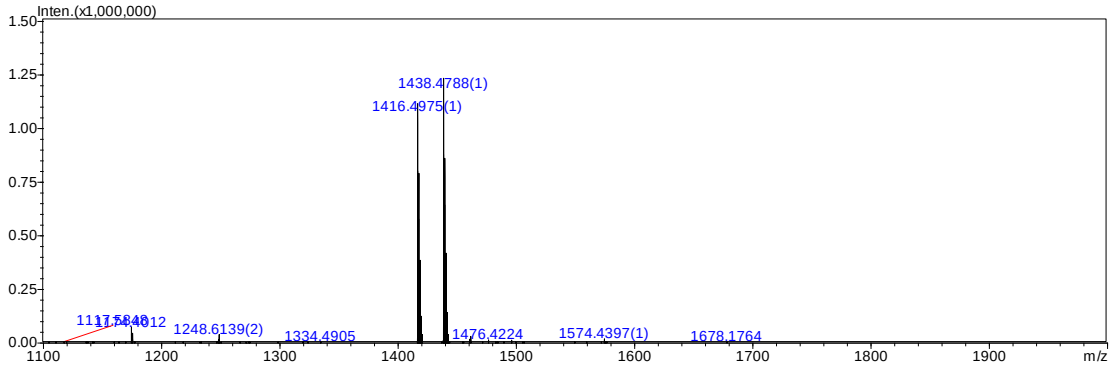

Event#: 2 MS(E-)

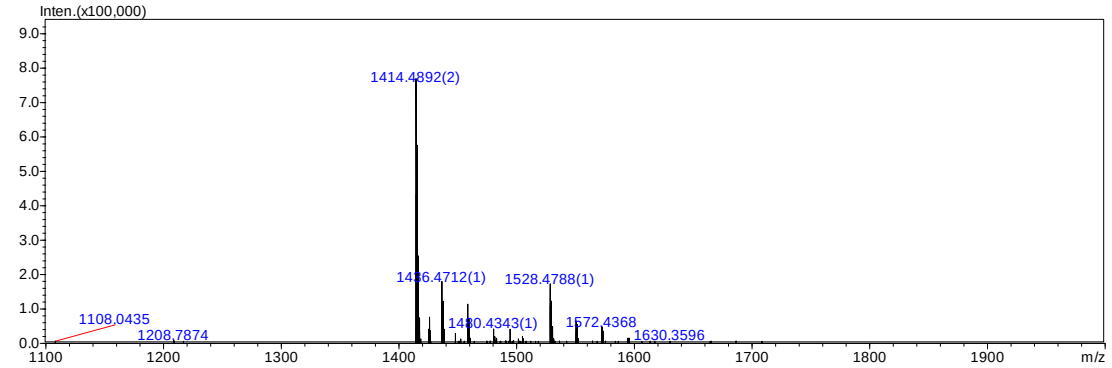

Figure S9. HRMS (ESI) Spectrum of BCDX-QUI-2, Related to Scheme 1.

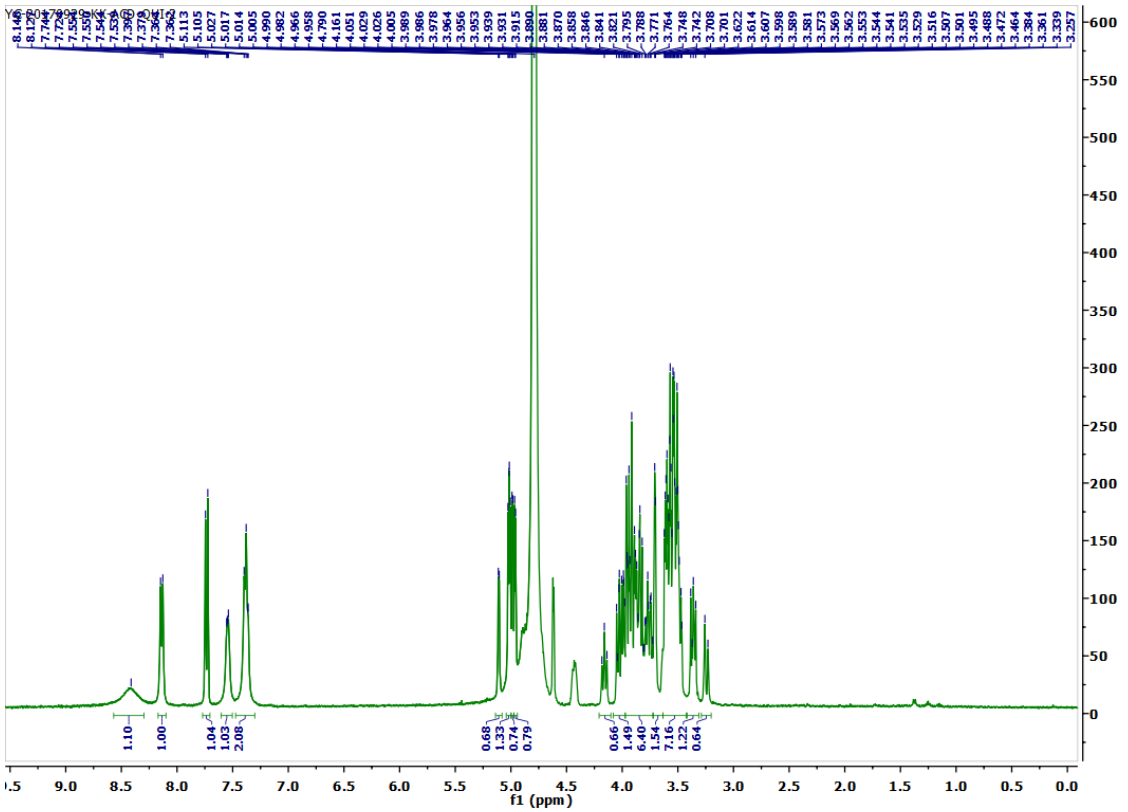

Figure S10. ^{1}H NMR Spectrum of ACDX-QUI-2 (D_2O, 400 MHz, 25 °C), Related to Scheme 1.

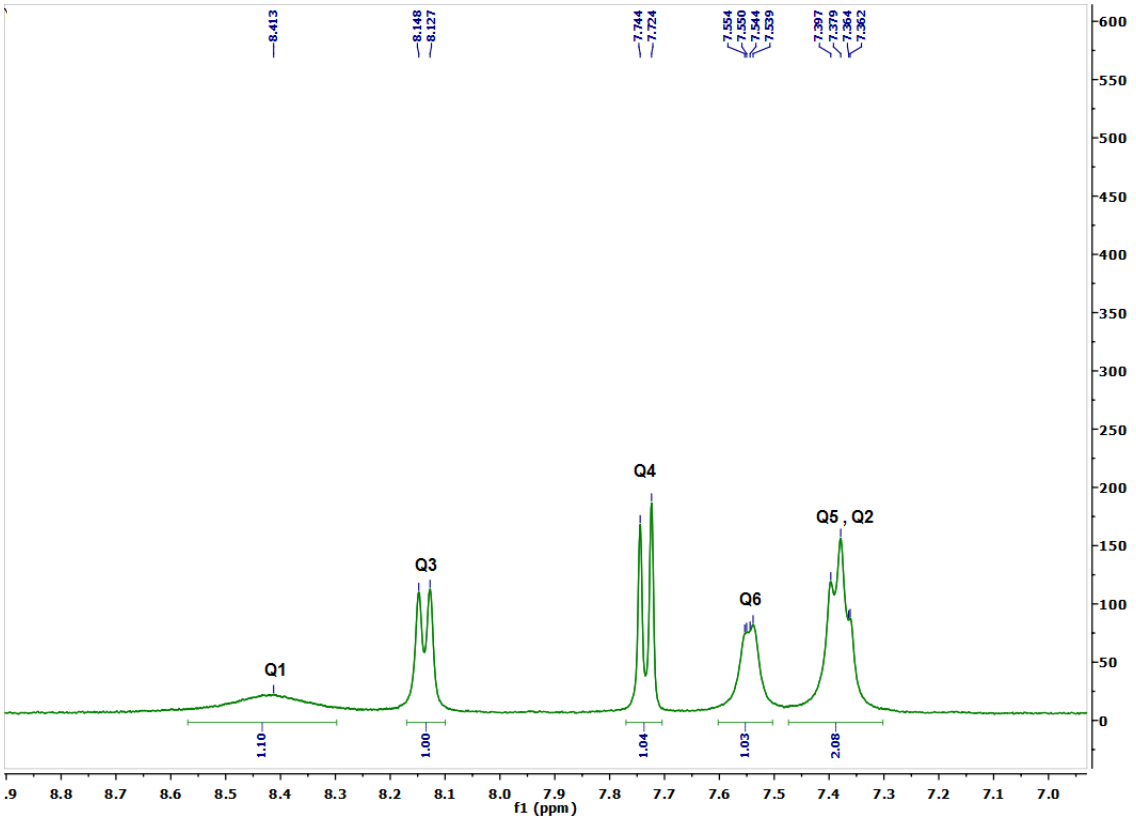

Figure S11. Expanded ^{1}H NMR Spectrum of ACDX-QUI-2 (D_2O, 400 MHz, 25 °C), Related to Scheme 1.

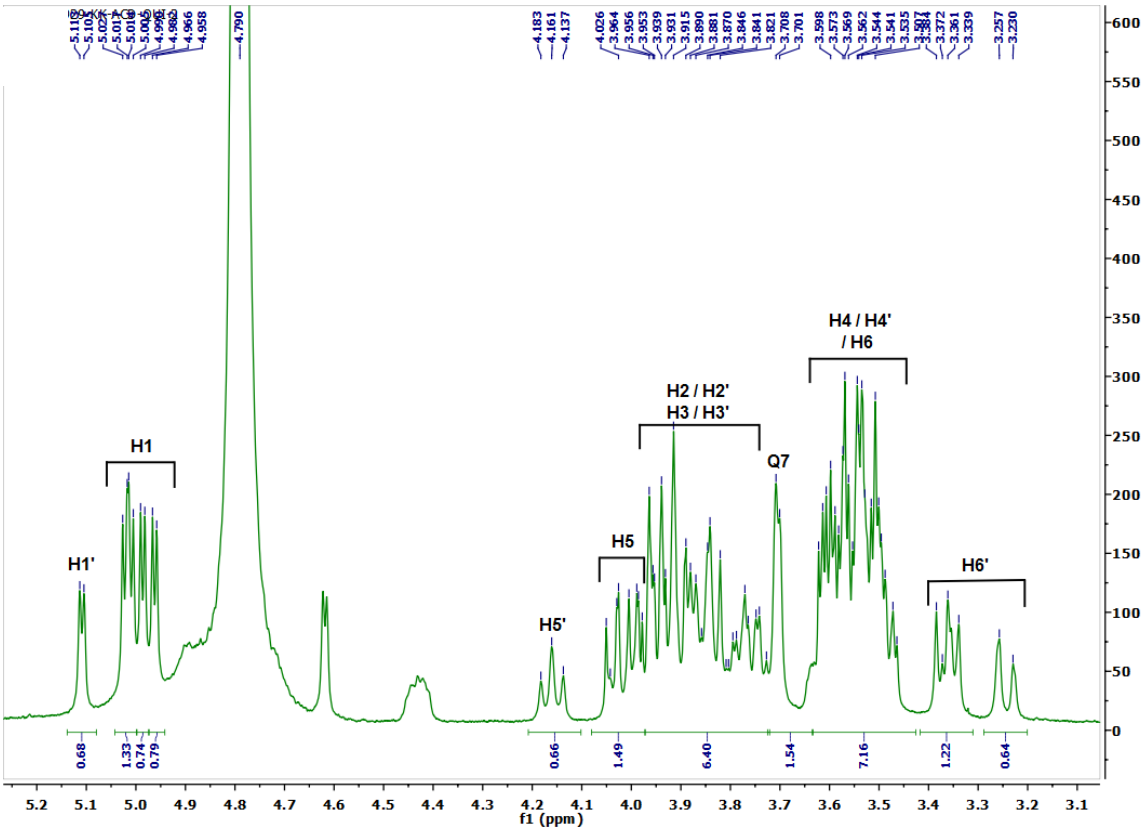

Figure S12. Expanded ^{1}H NMR Spectrum of ACDX-QUI-2 (D_2O, 400 MHz, 25 °C), Related to Scheme 1.

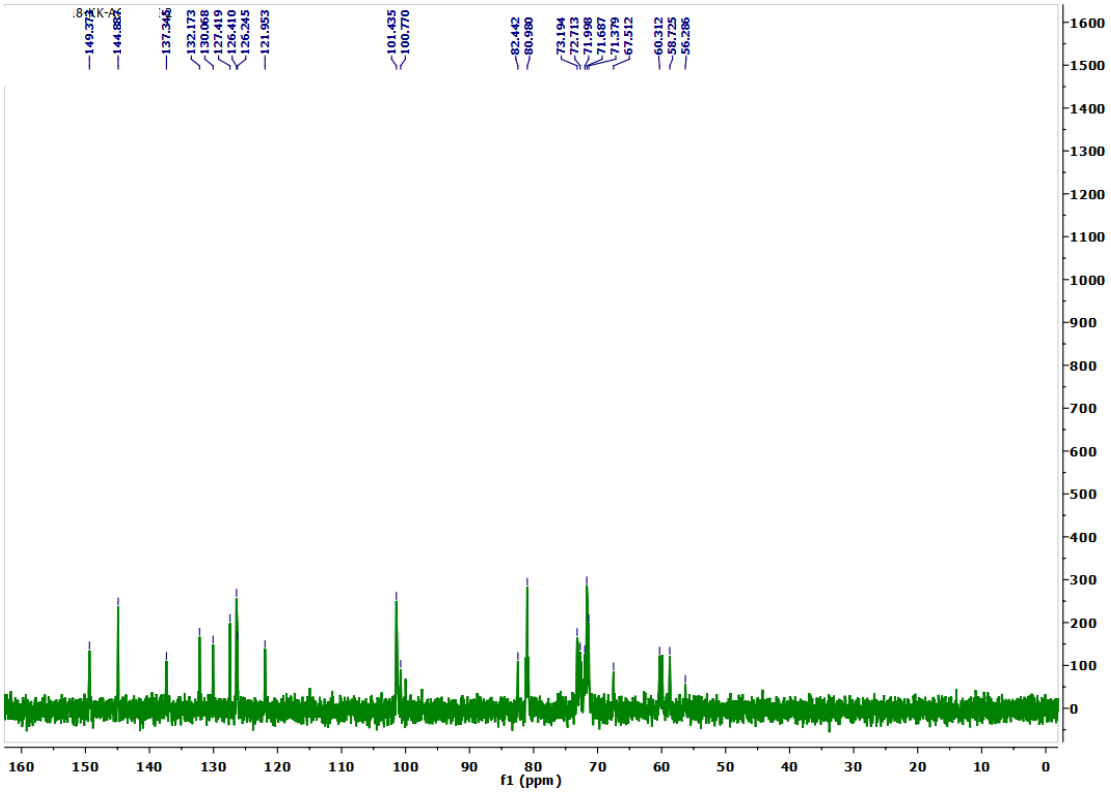

Figure S13. ^{13}C NMR Spectrum of ACDX-QUI-2 (D_2O, 101 MHz, 25 °C), Related to Scheme 1.

ACDX-QUI-2 ESI+

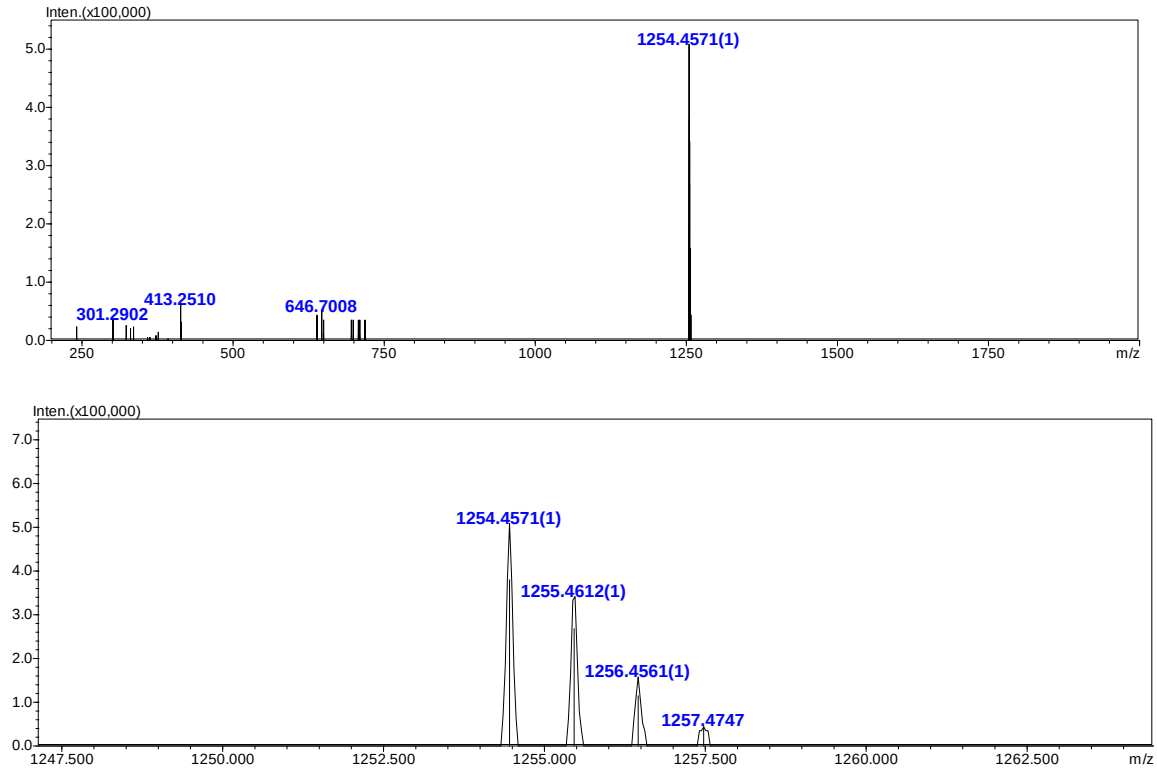

Figure S14. HRMS (ESI) Spectrum of ACDX-QUI-2, Related to Scheme 1.

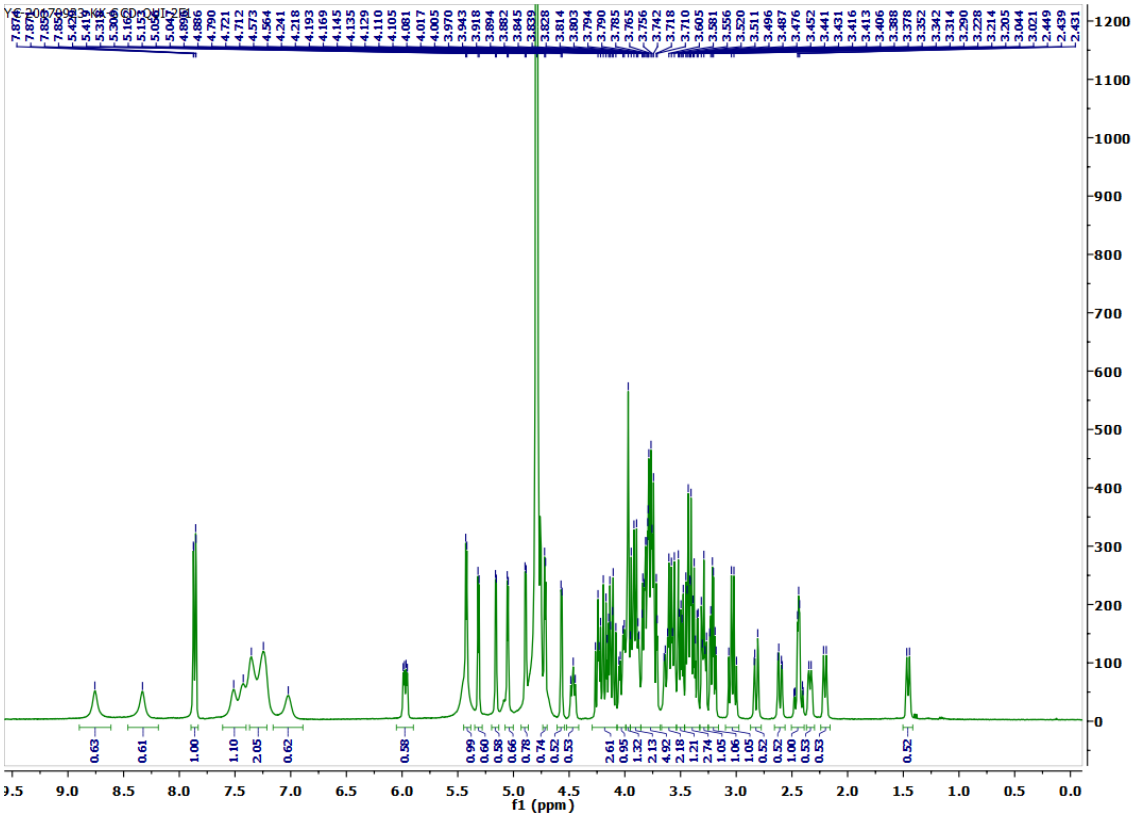

Figure S15. ^{1}H NMR Spectrum of GCDX-QUI-2 (D_2O, 400 MHz, 25 °C), Related to Scheme 1.

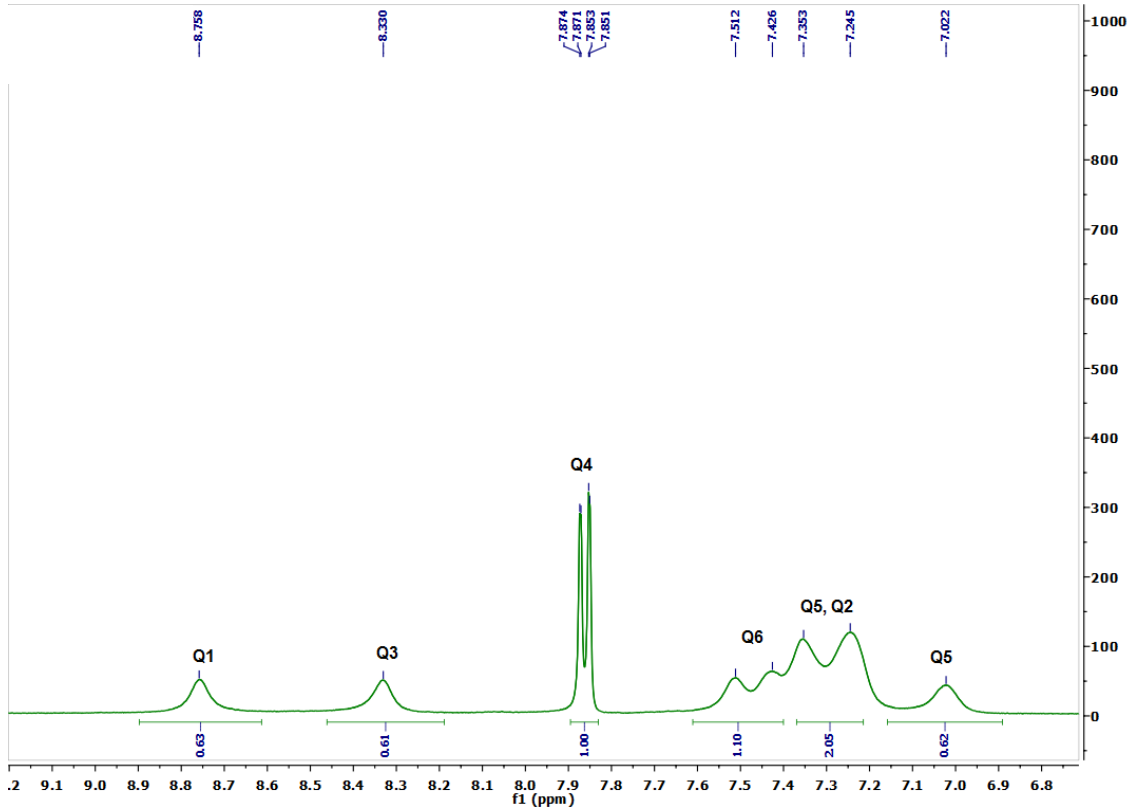

Figure S16. Expanded ^{1}H NMR Spectrum of GCDX-QUI-2 (D_2O, 400 MHz, 25 °C), Related to Scheme 1.

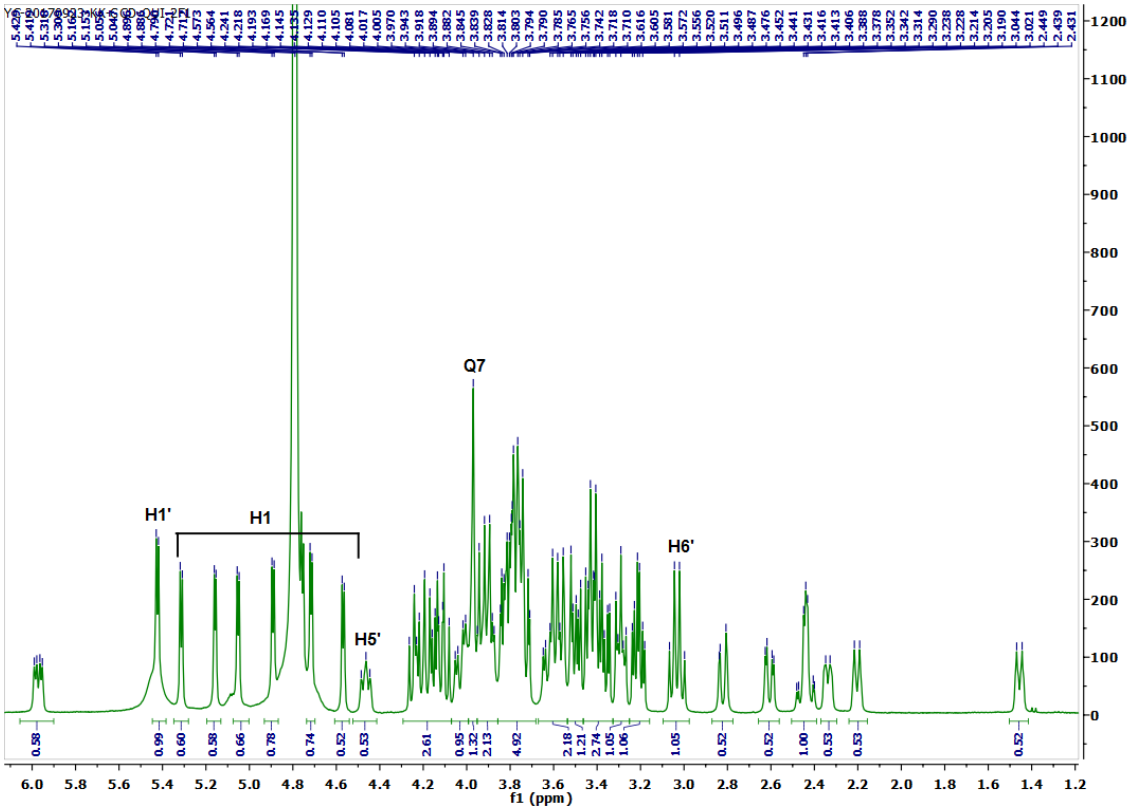

Figure S17. Expanded ^{1}H NMR Spectrum of GCDX-QUI-2 (D_2O, 400 MHz, 25 °C), Related to Scheme 1.

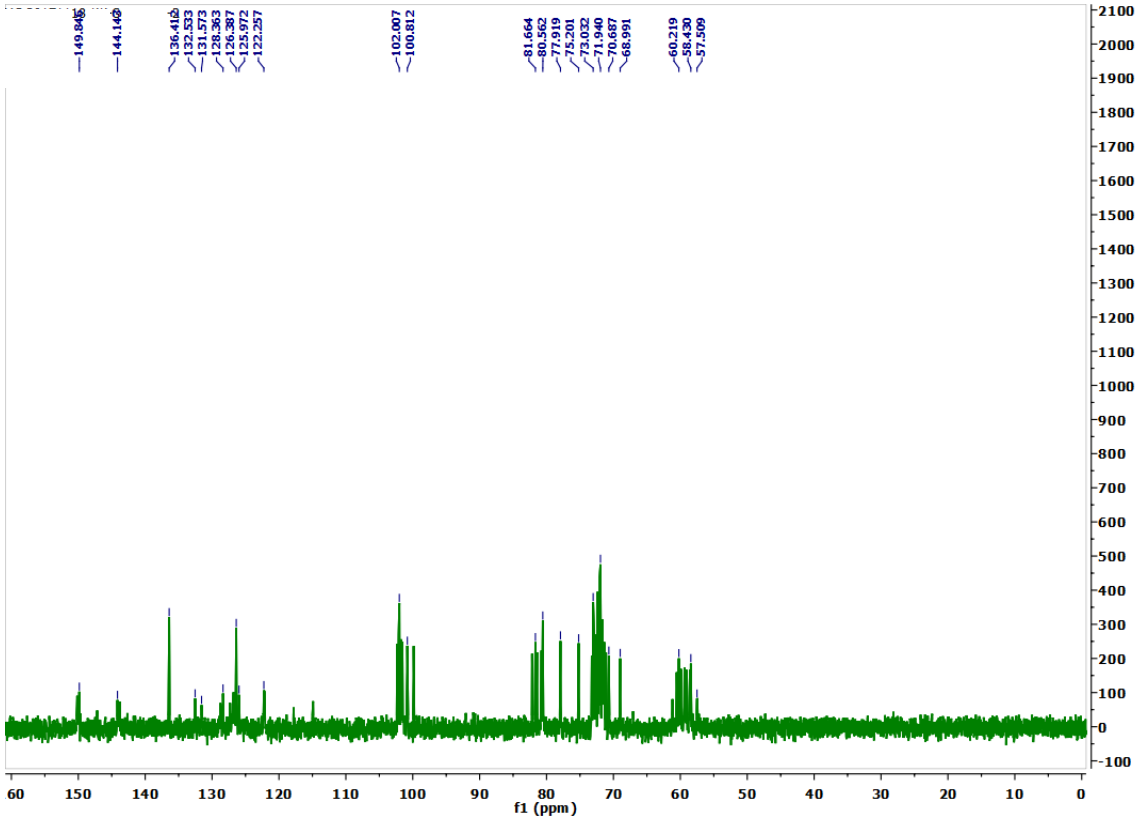

Figure S18. ^{13}C NMR Spectrum of GCDX-QUI-2 (D_2O, 101 MHz, 25 °C), Related to Scheme 1.

GCDX-QUI-2 ESI+

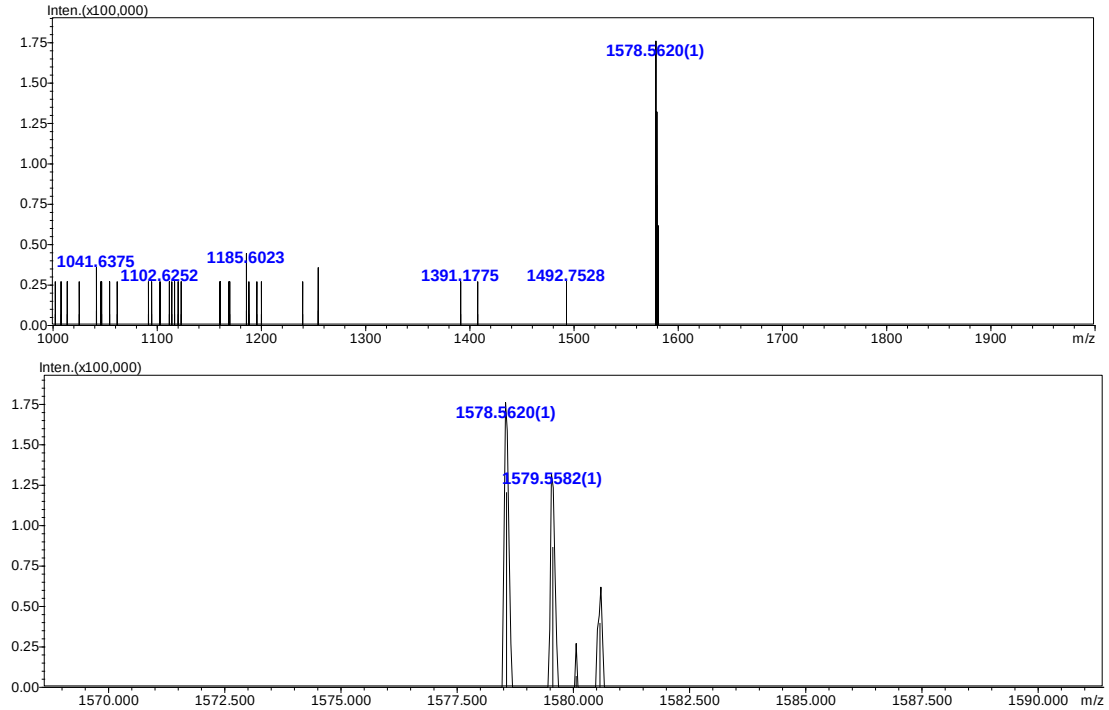

Figure S19. HRMS (ESI) Spectrum of GCDX-QUI-2, Related to Scheme 1.

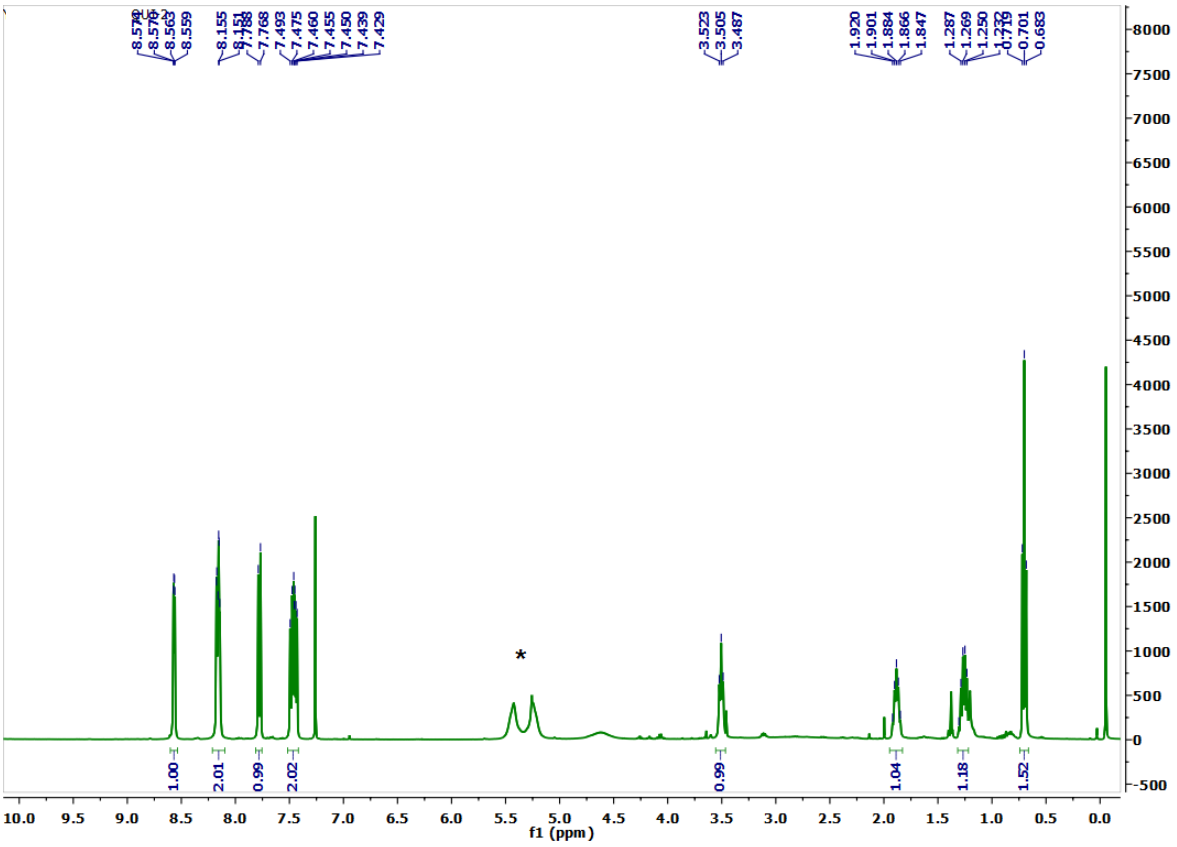

Figure S20. ^{1}H NMR Spectrum of Bu-QUI-2 ($CDCl_3$, 400 MHz, 25 °C) (*solvent impurity), Related to Scheme 2.

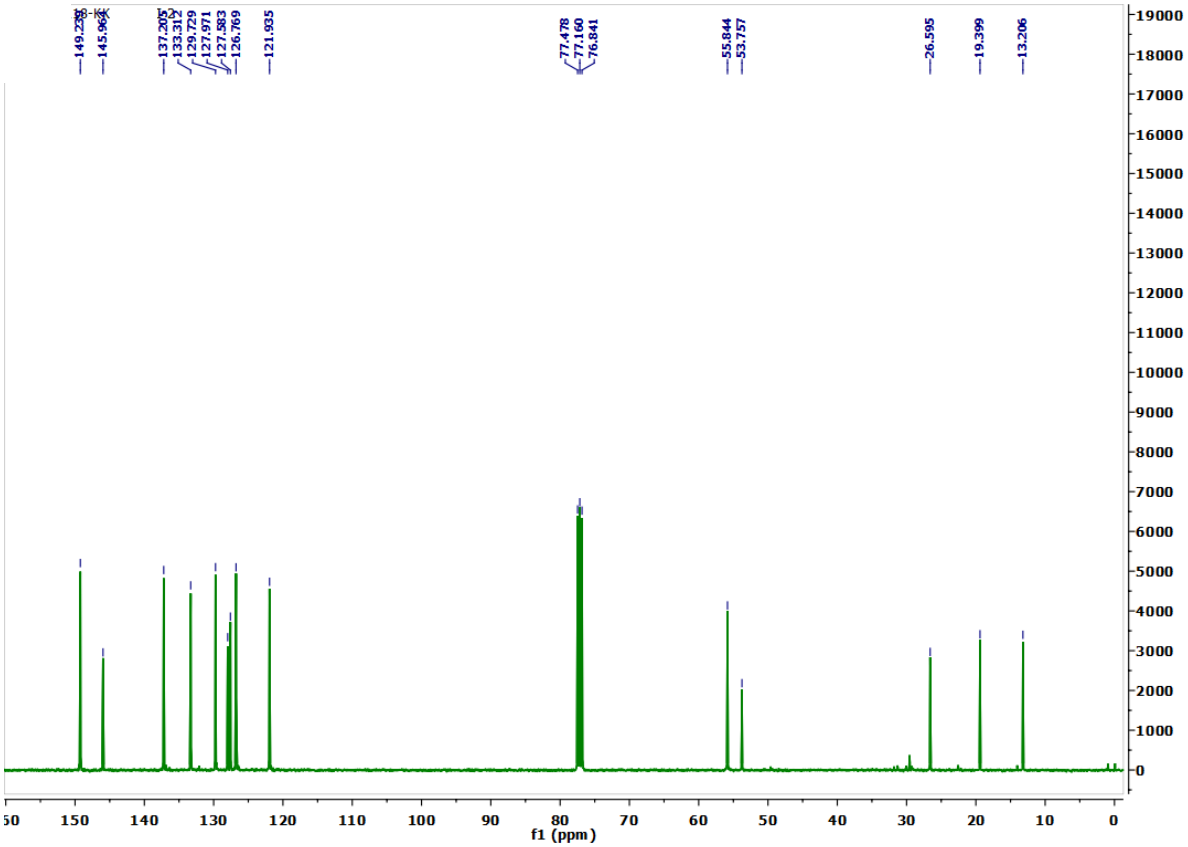

Figure S21. ^{13}C NMR Spectrum of Bu-QUI-2 ($CDCl_3$, 101 MHz, 25 °C), Related to Scheme 2.

Bu-QUI-2 MS(E+)

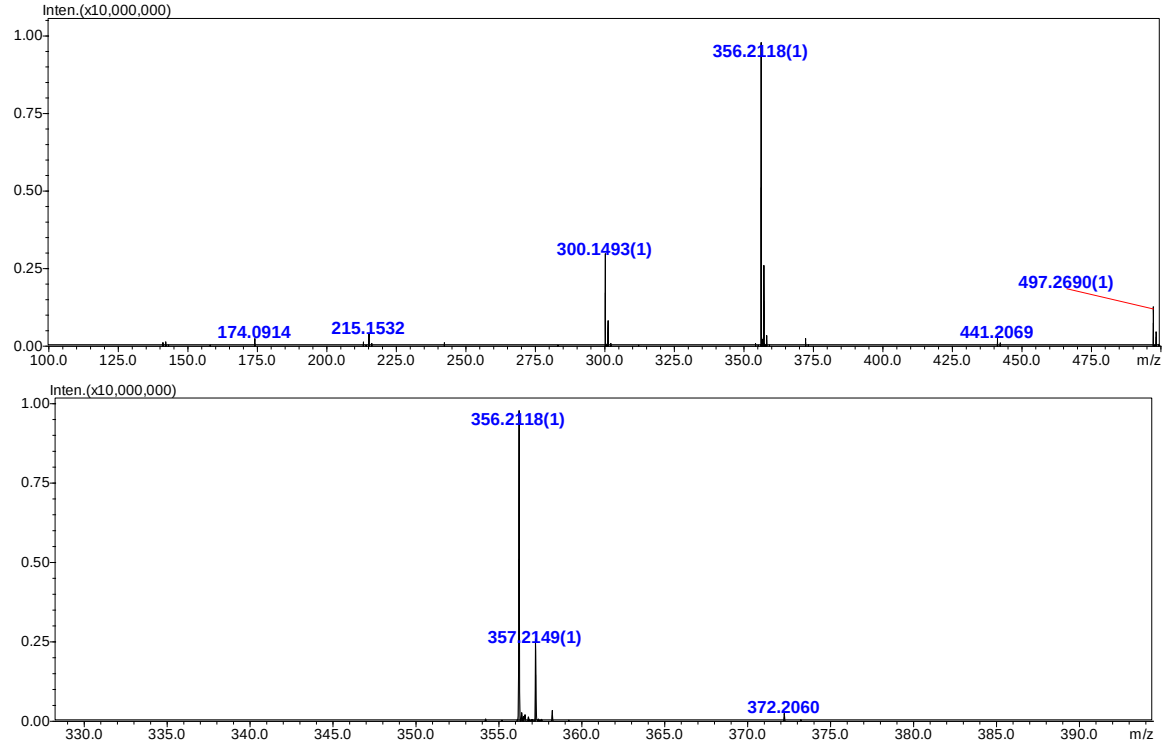

Figure S22. HRMS (ESI) Spectrum of Bu-QUI-2, Related to Scheme 2.

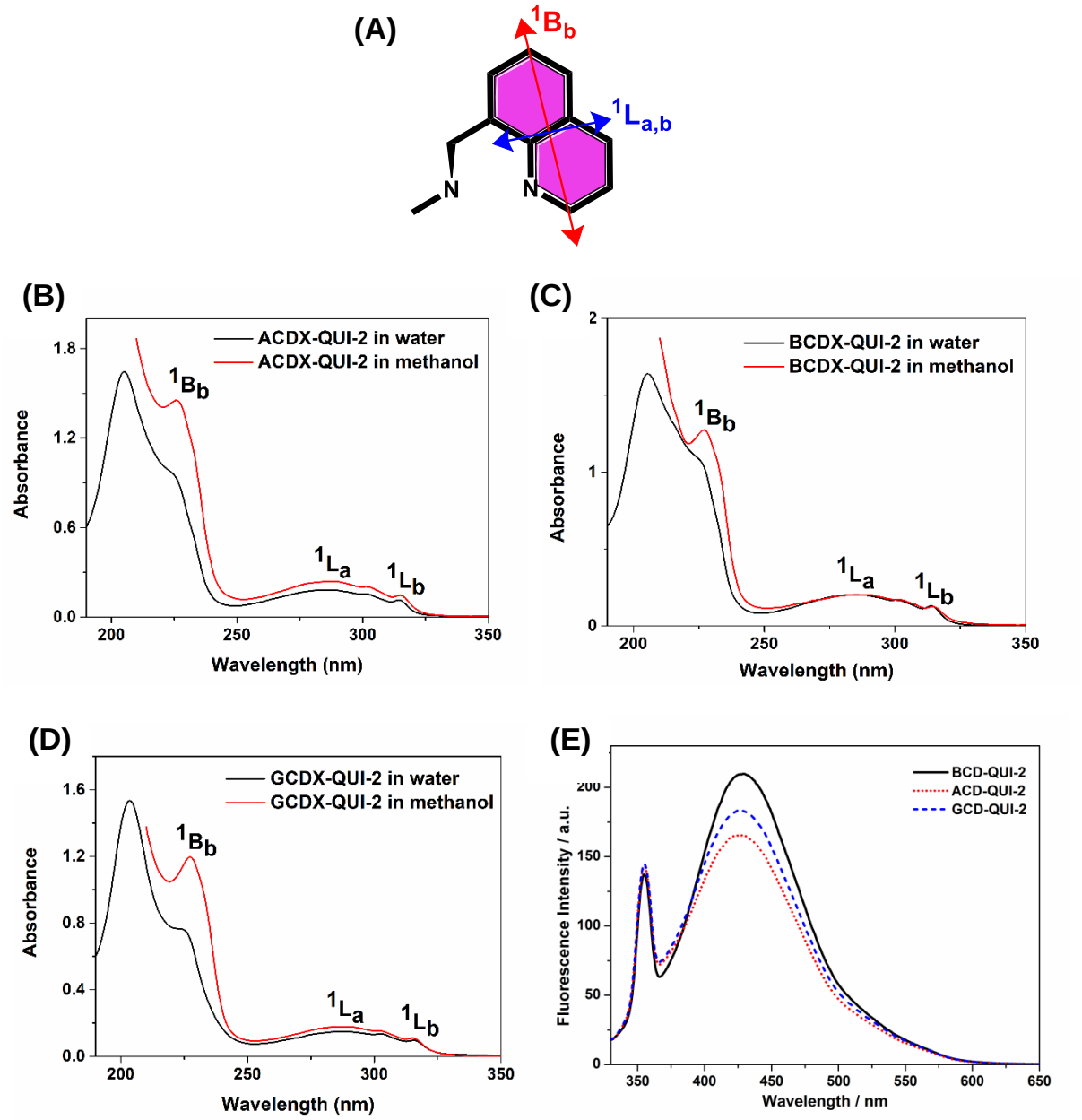

Figure S23. (A) The orientations of the absorption transition moments of quinoline chromophore. (B) & (C) Absorption and (D) & (E) fluorescence (λ_{exc} = 315 nm, λ_{em} = 427 nm) spectrum of CDX-QUI-2 (ACDX-QUI-2: 39.5 µM; BCDX-QUI-2: 36.8 µM; and GCDX-QUI-2: 31.7 µM) in water and methanol. The orientations of the absorption transition moments for both ^1B_b and $^1L_{a,b}$ absorption bands are shown in the inset, Related to Scheme 1, Figure 1 and Figure 2.

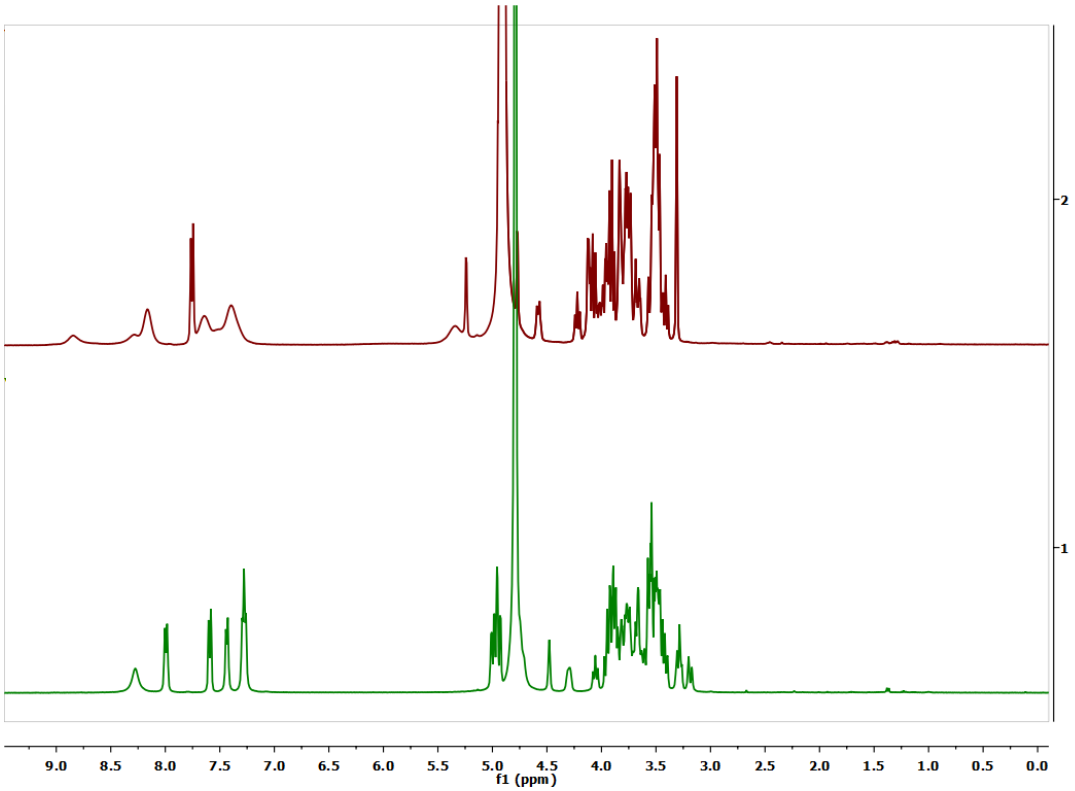

Figure S24. Comparison of ^{1}H NMR spectrum (400 MHz, 25 °C) of ACDX-QUI-2 in CD_3OD (top) and D_2O (bottom), Related to Figure 1.

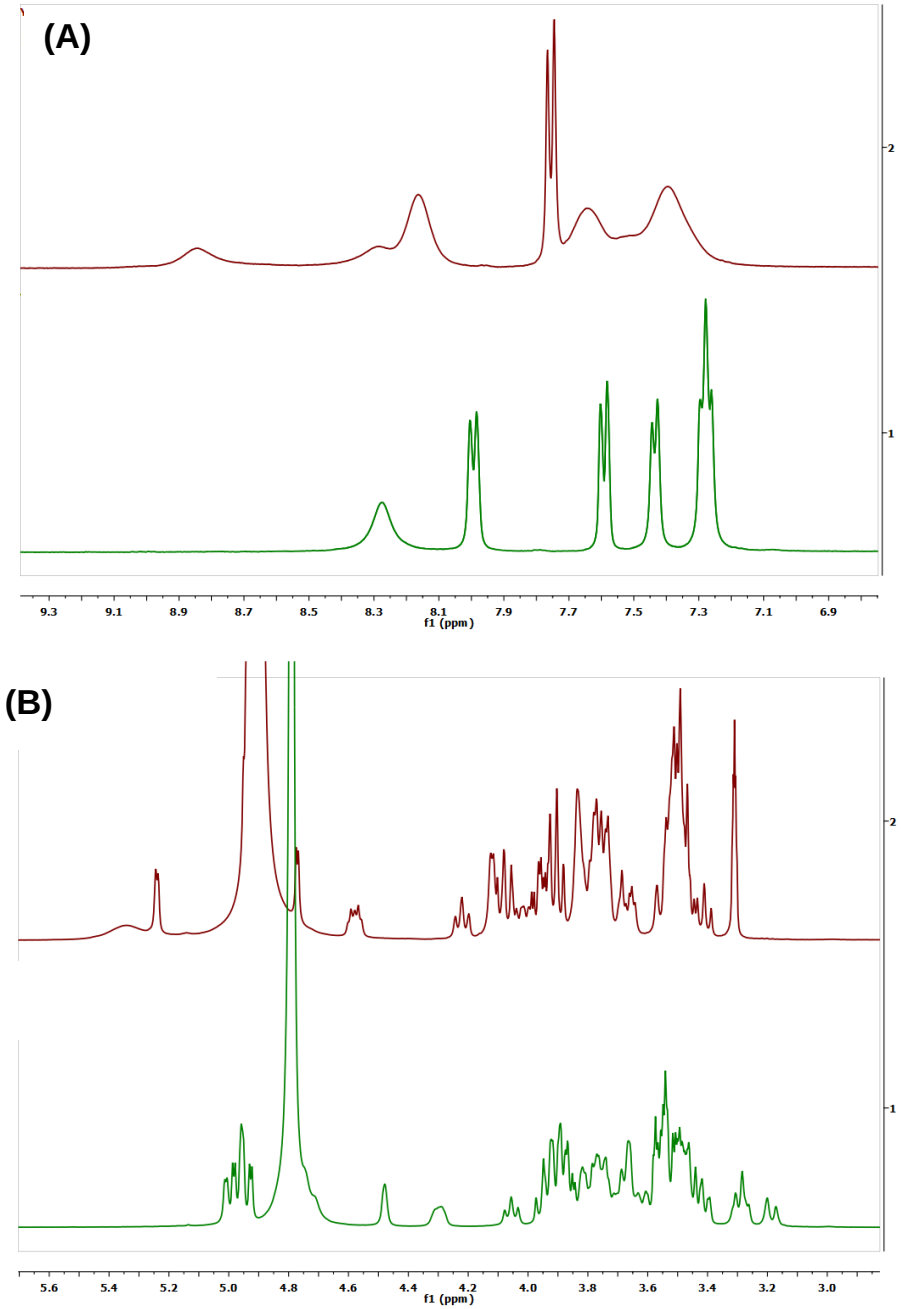

Figure S25. Expansion spectra of Figure S24 in the (A) aromatic proton region and (B) CDX proton region, Related to Figure 1.

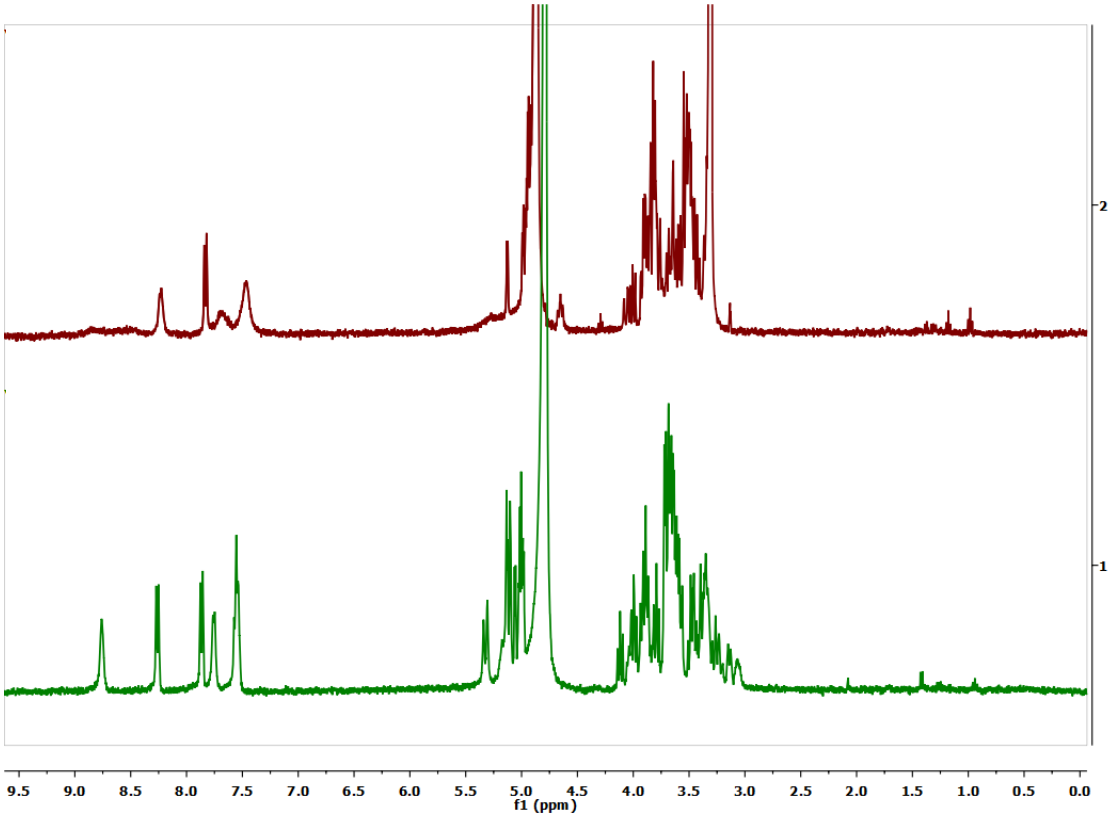

Figure S26. Comparison of ^{1}H NMR spectrum (400 MHz, 25 °C) of BCDX-QUI-2 in CD_3OD (top) and D_2O (bottom), Related to Figure 1 and Figure 2.

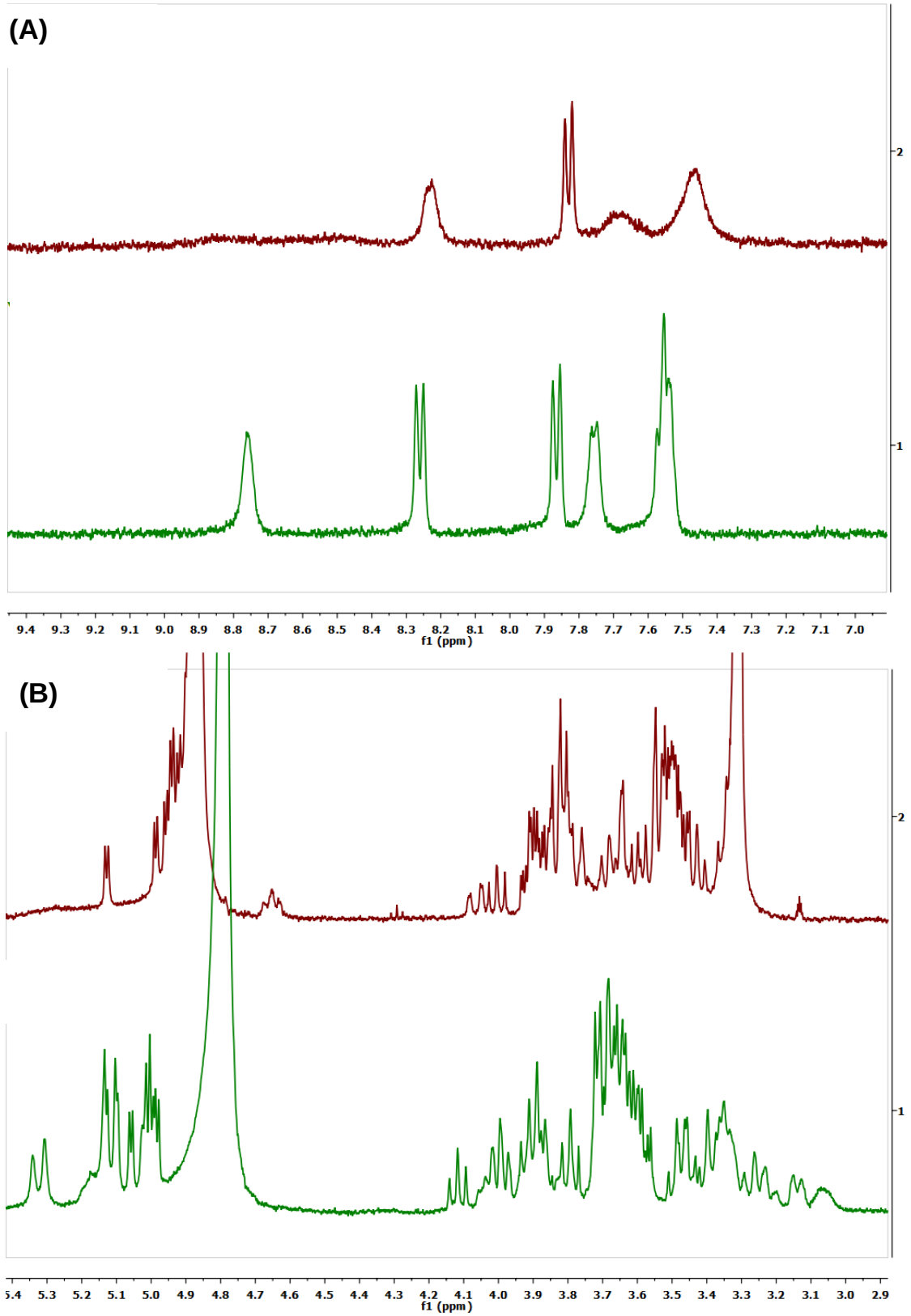

Figure S27. Expansion spectra of Figure S26 in the (A) aromatic proton region (B) CDX proton region, Related to Figure 1 and Figure 2.

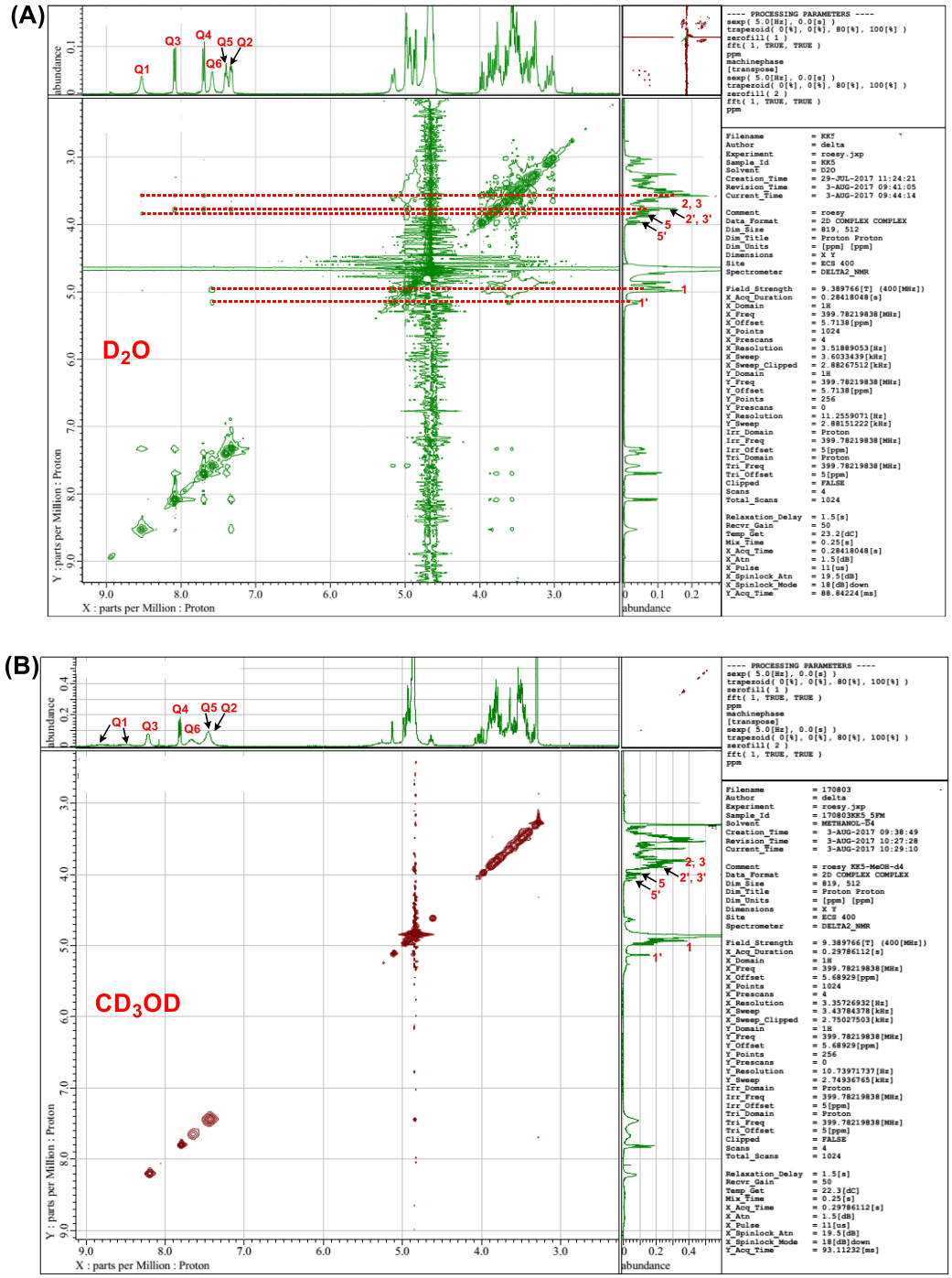

Figure S28. ROESY Spectrum of BCDX-QUI-2 in (A) D_2O and (B) CD_3OD 25 °C with a mixing time of 250 ms, Related to Figure 1 and Figure 2.

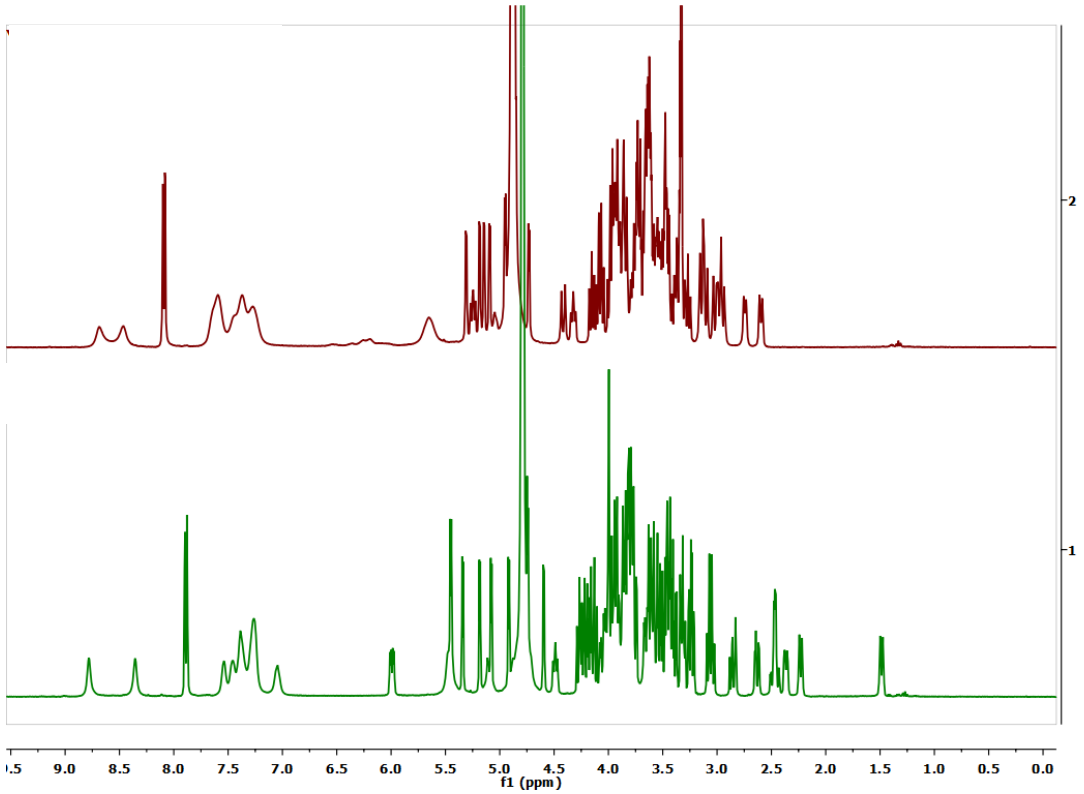

Figure S29. Comparison of ^{1}H NMR spectrum (400 MHz, 25 °C) of GCDX-QUI-2 in CD_3OD (top) and D_2O (bottom), Related to Figure 1.

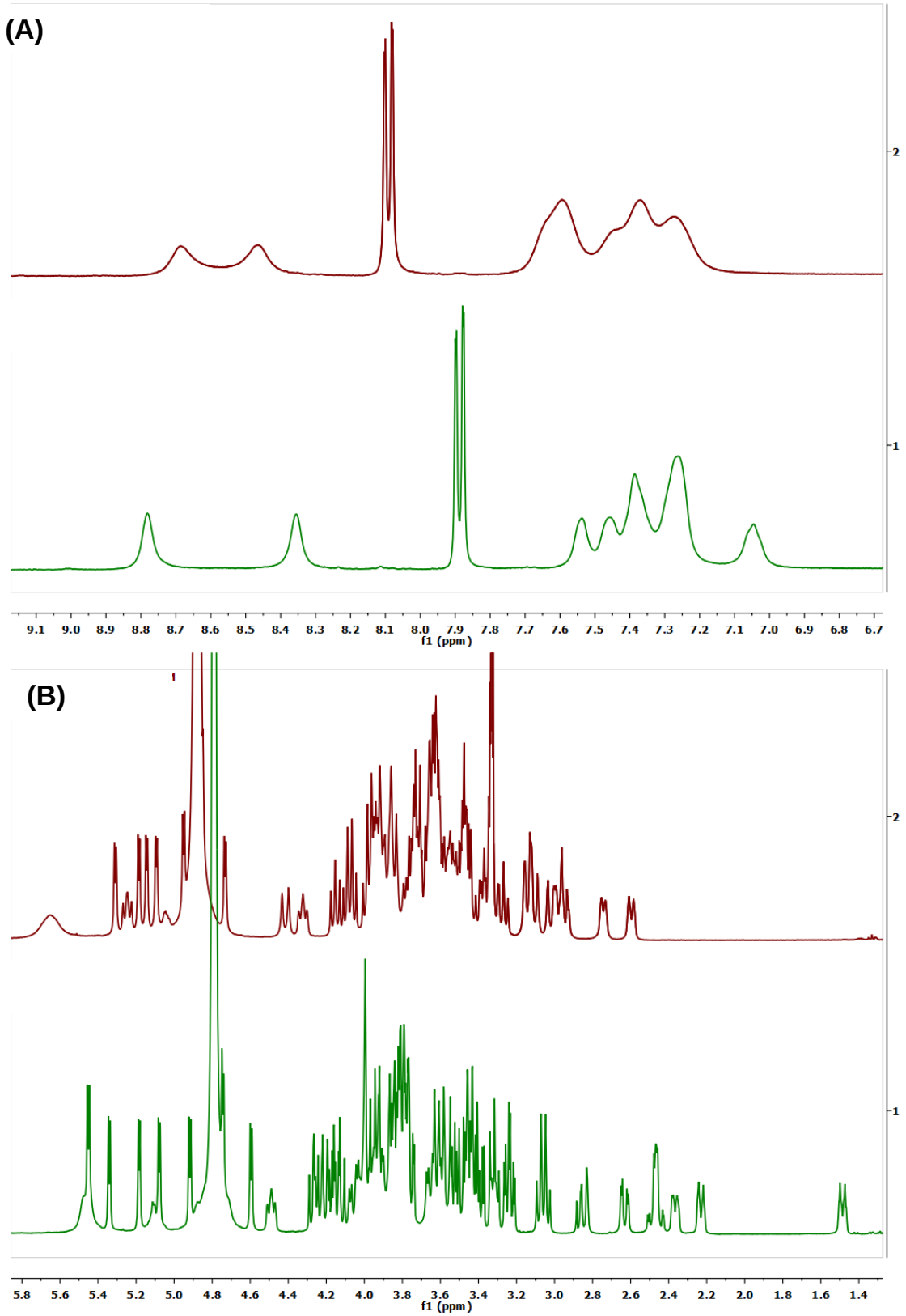

Figure S30. Expansion spectra of Figure S29 in the (A) aromatic proton region and (B) CDX proton region, Related to Figure 1.

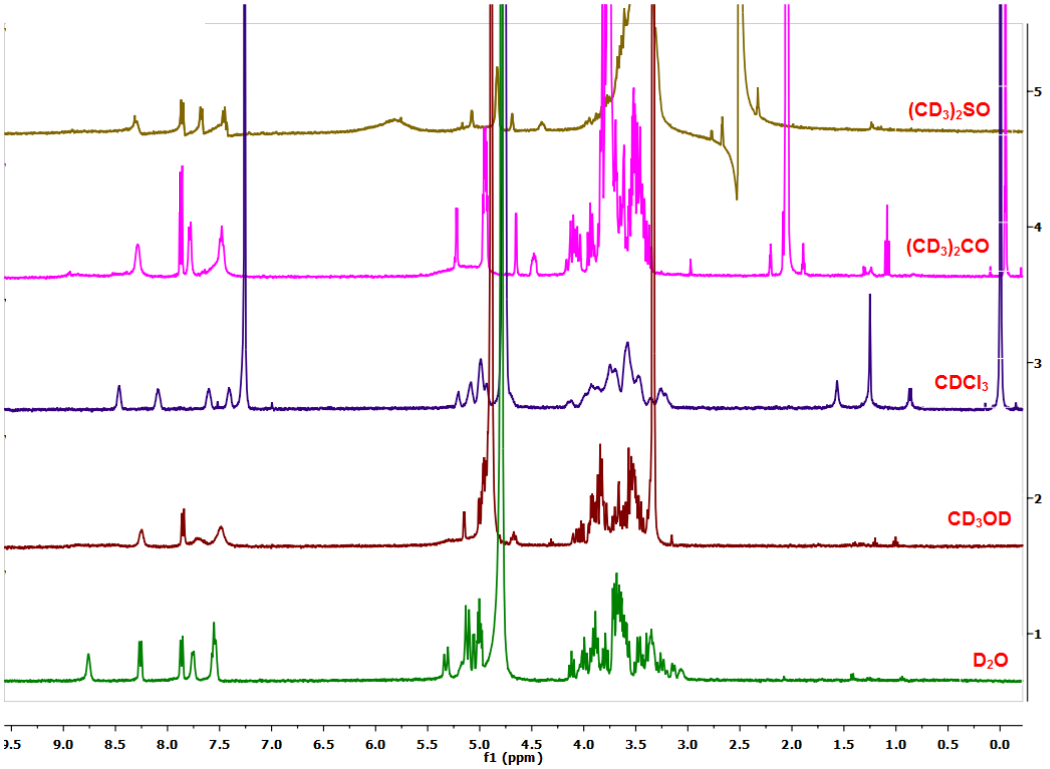

Figure S31. ^{1}H NMR Spectrum of BCDX-QUI-2 (D_2O, CD_3OD, $CDCl_3$, Acetone-d_6, and DMSO-d_6, 400 MHz, 25 °C), Related to Figure 1.

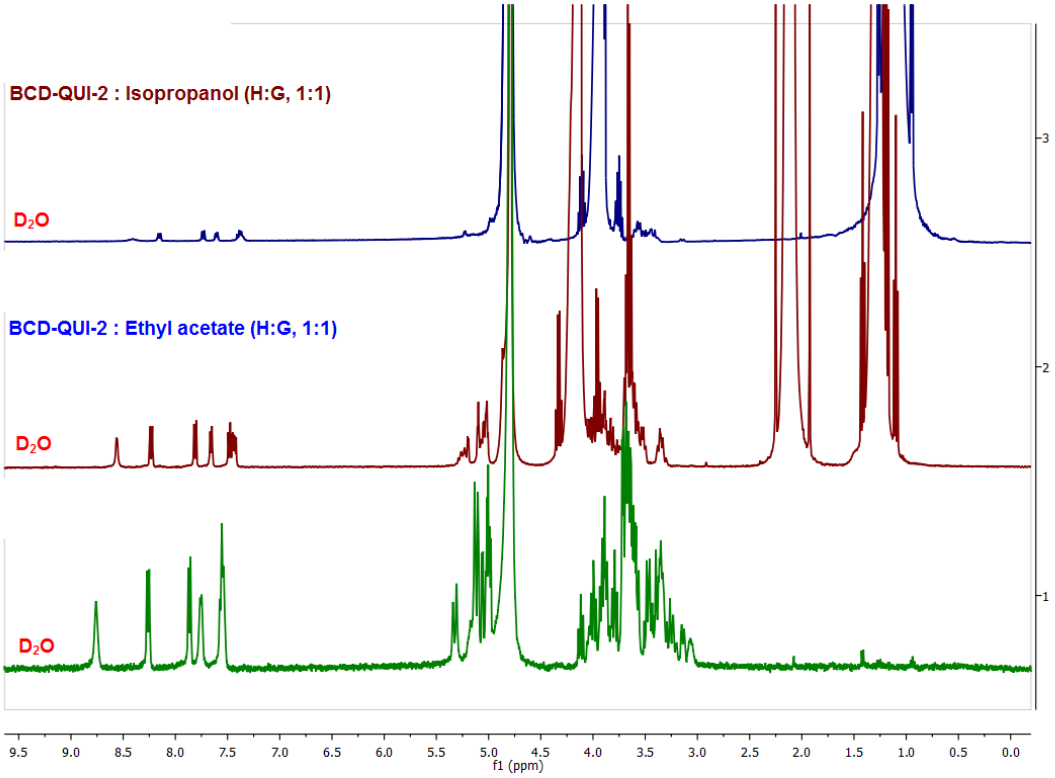

Figure S32. ^{1}H NMR Spectrum of 1:1 complex of BCDX-QUI-2 with ethyl acetate and isopropanol (D_2O, 400 MHz, 25 °C), Related to Figure 1.

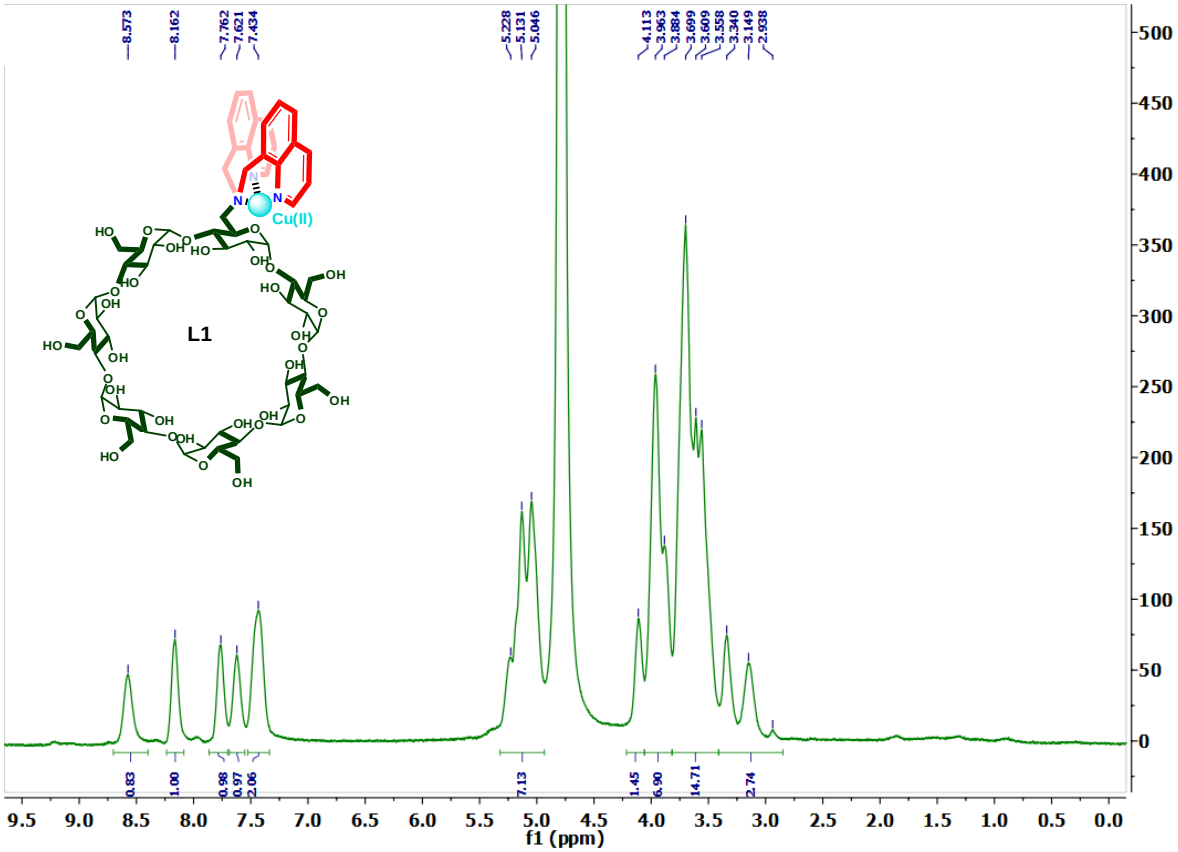

Figure S33. ^{1}H NMR Spectrum of probe **L1** (D_2O, 400 MHz, 25 °C), Related to Scheme 2.

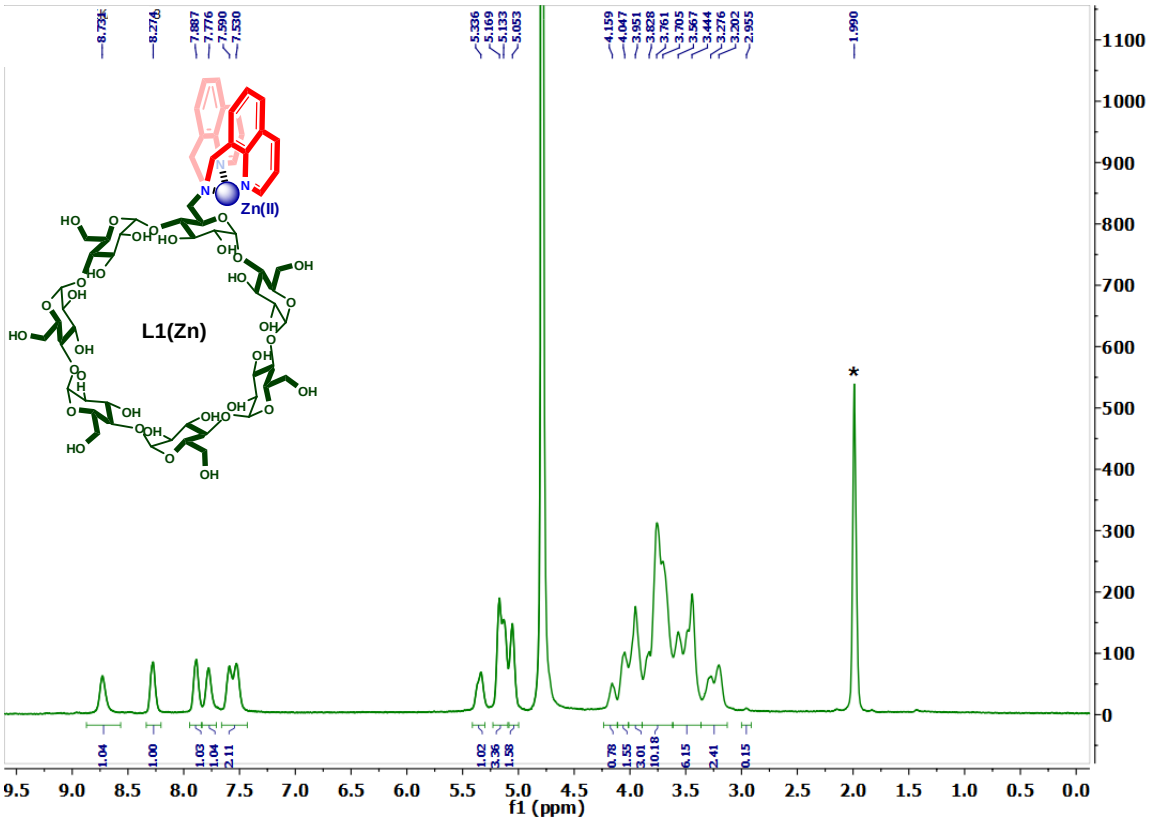

Figure S34. ^{1}H NMR Spectrum of probe **L1(Zn)** (D_2O, 400 MHz, 25 °C) (*CH_3COO^-), Related to Scheme 2.

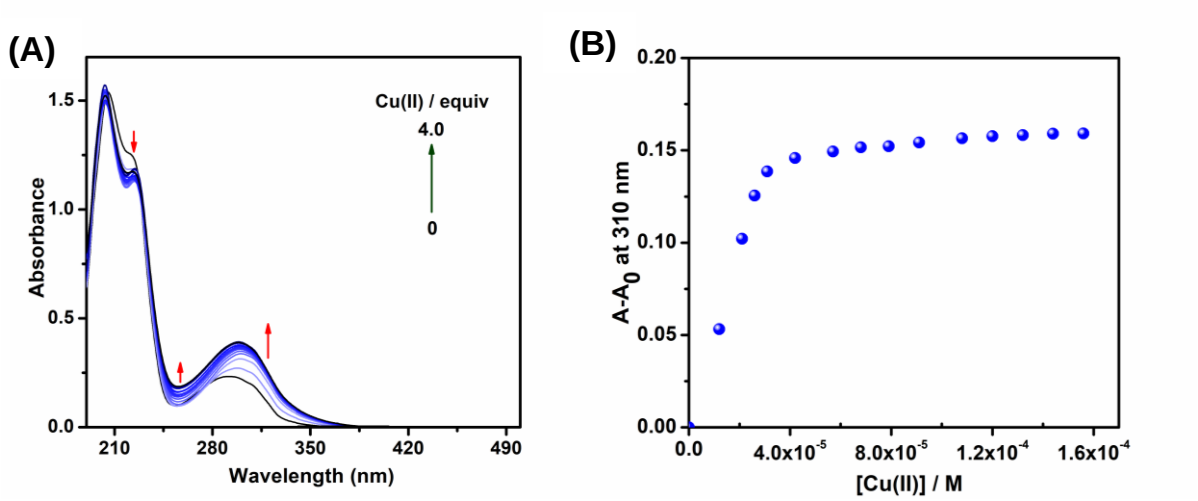

Figure S35. (A) UV-vis absorption spectra and (B) titration curve at 310 nm for BCDX-QUI-2:Cu(II) complex (**L1**) in water, at 25 °C. [BCDX-QUI-2] = 3.68 × 10^{-5} M, [Cu(II)] = 0 – 1.47 × 10^{-4} M, Related to Scheme 2.

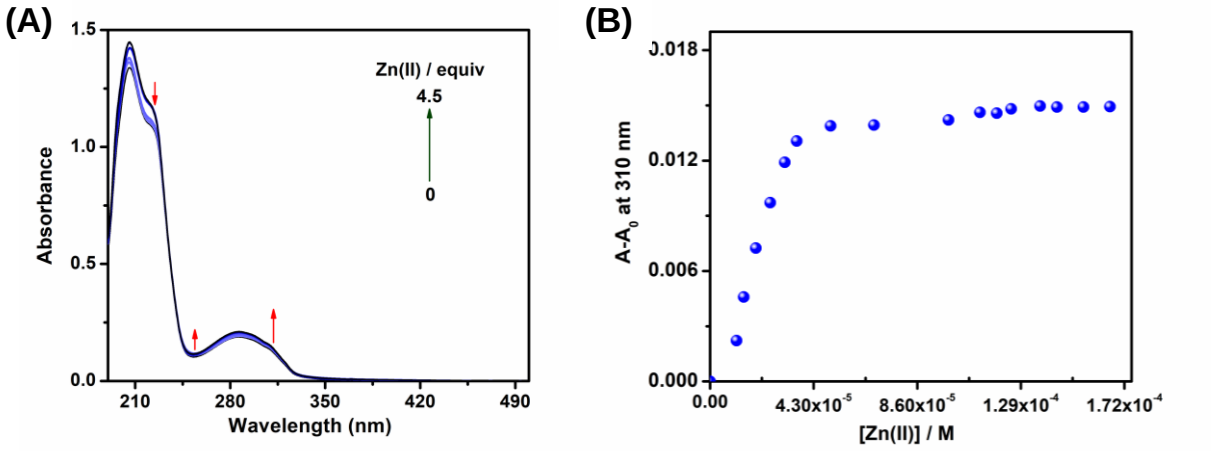

Figure S36. (A) UV-vis absorption spectra and (B) titration curve at 310 nm for BCDX-QUI-2: Zn (II) complex [**L1(Zn)**] in water, at 25 °C. [BCDX-QUI-2] = 3.68 × 10^{-5} M, [Zn(II)] = 0 - 1.66 × 10^{-4} M, Related to Scheme 2.

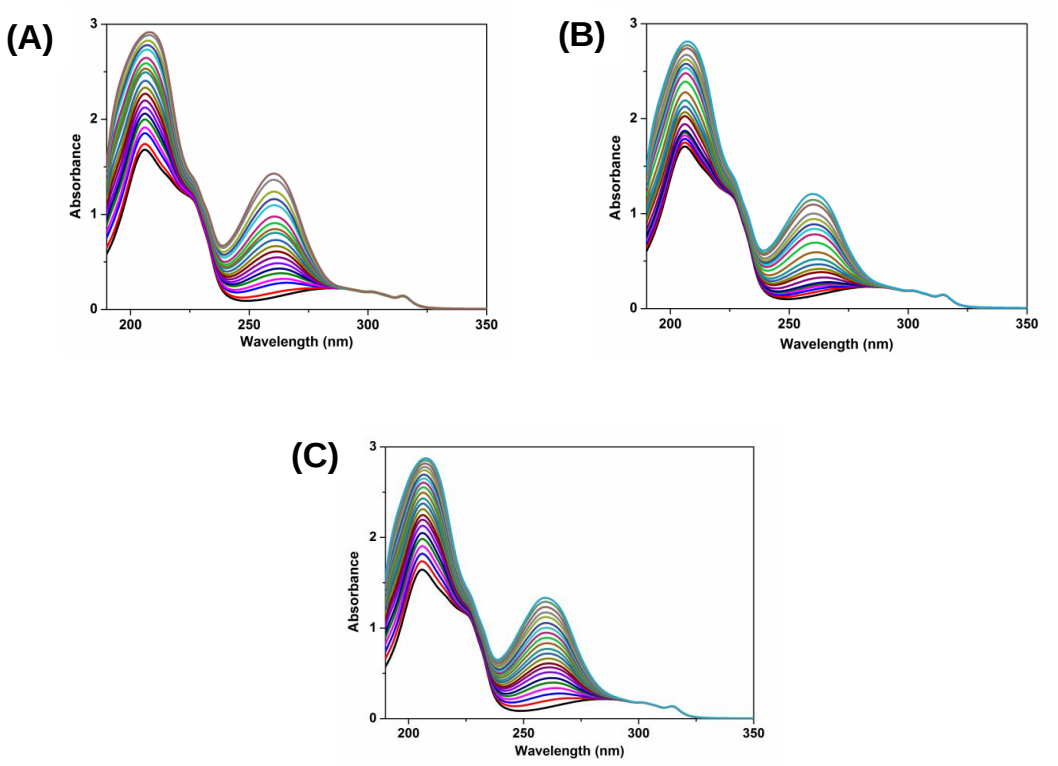

Figure S37. UV-vis absorption spectral changes for receptor BCDX-QUI-2 (37 μM) with nucleotides (A) AMP, (B) ADP and (C) ATP in aqueous medium at room temperature, Related to Scheme 1.

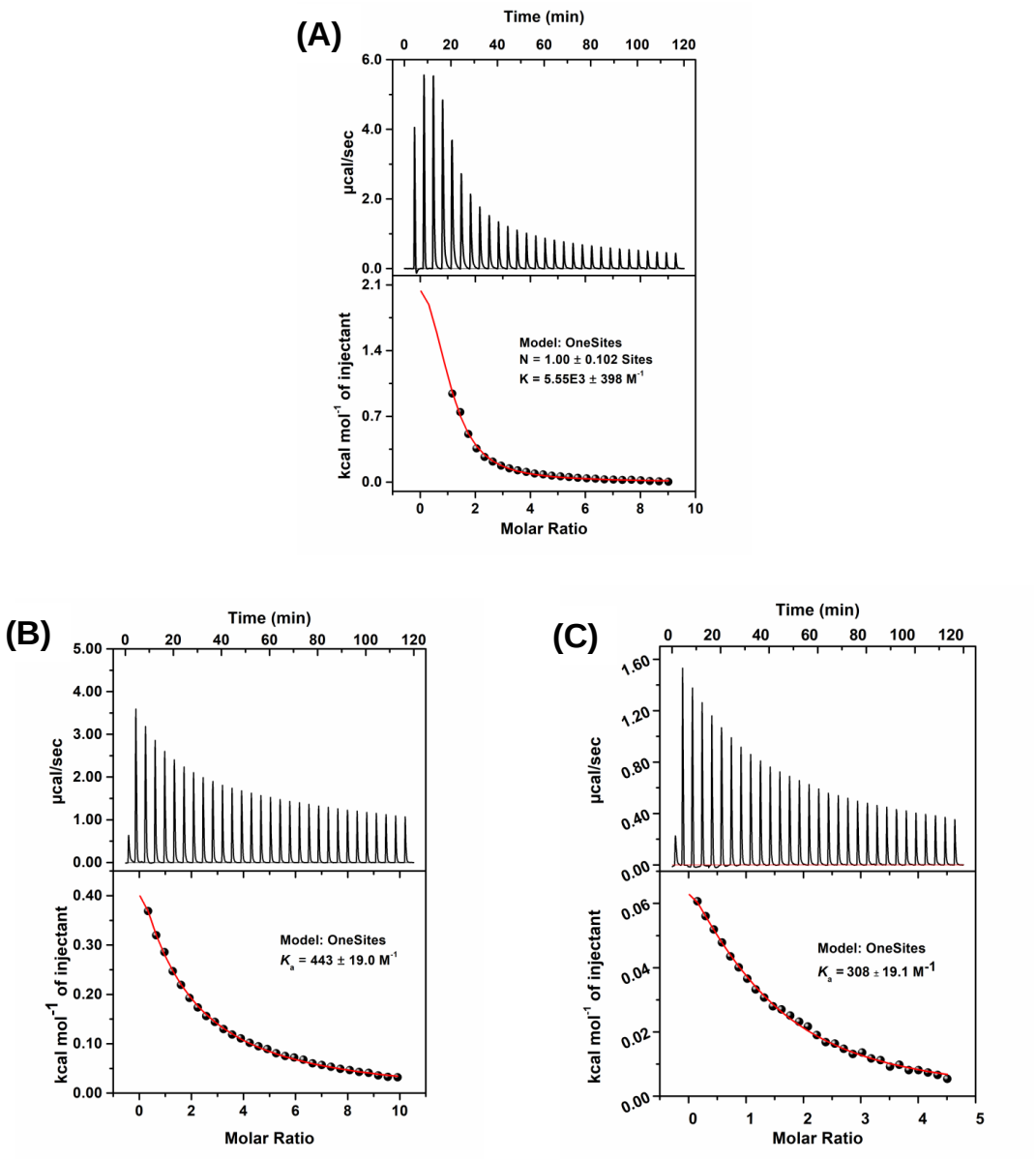

Figure S38. ITC titration of receptor BCDX-QUI-2 into the aqueous solution of nucleotides (A) AMP, (B) ADP and (C) ATP at 25 °C, Related to Scheme 1.

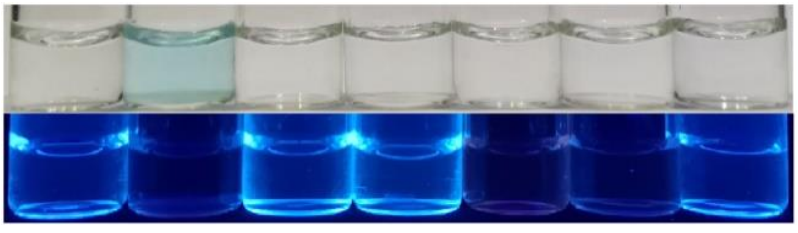

Figure S39. Color change of probe **L1** upon addition of nucleotides and inorganic phosphates under (top row) day light and (bottom row) illumination by a UV lamp (365 nm). From left to right: control (**L1** alone), **L1** + AMP, **L1** + ADP, **L1** + ATP, **L1** + Pi, **L1** + PPi and **L1** + triPi, Related to Scheme 3 and Figures 3, 4, 5, 6 and 7.

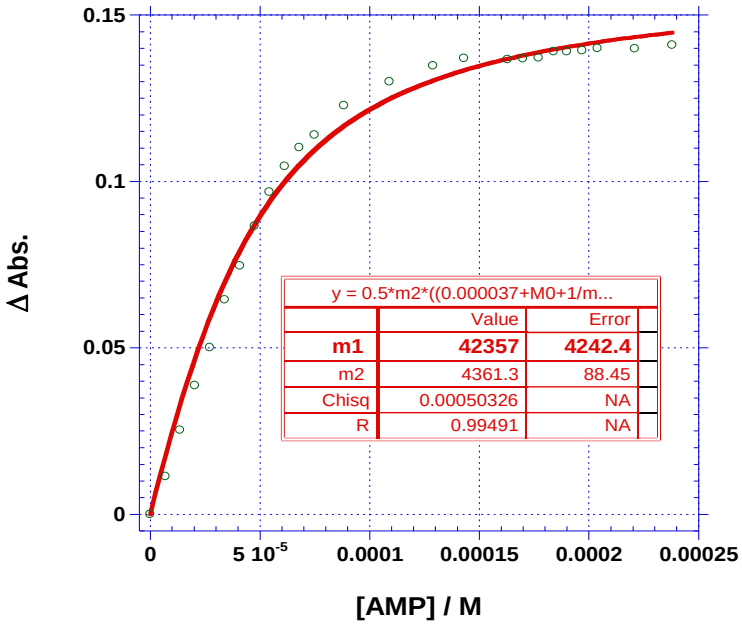

Figure S40. Binding constant plot for probe **L1** with AMP in aqueous medium at room temperature, Related to Table 1.

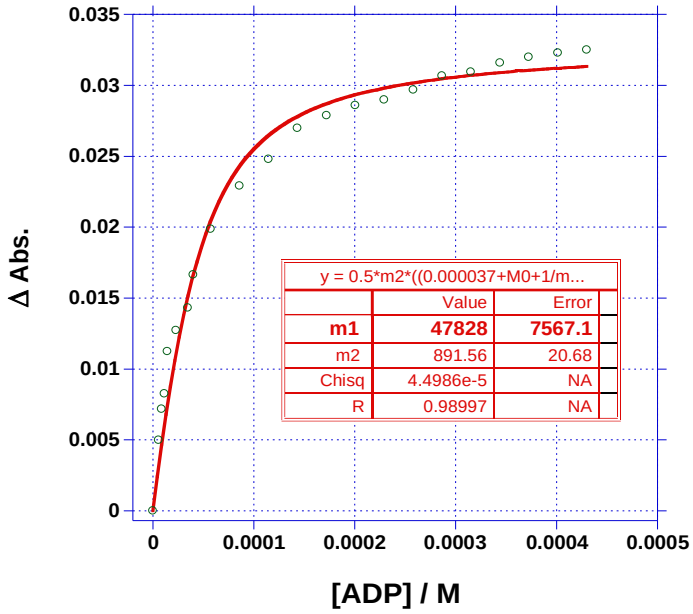

Figure S41. Binding constant plot for probe **L1** with ADP in aqueous medium at room temperature, Related to Table 1.

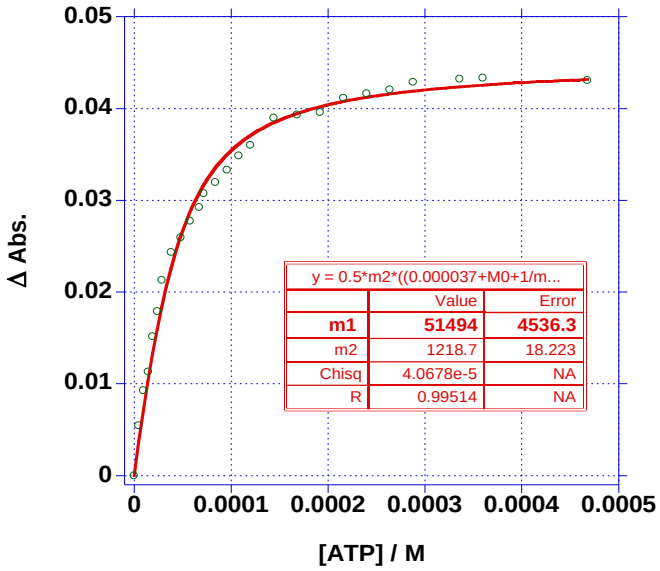

Figure S42. Binding constant plot for probe **L1** with ATP in aqueous medium at room temperature, Related to Table 1.

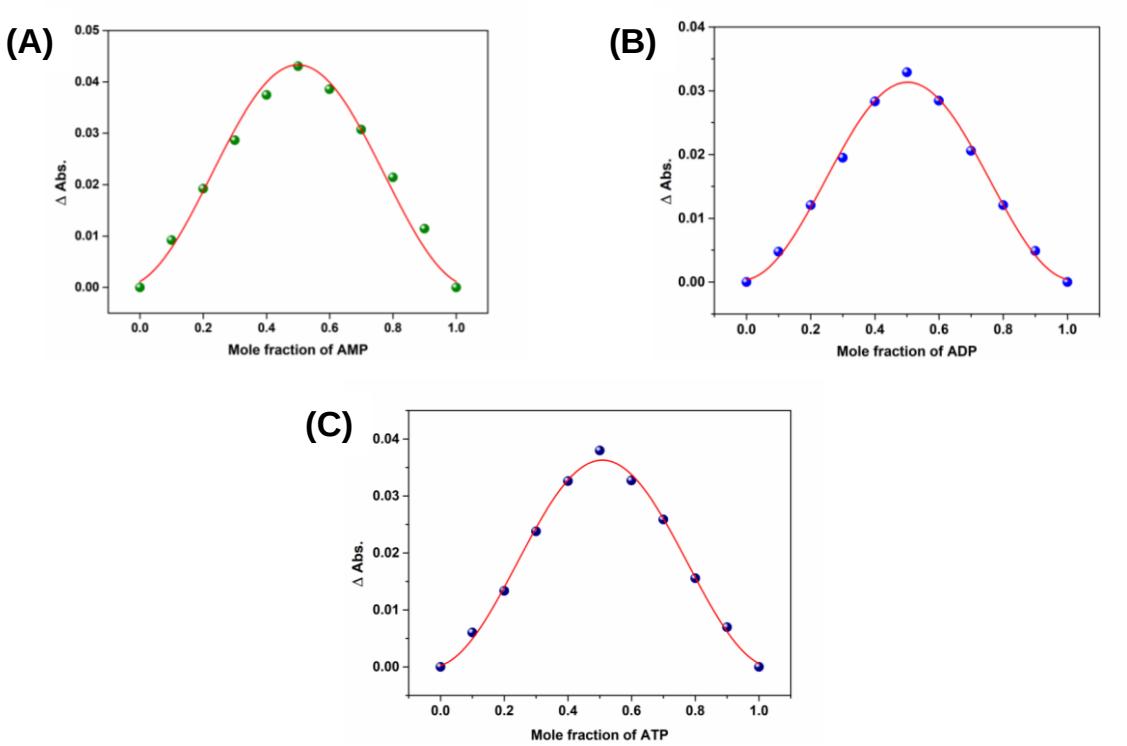

Figure S43. Job's plot of probe **L1** with nucleotides (A) AMP, (B) ADP, and (C) ATP in aqueous medium at room temperature (λ_{max} = 315 nm). [**L1**] • [AMP] = 5 × 10^{-5} M; [**L1**] • [ADP] = 5 × 10^{-5} M; [**L1**] • [ATP] = 5 × 10^{-5} M, Related to Table 1 and Scheme 2.

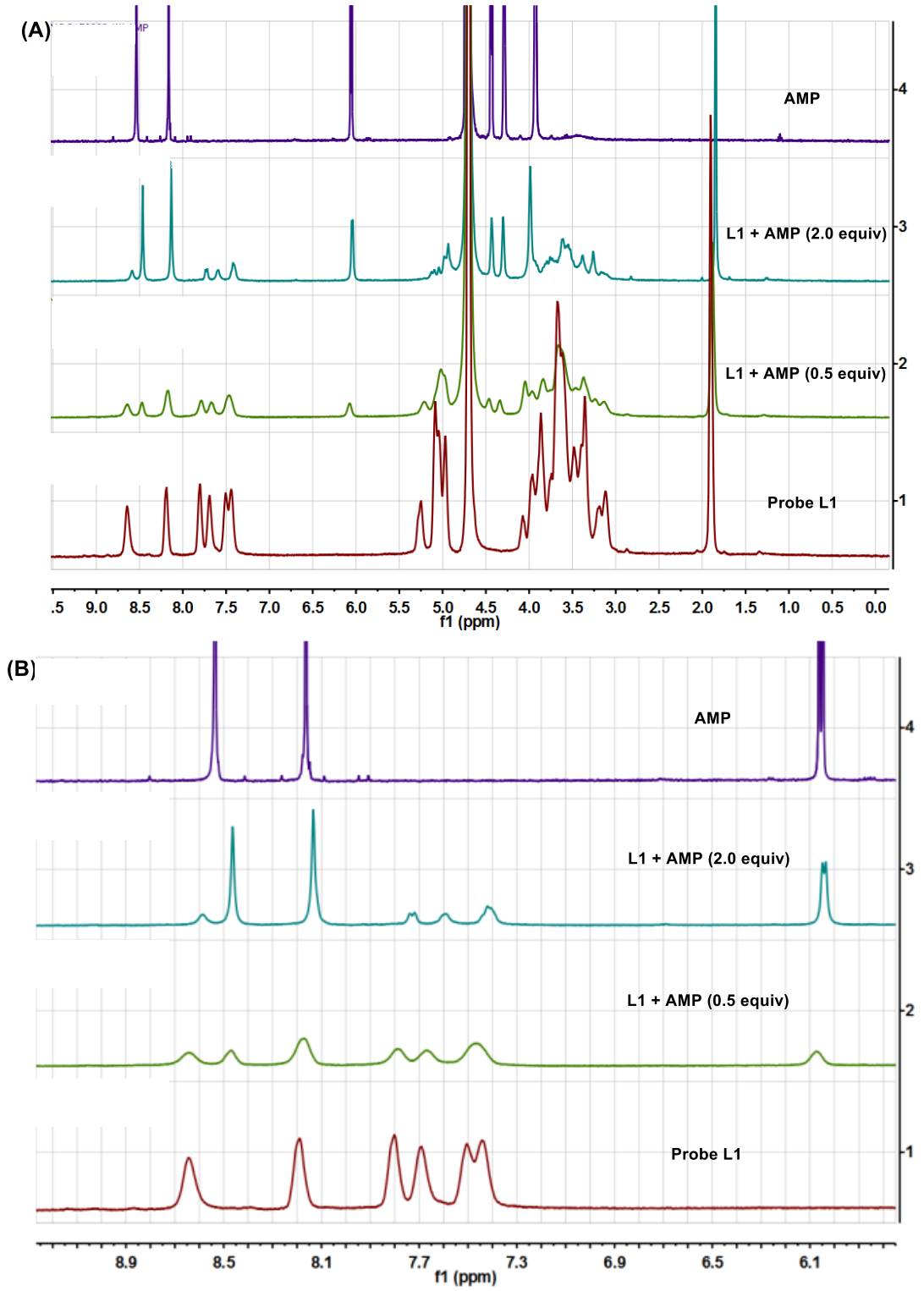

Figure S44. (A) Comparison of ^{1}H NMR spectrum of probe **L1** by adding different equiv. of AMP (D_2O, 400 MHz, 25 °C). (B) Expanded spectrum of (A), Related to Scheme 3.

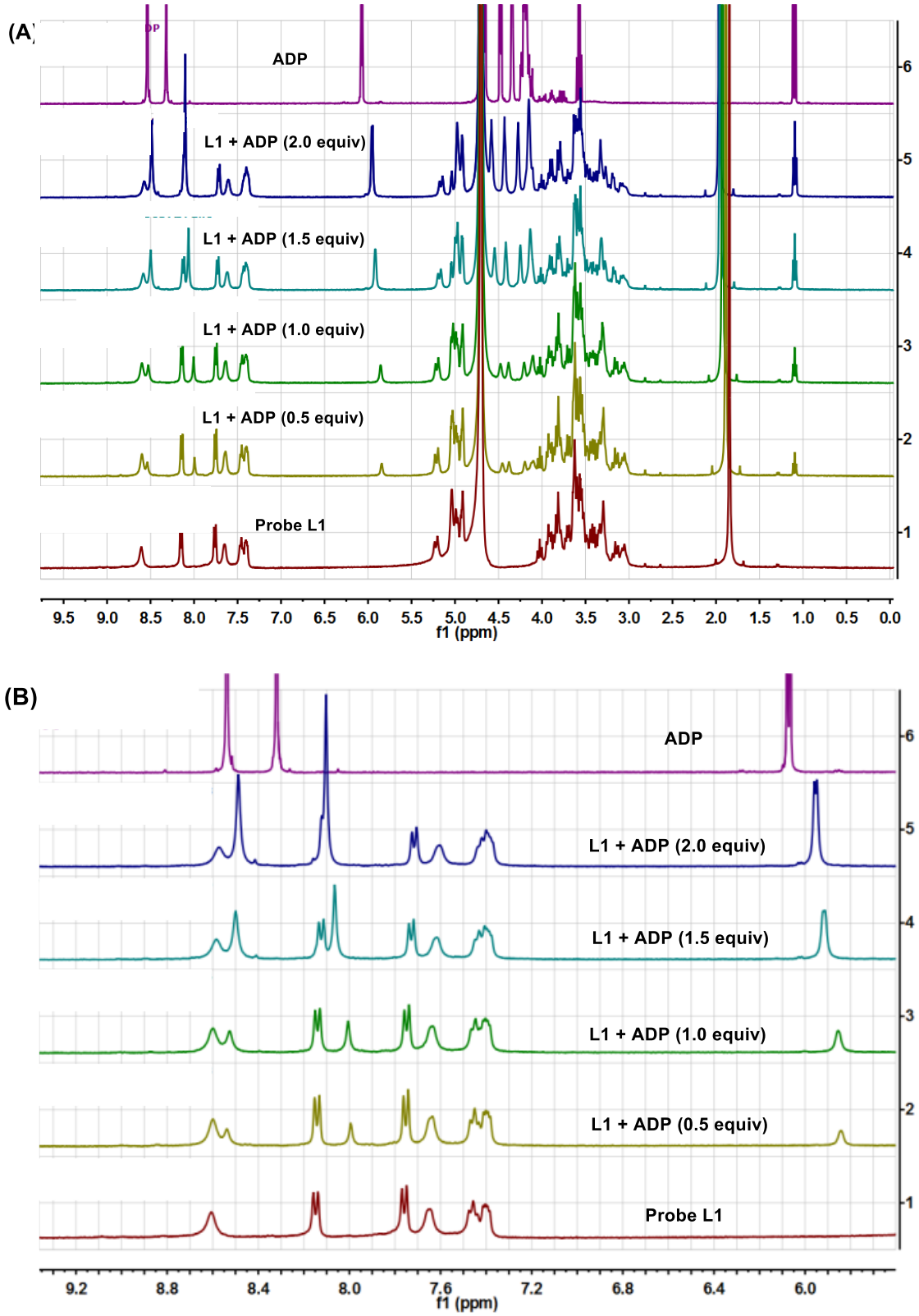

Figure S45. (A) Comparison of ^{1}H NMR spectrum of probe **L1** by adding different equiv. of ADP (D_2O, 400 MHz, 25 °C). (B) Expanded spectrum of (A), Related to Scheme 3.

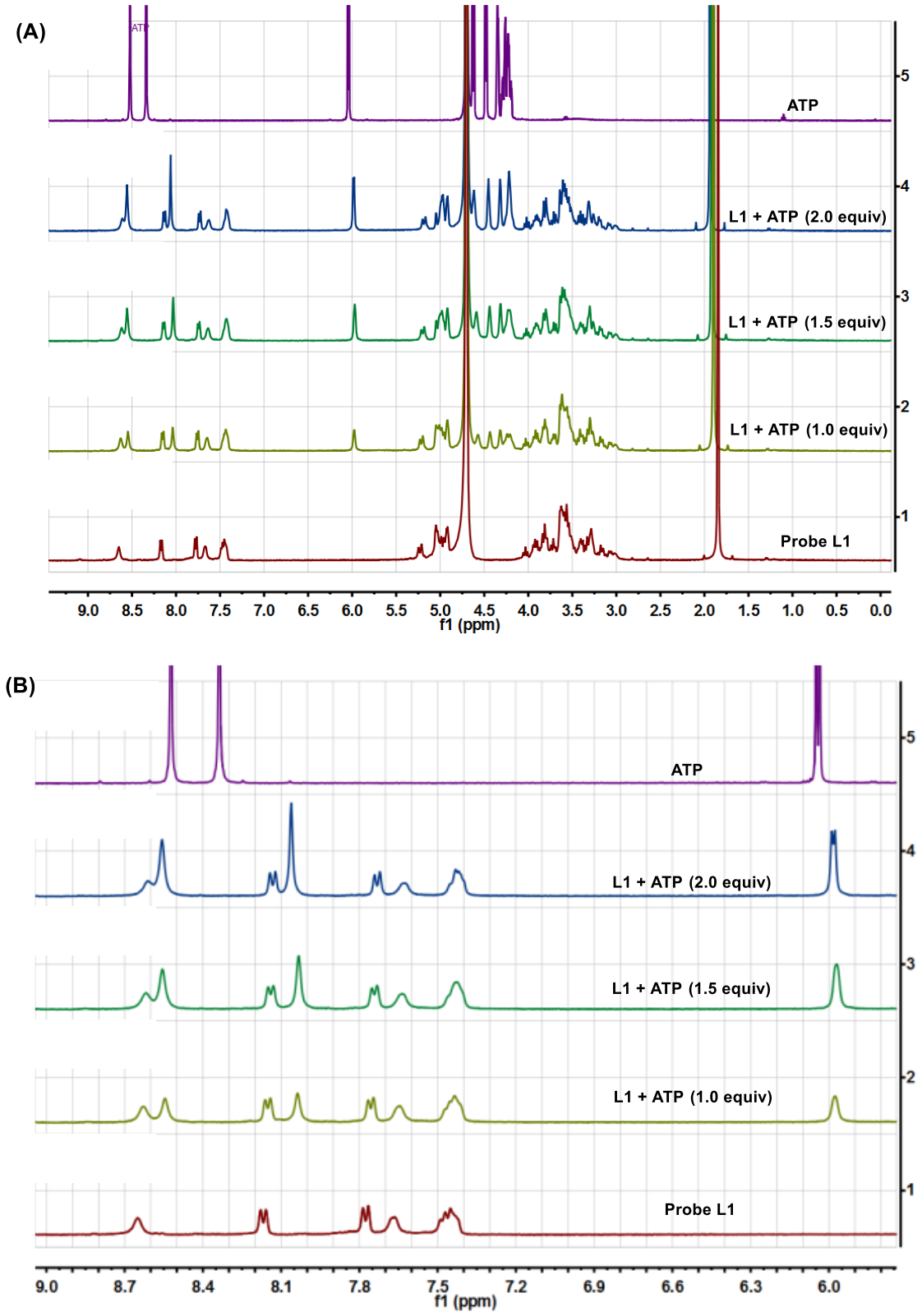

Figure S46. (A) Comparison of ^{1}H NMR spectrum of probe **L1** by adding different equiv. of ATP (D_2O, 400 MHz, 25 °C). (B) Expanded spectrum of (A), Related to Scheme 3.

(A) Probe L2 Vs nucleotides

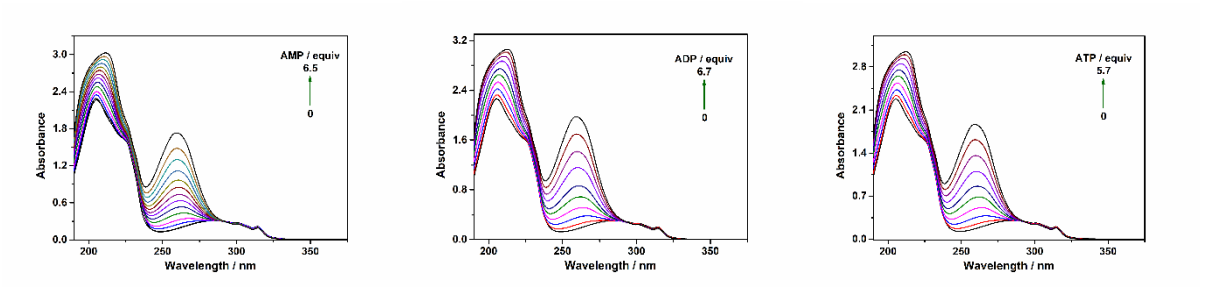

(B) Probe L3 Vs nucleotides

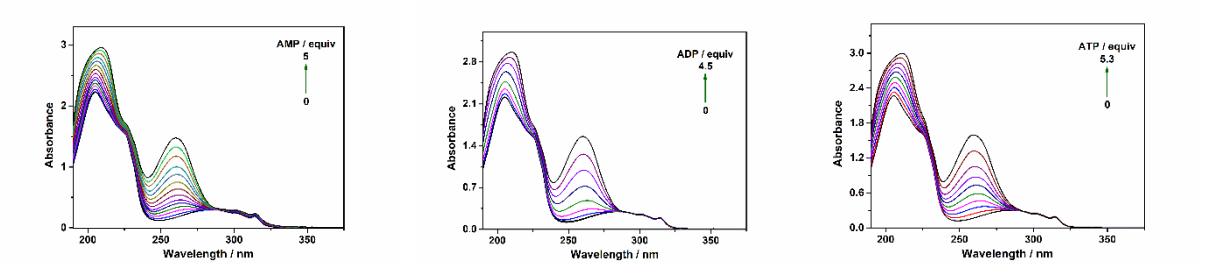

(C) Probe L2 Vs nucleotides

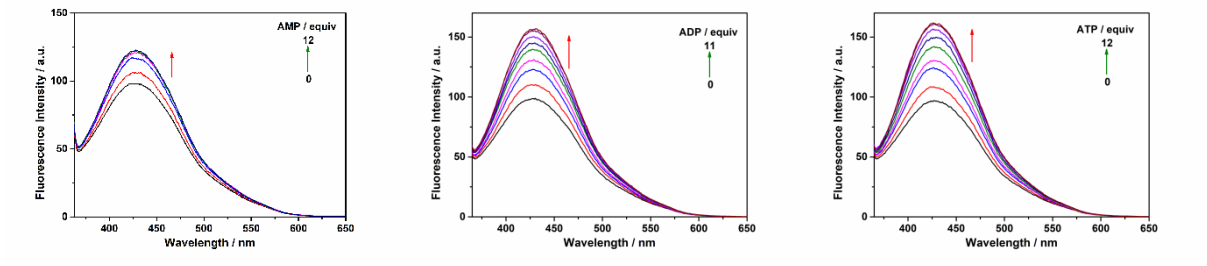

(D) Probe L3 Vs nucleotides

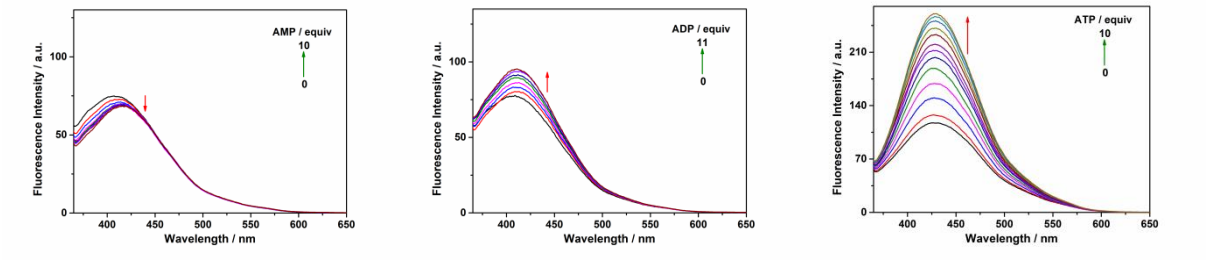

Figure S47. (A) & (B) UV-vis absorption and (C) and (D) fluorescence spectral changes ($\lambda_{exc.}$ = 315 nm) of probe **L2** (A & C) and **L3** (B & D; 37 µM) upon addition of nucleotides (AMP, ADP and ATP), respectively in water at room temperature, Related to Scheme 3 and Figure 9.

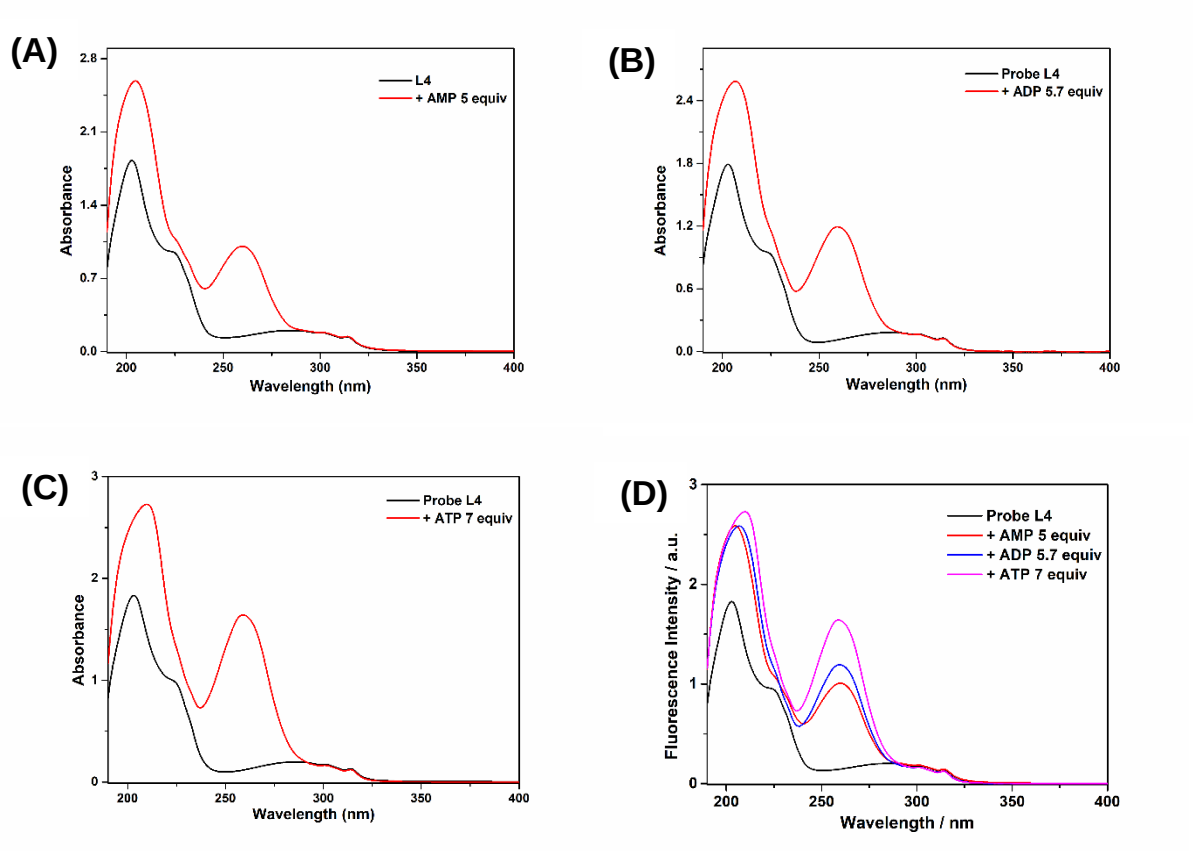

Figure S48. UV-vis absorption spectral change of control compound **L4** (Bu-QUI-2:Cu(II), 42 µM) upon addition of nucleotides (A) AMP, (B) ADP, and (C) ATP in aqueous medium at room temperature. (D) Combined spectra of **L4**:nucleotide complexes, Related to Schemes 2 and 3.

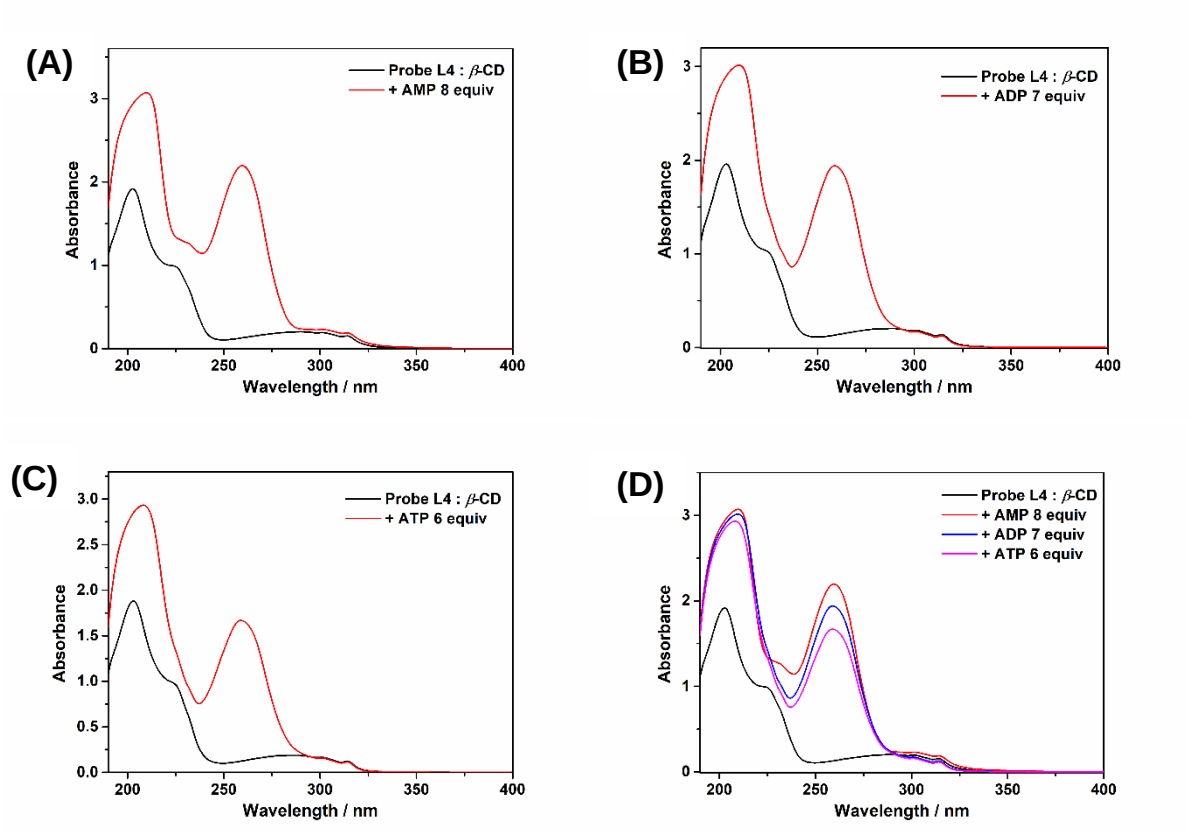

Figure S49. UV-vis absorption spectral changes of control compound **L4** (42 μM) and *β*-CDX (10 equiv) upon addition of nucleotides (A) AMP, (B) ADP, and (C) ATP in aqueous medium at room temperature. (D) Combined spectra of **L4**:*β*-CDX:nucleotide complexes, Related to Schemes 2 and 3.

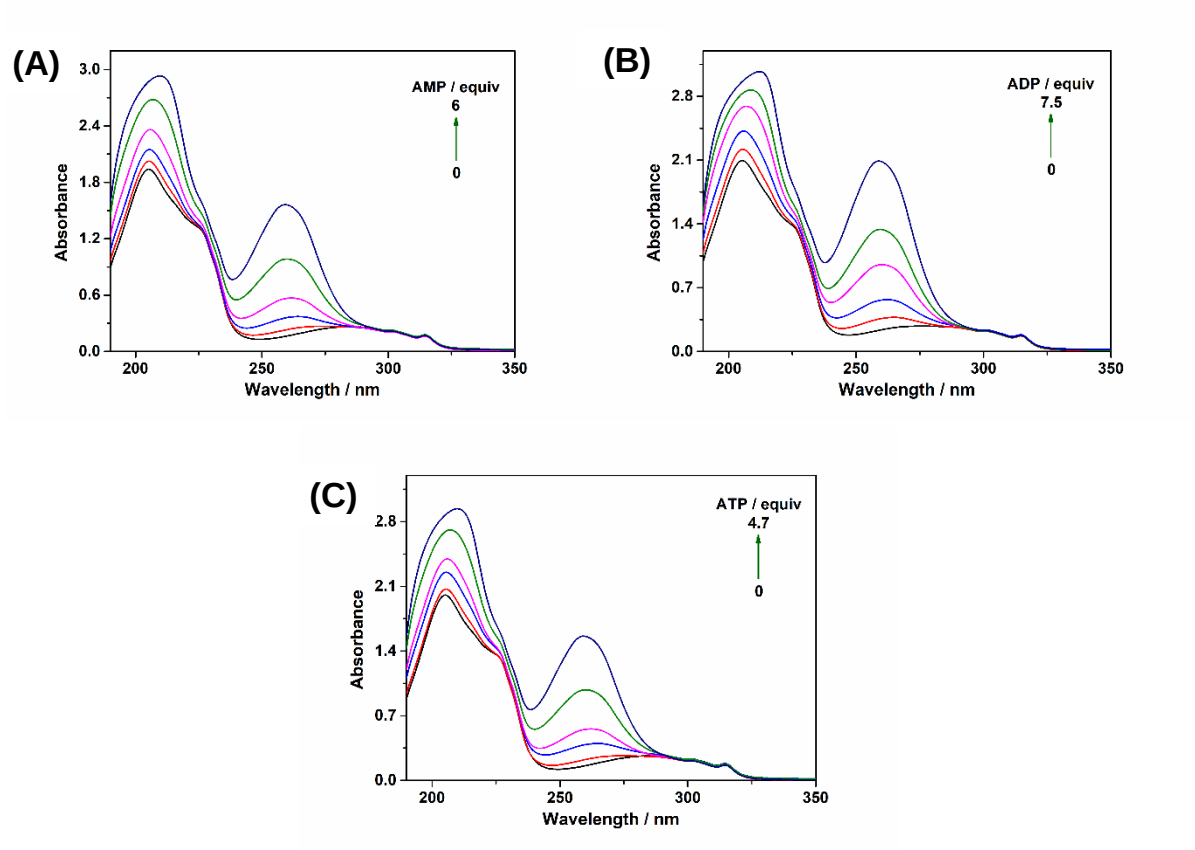

Figure S50. UV-vis absorption spectral changes ($\lambda_{exc.}$ = 315 nm) of probe **L1**:1-adamantanecarboxylic acid (1-AdCA) complex (1:1, H:G ratio) upon addition of nucleotides (A) AMP, (B) ADP, and (C) ATP in aqueous medium at room temperature, Related to Schemes 2 and 3.

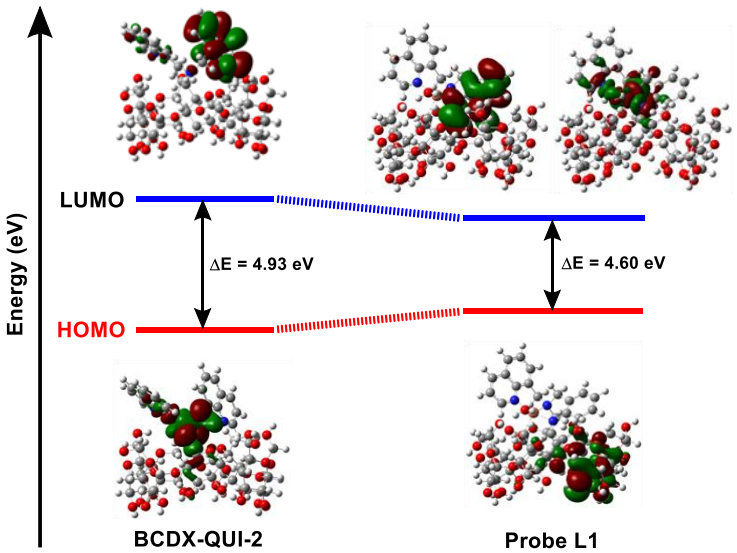

Figure S51. DFT optimized structures, HOMO-LUMO energy levels and the interfacial plots of the orbitals for BCDX-QUI-2 and the differentiating probe **L1**, Related to Figure 10.

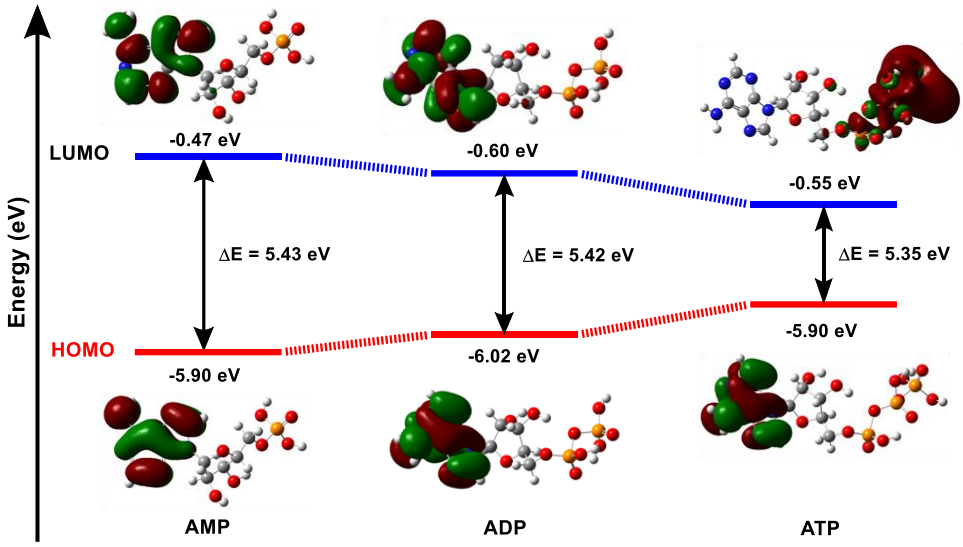

Figure S52. DFT optimized structures, HOMO-LUMO energy levels and the interfacial plots of the orbitals for AMP, ADP and ATP, Related to Figure 10.

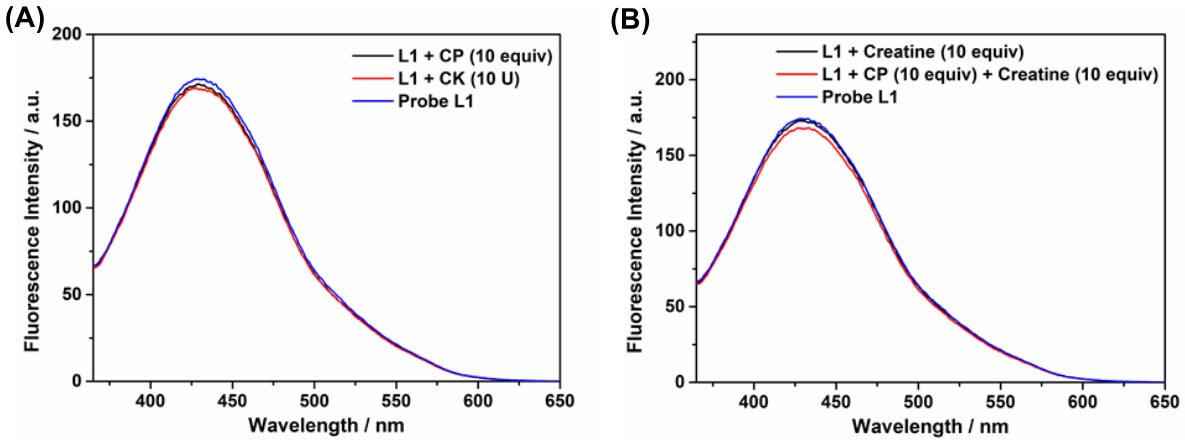

Figure S53. Fluorescence spectra of the solution of (A) probe **L1** (37 μM), **L1** + CP (10 equiv) and **L1** + CK (10 equiv) and (B) probe **L1** (37 μM), **L1** + creatine (10 equiv) and **L1** + CP (10 equiv) + creatine (10 equiv) in water, Related to Scheme 4 and Figure 11.

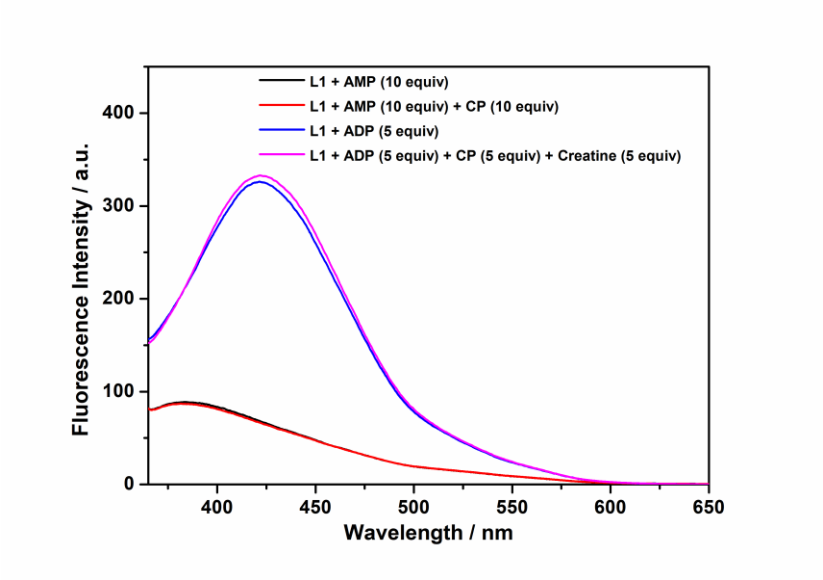

Figure S54. Fluorescence spectra of the solution of probe **L1** (37 µM) + AMP (10 equiv), **L1**+ CP (10 equiv), **L1** + ADP (5 equiv) and **L1** + ADP (5 equiv) + CP (5 equiv) + creatine (5 equiv) in water, Related to Scheme 4 and Figure 11.

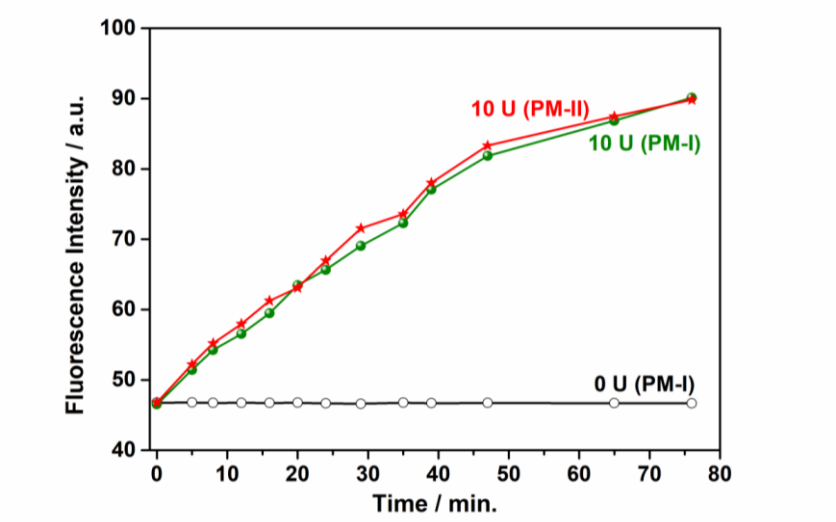

Figure S55. Time-trace plots of CK catalysed AMP phosphorylation monitored by emission intensity at 427 nm (λ_{exc} = 315 nm) in two different methods PM-I and PM-II, [AMP] = 370 µM, [CP] = 13 equiv, [CK] = 0 and 10 units, MES buffer (10 mM, pH = 6.5) at 37 °C, Related to Scheme 4 and Figure 11.

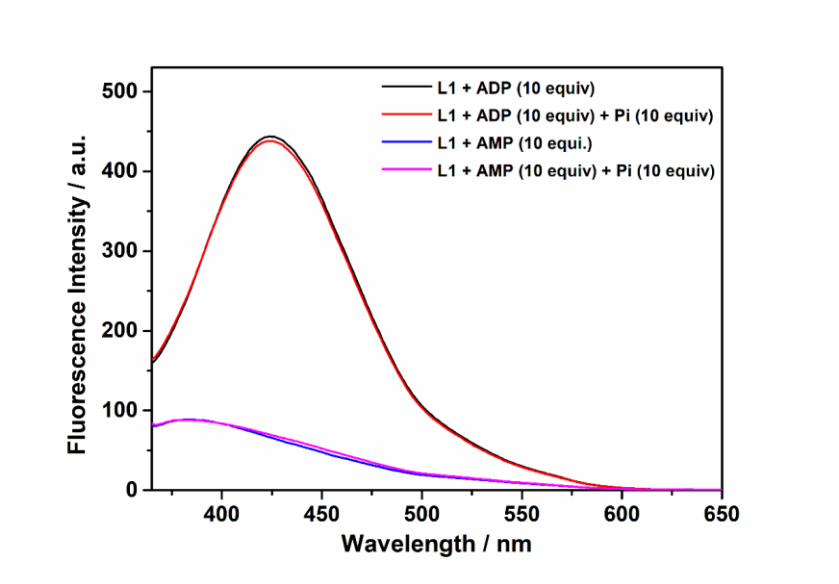

Figure S56. Fluorescence spectra of the solution of probe **L1** (37 μM) + ADP (10 equiv), **L1** (37 μM) + ADP (10 equiv) + Pi (10 equiv), **L1** (37 μM) + AMP (10 equiv) and **L1** (37 μM) + AMP (10 equiv) + Pi (10 equiv) in water, Related to Scheme 4 and Figure 11.

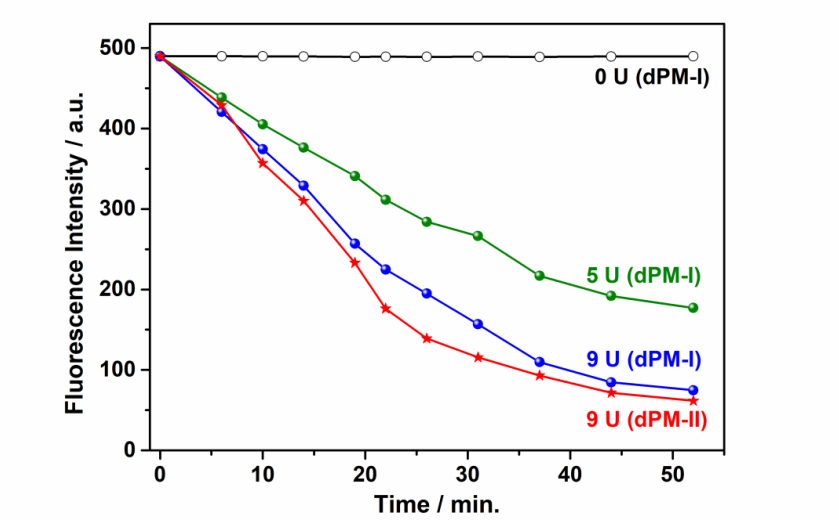

Figure S57. Time-trace plots of apyrase catalysed ADP dephosphorylation monitored by emission intensity at 427 nm (λ_{exc} = 315 nm) in two different methods PM-I and PM-II, [ADP] = 370 μM, [apyrase] = 0, 5 and 9 units, HEPES buffer solution (10 mM, pH = 7.4) at 37 °C, Related to Scheme 4 and Figure 11.

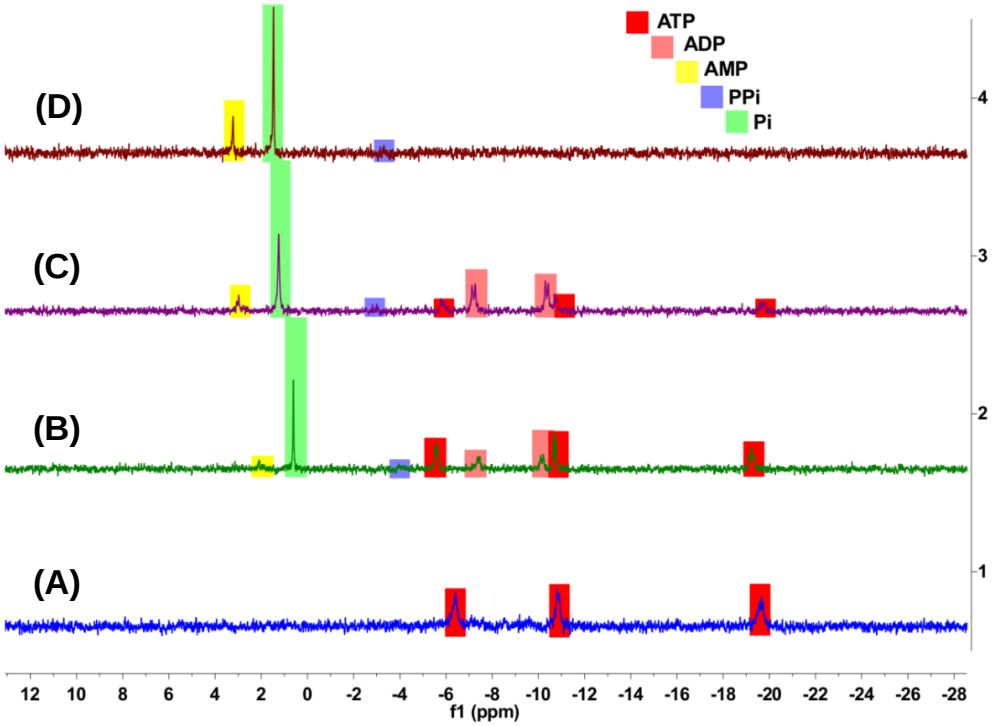

Figure S58. Monitoring the hydrolytic apyrase enzyme catalyzed dephosphorylation of ATP → ADP → AMP and Pi using ^{31}P NMR spectra (400 MHz) in HEPES buffer solution (D_2O, 10 mM, pH = 7.4) at 25 °C. (A) probe **L1(Zn)**:ATP - apyrase mixture; the reaction mixture was quenched the apyrase hydrolysis with EDTA (250 μM) at different time intervals, (B) after 10 min.; (C) after 20 min.; (D) completion of the reaction, Related to Scheme 4 and Figures 8 and 11.

Supplemental Tables

Table S1. Association constants (k_a) determined for receptor BCDX-QUI-2 and nucleotides in aqueous medium at room temperature, Related to Scheme 1.[a]

Host	Guest	k_a / M^{-1}
BCDX-QUI-2	AMP [b]	5.55 x 10^3
BCDX-QUI-2	ADP [b]	443
BCDX-QUI-2	ATP [b]	308
BCDX-QUI-2	Other anions [c]	-

[a] All of the nucleotides were added as sodium salts. [b] Determined using ITC measurements. [c] Other anions – not determined

Transparent Methods

Materials: α-Cyclodextrin (CDX) (Junsei, Japan), β-CDX (BODI, China), γ-CDX (Junsei, Japan), 1-butylamine (Adamas, China), and 8-bromomethylquinoline (Adamas, China) were purchased and are used as received without further purification. Nucleotides such as AMP, ADP, and ATP, as well as the corresponding inorganic phosphates Pi, PPi, and triPi were purchased from Aladdin (China) and used as received without further purification. Double distilled deionized water and HPLC grade solvents were used for all spectral measurements. All other chemicals and solvents were purchased from Adamas-beta, Amethyst, or Oceanpak and used as received without further purification.

Methods: Reverse phase chromatography was used to separate the CDX derivatives and water-soluble compounds using an ODS-SM-50C column and water - 90% EtOH/MeOH (v/v) (linear elution) in water as eluent. Nuclear magnetic resonance spectroscopy (NMR) was acquired on a Bruker Ascend 400 (400 MHz) instrument using TMS as an internal standard at 298 K. Coupling constants are reported in Hz and chemical shifts (δ) in ppm [relative to TMS (0.00) or residual solvent peaks; for ^{1}H ($CDCl_3$: 7.26, DMSO-d_6: 2.50, D_2O: 4.79, CD_3CN: 1.94, CD_3OD: 3.31) and ^{13}C ($CDCl_3$: 77.16, DMSO-d_6: 39.52, CD_3CN: 1.32, 118.26, CD_3OD: 49.00)] (Gottlieb et al., 1997). Multiplicities were assigned as s (singlet), d (doublet), t (triplet), q (quartet), m (multiplet) and brs (broad singlet). 2D NMR COSY and ROESY were recorded, if necessary; ROESY spectrum were obtained using a Bruker Ascend 400 (400 MHz) instrument in D_2O/CD_3OD at 25 °C with a mixing time of 250 ms. Ultraviolet-visible absorption spectroscopy (UV-Vis.) measurements were recorded using a JASCO V-650 double beam spectrophotometer with PMT detector. UV-Vis. analyses were done using JASCO-Spectral manager and the calculations were done in Microsoft Origin software. Fluorescence spectroscopy was recorded using JASCO FP-8500 or Fluoromax-4 (attached with TCSPC) spectrofluorometer (HORIBA JOBIN YVON) with the excitation slit set at 5.0 nm band pass and emission at 5.0 nm band pass in 1 x 1 cm quartz cell. Emission calculations were done using Microsoft Origin software. Circular dichroism spectroscopy (CD) was measured on a JASCO J-1500 spectropolarimeter with PMT detector in the wavelength range 190-900 nm. For these studies, solutions were of less or higher concentration than those for spectrophotometric studies. Sample cell temperature was controllable in the range from -90 °C to 100 °C. Mass spectral data were obtained using Electrospray Ionization Mass Spectrometry (ESI-MS). Isothermal titration calorimetry (ITC) data were recorded by using a VP-ITC MicroCalorimeter.

Mass spectral analysis: ESI-MS analysis was performed in the positive/negative ion mode on a liquid chromatography-ion trap mass spectrometer (Waters® Q-Tof Premier™, Waters Corporation, USA). The samples were introduced into the ion source by direct nanoflow method at different flow rates. The high-resolution *m/z* rang up to 100,000.

Synthesis and characterization of CDX receptors and control compounds: The detailed synthetic procedures for the synthesis of mono-6-deoxy-6-amino-*α*-/*β*-/*γ*-CDX derivatives (Mono-6-NH2-ACDX/BCDX/GCDX) (Scheme S2), mono-*N*-bis-(8-methylquinolyl)-tethered CDX derivatives (CDX-QUI-2) (Scheme S3), reference compound Bu-QUI-2 (Scheme S4), and probes **L1/L1(Zn), L2, L3, L4** (Scheme S5).

Synthesis and characterization of mono-aminocyclodextrins (Mono-6-NH_2-ACDX/BCDX/GCDX): Mono-6-amino-*α*-CDX (mono-6-NH_2-ACDX), mono-6-amino-*β*-CDX (mono-6-NH_2-BCDX) and mono-6-amino-*γ*-CDX (mono-6-NH_2-GCDX) were synthesized and purified according to the procedure described in the literature (Scheme S2) (Tang, and Ng, 2008). The product was dried for 24 h under vacuum at 60 °C and then stored in a vacuum desiccator and are characterized by ^{1}H and ^{13}C-NMR, and ESI-MS analysis, which were in accordance with literature reports (Tang, and Ng, 2008).

Synthesis and characterization of mono-*N*-bis-(8-methylquinolyl) tethered CDX derivatives (Scheme S3, CDX-QUI-2): To a dry DMF solution (10 mL) of mono-6-NH_2-ACDX/BCDX/GCDX (0.971 g; 1.133 g; 1.296 g, 1 mmol), 8-bromomethylquinoline (0.489 g, 2.2 mmol) and DIPEA (0.2 mL) were added drop-wise. The reaction mixture was stirred at 80 °C for 24 h under a nitrogen atmosphere, then the solvent was removed under vacuum. The residue was dissolved in a small amount of DMF and then added drop-wise to acetone (300 mL). The resulting white precipitate was filtered and washed successively with acetone (20 mL x 4) to give the crude product. The crude product was loaded onto the preparative reverse phase column (ODS-SM-50C) and eluted with a linear gradient ranging from water to 40% (v/v) methanol-water. The desired fraction was collected, and the eluent was evaporated/lyophilized to yield the desired products as white powders. **Mono-[6-deoxy-6-*N*-bis(8-methylquinolyl)]-*α*-cyclodextrin (ACDX-QUI-2)** (yield 85%) ^{1}H NMR (400 MHz, D_2O, δ ppm): 8.41 (s, 1H), 8.14 (d, J = 8.2 Hz, 1H), 7.73 (d,

J = 8.3 Hz, 1H), 7.55 (dd, *J* = 4.3, 1.8 Hz, 1H), 7.38 (dd, *J* = 10.0, 4.1 Hz, 2H), 5.11 (d, *J* = 3.3 Hz, 1H), 5.02 (dd, *J* = 4.9, 3.7 Hz, 1H), 4.99 (d, *J* = 3.4 Hz, 1H), 4.96 (d, *J* = 3.4 Hz, 1H), 4.16 (t, *J* = 9.1 Hz, 1H), 4.01 (ddd, *J* = 10.7, 6.5, 3.2 Hz, 1H), 3.97 - 3.72 (m, 6H), 3.70 (d, *J* = 2.9 Hz, 2H), 3.63 - 3.43 (m, 7H), 3.36 (dd, *J* = 11.3, 6.8 Hz, 1H), 3.24 (d, *J* = 11.1 Hz, 1H). ^{13}C NMR (101 MHz, D_2O, δ ppm) : 149.37, 144.89, 137.35, 132.17, 130.07, 127.42, 126.41, 126.24, 121.95, 101.43, 100.77, 82.44, 80.98, 73.19, 72.71, 72.00, 71.69, 71.38, 67.51, 60.31, 58.73, 56.29. HRMS (ESI) *m/z* calcd. for $C_{56}H_{76}N_3O_{29}$ $[M + H]^+$ 1254.4564, found 1254.4571.

Mono-[6-deoxy-6-*N*-bis(8-methylquinolyl)]-*β*-cyclodextrin (BCDX-QUI-2) (yield 90%) ^{1}H NMR (400 MHz, D_2O, δ ppm): 8.67 (s, 1H), 8.17 (d, *J* = 8.5 Hz, 1H), 7.78 (d, *J* = 8.3 Hz, 1H), 7.67 (d, *J* = 6.1 Hz, 1H), 7.52 – 7.40 (m, 2H), 5.24 (d, *J* = 14.2 Hz, 1H), 5.04 (d, *J* = 3.5 Hz, 1H), 5.02 (s, 1H), 4.97 (d, *J* = 3.7 Hz, 1H), 4.96 – 4.87 (m, 2H), 4.07 – 3.99 (m, 1H), 3.98 – 3.87 (m, 2H), 3.80 (dt, *J* = 12.8, 8.8 Hz, 2H), 3.74 – 3.67 (m, 1H), 3.66 – 3.46 (m, 7H), 3.44 – 3.33 (m, 2H), 3.32 – 3.22 (m, 3H), 3.21 – 3.09 (m, 2H), 3.05 (d, *J* = 8.9 Hz, 1H), 2.98 (s, 1H). ^{13}C NMR (101 MHz, CD_3OD, δ ppm) : 149.37, 144.89, 137.35, 132.17, 130.07, 127.42, 126.41, 126.24, 121.95, 101.43, 100.77, 82.44, 80.98, 73.19, 72.71, 72.00, 71.69, 71.38, 67.51, 60.31, 58.73, 56.29. HRMS (ESI) *m/z* calcd. for $C_{62}H_{85}N_3O_{34}Na$ $[M + Na]^+$ 1438.4912, found 1438.4788; $C_{62}H_{86}N_3O_{34}$ $[M + H]^+$ 1416.5093, found 1416.4975; $C_{62}H_{84}N_3O_{34}$ $[M - H]^+$ 1414.4936, found 1414.4892.

Mono-[6-deoxy-6-*N*-bis(8-methylquinolyl)]-*γ*-cyclodextrin (GCDX-QUI-2) (yield 82%) ^{1}H NMR (400 MHz, D_2O, δ ppm) : 8.76 (s, 1H), 8.33 (s, 1H), 7.86 (dd, *J* = 8.2, 1.0 Hz, 1H), 7.47 (d, *J* = 34.3 Hz, 1H), 7.30 (d, *J* = 43.4 Hz, 2H), 7.02 (s, 1H), 5.97 (dd, *J* = 10.3, 4.6 Hz, 1H), 5.42 (d, *J* = 4.1 Hz, 1H), 5.31 (d, *J* = 3.9 Hz, 1H), 5.16 (d, *J* = 3.2 Hz, 1H), 5.05 (d, *J* = 3.6 Hz, 1H), 4.89 (d, *J* = 4.0 Hz, 1H), 4.72 (d, *J* = 3.6 Hz, 1H), 4.57 (d, *J* = 3.9 Hz, 1H), 4.52 - 4.41 (m, 1H), 4.29 - 4.07 (m, 3H), 4.03 (dd, *J* = 14.2, 4.8 Hz, 1H), 3.97 (s, 1H), 3.91 (dt, *J* = 8.2, 3.2 Hz, 2H), 3.86 - 3.68 (m, 5H), 3.67 - 3.54 (m, 2H), 3.54 - 3.46 (m, 1H), 3.46 - 3.33 (m, 3H), 3.33 - 3.25 (m, 1H), 3.21 (td, *J* = 9.5, 3.7 Hz, 1H), 3.03 (dd, *J* = 18.4, 9.2 Hz, 1H), 2.87 - 2.78 (m, 1H), 2.61 (dd, *J* = 12.6, 3.1 Hz, 1H), 2.50 - 2.39 (m, 1H), 2.34 (d, *J* = 8.1 Hz, 1H), 2.20 (d, *J* = 9.8 Hz, 1H), 1.46 (d, *J* = 9.9 Hz, 1H). ^{13}C NMR (101 MHz, D_2O, δ ppm) : 149.37, 144.89, 137.35, 132.17, 130.07, 127.42, 126.41, 126.24, 121.95, 101.43, 100.77, 82.44, 80.98, 73.19, 72.71, 72.00, 71.69, 71.38, 67.51, 60.31, 58.73, 56.29. HRMS (ESI) *m/z* calcd. for $C_{68}H_{96}N_3O_{39}$ $[M + H]^+$ 1578.5621, found 1578.5620.

Synthesis and Characterization of control molecule, (Scheme S4, Bu-QUI-2): To a dry DCM solution (15 mL) of 1-butylamine (0.073 g, 1 mmol), 8-bromomethylquinoline (0.489 g, 2.2 mmol) and K_2CO_3 (3 equiv) were added. The reaction mixture was stirred at 70 °C for 12 h under a nitrogen atmosphere, then the solvent was removed under vacuum. The crude product was loaded in the column chromatography (silica gel, 200-400 mesh) and eluted with 20% ethyl acetate-petroleum ether. The desired product was obtained as yellowish viscus liquid. ***N,N*-bis(quinolin-8-ylmethyl)butan-1-amine (Bu-QUI-2)** (yield 92%) ^{1}H NMR (400 MHz, $CDCl_3$, δ ppm): 8.57 (dd, *J* = 4.2, 1.5 Hz, 1H), 8.21 - 8.10 (m, 2H), 7.78 (d, *J* = 8.2 Hz, 1H), 7.52 - 7.42 (m, 2H), 3.51 (t, *J* = 7.1 Hz, 1H), 1.95 - 1.83 (m, 1H), 1.27 (dt, *J* = 14.8, 7.4 Hz, 1H), 0.70 (t, *J* = 7.3 Hz, 2H). ^{13}C NMR (101 MHz, $CDCl_3$, δ ppm): 149.24, 145.96, 137.21, 133.31, 129.73, 127.97, 127.58, 126.77, 121.93, 55.84, 53.76, 26.60, 19.40, 13.21. HRMS (ESI) *m/z* calcd. for $C_{24}H_{26}N_3$ $[M + H]^+$ 356.2127, found 356.2118.

Preparation and characterization of probe L1/L1(Zn) (Scheme S5) (Xue et al., 2016; Hu et al., 2012; Zhao et al., 2010)**:** To an aqueous solution (2 mL) of BCDX-QUI-2 (0.079 g, 0.056 mmol) was added a dilute aqueous solution of a slight excess of $Cu(ClO_4)_2 \cdot 6H_2O$ or $Zn(CH_3COO)_2 \cdot 6H_2O$ (0.062 mmol) and the mixture was stirred at room temperature for 6 h. The resulting solution was evaporated down to 1 ml under reduced pressure and then poured into acetone (30 mL). The resulting white precipitate was filtered and washed successively with acetone (20 mL x 4) to give the product (similar procedure was used to prepare the probes **L2-4**). Then the aqueous solution of the complex was lyophilized to give the pure complex as a slightly light blue solid in 78% yield. **Probe L1**: ^{1}H NMR (400 MHz, D_2O, δ ppm): 8.57 (s, 1H), 8.16 (s, 1H), 7.76 (s, 1H), 7.62 (s, 1H), 7.43 (s, 2H), 5.32 - 4.93 (m, 7H), 4.11 (s, 1H), 3.92 (d, *J* = 31.6 Hz, 7H), 3.82 – 3.41 (m, 15H), 3.41 – 2.85 (m, 3H). **Probe L1(Zn) :** ^{1}H NMR (400 MHz, D_2O, δ ppm) 8.73 (s, 1H), 8.27 (s, 1H), 7.89 (s, 1H), 7.78 (s, 1H), 7.56 (d, *J* = 24.2 Hz, 2H), 5.34 (s, 1H), 5.15 (d, *J* = 14.6 Hz, 3H), 5.05 (s, 2H), 4.16 (s, 1H), 4.05 (s, 2H), 3.95 (s, 3H), 3.76 (t, *J* = 24.6 Hz, 10H), 3.51 (d, *J* = 49.4 Hz, 6H), 3.24 (d, *J* = 29.4 Hz, 2H), 2.96 (s, 1H).

Preparation of stock solutions: Stock solutions (ACDX-QUI-2 = 7.9 x 10^{-4} M; BCDX-QUI-2 = 7.06 x 10^{-4} M; GCDX-QUI-2 = 6.3 x 10^{-4} M and probes **L1-L4**) of the modified CDXs (CDX-QUI-2) used for all sensing studies were prepared by dissolving 0.001g of the requisite CDX-QUI-2 derivative in 1 mL of double-distilled water or methanol. A stock solution of the control compound Bu-QUI-2 (2.8 x 10^{-3} M) was prepared by

dissolving 0.001 g of Bu-QUI-2 in MeOH (1 mL). All of the stock solutions of the anionic analytes (AMP, ADP, ATP, Pi, PPi, and triPi) were prepared from the corresponding sodium salts (0.002 g) in double distilled water.

DFT calculations: Quantum mechanical calculations based on the density functional theory (DFT) and time-dependent density function theory (TD-DFT) were carried out using the Gaussian 09 program (Frisch et al., 2010). These studies were used to identify the binding pattern between the three different adenosine nucleotides and the probe **L1**. Theoretical investigation of individual molecules *viz.* BCDX-QUI-2, probe **L1** (BCDX-QUI-2:Cu^{2+} complex), and nucleotides (AMP, ADP, or ATP) were employed to gain additional support for binding considerations, and they were used to provide a theoretical basis for the photophysical properties of the formed inclusion complexes involved in the differential binding behaviour. The structures were optimized with the function of B3LYP with the basic set of 6-31G(d), while the 6-311G(d) basis set and LANL2DZ as additional input was used for Cu atom.

The individual optimization and calculation studies for probe **L1** (Figure S51), nucleotides (AMP, ADP and ATP) (Figure S52) and the respective complexes were performed. In the absence of nucleotides, probe **L1** exhibits moderate emission attributed to electron transfer from *N*-bis-8-methylamino part (HOMO) to the quinolyl scaffolds (LUMO) (Figure S51). In nucleotides, both HOMO and LUMO level electron clouds occupied in the adenine moiety. Upon complexation of AMP with probe **L1**, the phosphate group binds to the metal center and the hydrophobic adenine moiety occupies the CDX cavity, thus exhibiting quenched fluorescence (blue shifted) attributed to restricted photoinduced electron transfer (PET) from the adenine moiety to the quinolyl scaffold. Binding of probe **L1** binding with ATP/ADP exhibits enhanced fluorescence attributed to photoinduced electron transfer (PET) from the adenine moiety to the quinolyl scaffolds because the adenine moiety is located outside the electronic clouds of the CD cavity.

"*in-situ*" Monitoring of enzymatic phosphorylation and dephosphorylation (PM-I/II and dPM-I/II)

Phosphorylation Method I (PM-I): The enzymatic phosphorylation reaction was carried out by adding creatine phosphate (CP, 5 equiv) and various concentration of creatine kinase (CK, 0-10 U) to the aqueous buffer solution (pH 6.5, MES, 10 mM) containing AMP/ADP and the mixture was stirred at 37 ºC. From the reaction mixture, the aliquots were

collected at different time intervals. The emission enhancement at 427 nm was monitored using fluorescence spectroscopy for the solution containing the collected aliquot mixed with probe **L1** (37 μM) in water.

Phosphorylation Method II (PM-II): The enzymatic phosphorylation reactions was carried out as mentioned with above reaction condition and reactants along with probe **L1** (37 μM) in the aqueous buffer solution (pH 6.5, MES, 10 mM). From the reaction mixture, the aliquots were collected at different time intervals, diluted with the required volume of water and monitored the emission change at 427 nm using fluorescence spectroscopy.

Dephosphorylation Method I (dPM-I): The enzymatic dephosphorylation reaction was carried out by adding various concentration of apyrase (0-10 U) to the aqueous buffer solution (pH 7.4, HEPES, 10 mM) containing ATP/ADP and the mixture was stirred at 25 ºC. From the reaction mixture the aliquots were collected at different time intervals and the dephosphorylation process was quenched with the aid of ethylenediaminetetraacetic acid (EDTA, 90 μM) as a catalyst quencher (Butler, 2014). The emission enhancement at 427 nm was monitored using fluorescence spectroscopy for the solution containing the collected aliquot mixed with probe **L1** (37 μM) in water.

Dephosphorylation Method II (dPM-II): The enzymatic dephosphorylation reactions was carried out as mentioned with above reaction condition and reactants along with probe **L1** (37 μM) in the aqueous buffer solution (pH 7.4, HEPES, 10 mM). From the reaction mixture the aliquots were collected at different time intervals, and the dephosphorylation process was quenched with the aid of EDTA (90 μM) as a catalyst quencher. The aliquots were diluted with the required volume of water and monitored the emission change at 427 nm using fluorescence spectroscopy.

Supplemental References

Butler, S.J. (2014). Ratiometric detection of adenosine triphosphate (ATP) in water and real-time monitoring of apyrase activity with a tripodal zinc complex. Chem. Eur. J. *20*, 15768-15774.

Frisch, M.J., Trucks, G.W., Schlegel, H.B., Scuseria, G.E., Robb, M.A., Cheeseman, J.R., Scalmani, G., Barone, V., Mennucci, B., Petersson, G.A., Nakatsuji, H., Caricato, M.L., Li, X., Hratchian, H.P., Izmaylov, A.F., Bloino, J., Zheng, G., Sonnenberg, J.L., Hada, M., Ehara, M., Toyota, K., Fukuda, R., Hasegawa, J., Ishida, M., Nakajima, T., Honda, Y., Kitao, O., Nakai, H., Vreven, T., Montgomery, Jr., J.A., Peralta, J.E., Ogliaro, F., Bearpark, M., Heyd, J.J., Brothers, E., Kudin, K.N., Staroverov, V.N., Keith, T., Kobayashi, R., Normand, J., Raghavachari, K., Rendell, A., Burant, J.C., Iyengar, S.S., Tomasi, J., Cossi, M., Rega, N., Millam, J.M., Klene, M., Knox, J.E., Cross, J.B., Bakken, V., Adamo, C., Jaramillo, J., Gomperts, R., Stratmann, R.E., Yazyev, O., Austin, A.J., Cammi, R., Pomelli, C., Ochterski, J.W., Martin, R.L., Morokuma, K., Zakrzewski, V.G., Voth, G.A., Salvador, P., Dannenberg, J.J., Dapprich, S., Daniels, A.D., Farkas, O., Foresman, J.B., Ortiz, J.V., Cioslowski, J., and Fox, D.J. (2010). Gaussian 09. (Gaussian, Inc., Wallingford, CT).

Gottlieb, H.E., Kotlyar, V., and Nudelman, A. (1997). NMR chemical shifts of common laboratory solvents as trace impurities. J. Org. Chem. *62*, 7512-7515.

Hu, P., Liu, G.-F., Ji, L.-N., and Mao, Z.-W. (2012). Efficient promotion of phosphatediester cleavage by a face-to-face cyclodextrin dimer without metal. Chem. Commun. *48*, 5515-5517.

Tang, W., and Ng, S.-C. (2008). Facile synthesis of mono-6-amino-6-deoxy-α-, β-, γ-cyclodextrin hydrochlorides for molecular recognition, chiral separation and drug delivery. Nat. Protoc. *3(4)*, 691-697.

Xue, S.-S., Zhao, M., Ke, Z.-F., Cheng, B.-C., Su, H., Cao, Q., Cao, Z.K., Wang, J., Ji, L.-N., and Mao, Z.-W. (2016). Enantioselective hydrolysis of amino acid esters promoted by bis(β-cyclodextrin) copper complexes. Sci. Rep. *6*, 22080.

Zhao, M., Zhang, L. Chen, H.-Y. Wang, H.-L. Ji, L.-N., and Mao, Z.-W. (2010). Effect of hydrophobic interaction cooperating with double Lewis acid activation in a zinc(II) phosphodiesterase mimic. Chem. Commun. *46*, 6497-6499.